A Fluid Inclusion Study of the Little Nahanni LCT-Type Pegmatite Group, NWT Canada: Implications for the Nature and Origin of Fluids in LCT-Type Pegmatites and Pegmatite Evolution

by

Michael George Garrett Burns

A thesis submitted in partial fulfillment
of the requirements for the degree of
Master of Science (MSc) in Geology

The Faculty of Graduate Studies
Laurentian University
Sudbury, Ontario, Canada

THESIS DEFENCE COMMITTEE/COMITÉ DE SOUTENANCE DE THÈSE
Laurentian Université/Université Laurentienne
Faculty of Graduate Studies/Faculté des études supérieures

Title of Thesis
Titre de la these: A Fluid Inclusion Study of the Little Nahanni LCT-Type Pegmatite Group, NWT Canada: Implications for the Nature and Origin of Fluids in LCT-Type Pegmatites and Pegmatite Evolution

Name of Candidate
Nom du candidat: Burns, Michael

Degree
Diplôme: Master of Science

Department/Program
Département/Programme: Geology

Date of Defence
Date de la soutenance December 14, 2015

APPROVED/APPROUVÉ

Thesis Examiners/Examinateurs de thèse:

Dr. Daniel Kontak
(Supervisor/Directeur de thèse)

Dr. Andrew McDonald
(Committee member/Membre du comité)

Dr. Pedro Jugo
(Committee member/Membre du comité)

Dr. Alan Anderson
(External Examiner/Examinateur externe)

Approved for the Faculty of Graduate Studies
Approuvé pour la Faculté des études supérieures
Dr. David Lesbarrères
Monsieur David Lesbarrères
Acting Dean, Faculty of Graduate Studies
Doyen intérimaire, Faculté des études supérieures

Abstract

The Cretaceous (82 Ma) Little Nahanni Pegmatite Group , Canada, is a 15 km long swarm of LCT-type pegmatite dikes that intrude Precambrian to Lower Cambrian siliciclastic metapelites and carbonate rocks. The dykes are dominated by a primary assemblage of quartz, spodumene, K-feldspar ± muscovite lacking both graphic textures and core zones, but characterized by comb-textured spodumene and K-feldspar intergrowths. Varying degrees of albitization and lesser phyllic alteration accompany ore-grade oxide enrichment (Ta-Nb and Sn, respectively).A comprehensive fluid inclusion study using a wide variety of methods (petrography , CL, microthermometry, SEM/EDS evaporate mound analysis, LA ICP-MS, laser Raman spectroscopy, $\delta^{13}C$) on minerals (quartz, K-feldspar, albite, spodumene, muscovite, garnet, and tourmaline) from barren and mineralized samples indicate the fluid inclusions are secondary and appear to post-date pegmatite crystallization. The presence of secondary fluid inclusions may instead represent entrapment during the late-stage (sub-solidus to post crystallization) metasomatic evolution stage of the pegmatites. Three fluid types occur, and listed in paragenetic order are: (A) an aqueous-carbonic fluid (≤1 wt. % eq. NaCl) with varying X_{CO2} (0.1 to 0.78), purity (Tm_{CO2}= -57° to -61°C), and density; (B) a low-salinity (≤2 wt. % eq. NaCl) aqueous fluid; and (C) an aqueous-methane-nitrogen fluid. SEM-EDS analysis indicates that the fluids are Na (-K) - dominant, but with significant S and enrichment in transition and chalcophile elements. Fluid inclusion extracts have $\delta^{13}C$ values (-9.7 to -27.7‰; n=7) which indicates exchange of the fluids with the immediate, carbon-bearing wall rocks occurred. Collectively the data indicate: (1) fluids were trapped during the later, metasomatic stage of pegmatite evolution; (2) fluids were trapped at <2.5 kbars and <350°C with pressure fluctuating between lithostatic and hydrostatic; (3) variable degrees of fluid:rock interaction occurred with the exocontact zone, resulting in varying $XCO_2$and CO_2:CH_4 values; and (4) metasomatism and rare metal mineralization occurred in the presence of meteoric water. These findings indicate that the LNPG pegmatites are not a closed system, some of the carbonic component of H_2O-CO_2 fluids is exotic, and that low-salinity fluids of meteoric origin infiltrated during the subsolidus stage of pegmatite evolution.

Keywords

LCT-type Pegmatite, Fluid Inclusion, Little Nahanni Pegmatite Group, Evaporate Mound.

Co-Authorship Statement

I hereby declare that this thesis incorporates material that is in part a result of joint research undertaken in collaboration with Dr. Lee A. Groat and under the supervision of Dr. Daniel J. Kontak. The collaboration includes the field-research portion of the project which is limited to field research logistics, sample collection, sample setting description, and geological mapping. In addition, assistance with the $\delta^{13}C$ analysis was provided by Dr. Kontak, who selected, and submitted samples for analysis at Queen's University, Kingston, ON. Assistance with the LA-ICP-MS analysis and data collection was provided by Joseph Petrus, however all sample selection, preparation, data analysis and interpretation was performed by the author. Revisions and edits to the manuscript were also facilitated with assistance from Dr. Kontak, Dr. Groat, and Dr. Jugo. In all other aspects of the study, including the writing of the manuscript, the data collection, analysis and interpretation of microthermometric, SEM-EDS evaporate mound, laser Raman, and petrographic studies, the work was performed by the author. The contribution of co-authors was primarily through the provision of discussion of results, and obtaining information regarding the field-setting of collected samples for contextual comparison in the lab.

Acknowledgements

I am gratefully appreciative of the assistance of my supervisor, Dr. Daniel Kontak, as a respected mentor, teacher and fellow researcher who helped me grow both as a person and student, and for providing much appreciated support and encouragement throughout this project. In addition I would like to acknowledge and thank Dr. Lee Groat for his mentorship and introduction to pegmatites, Dr. Dan Marshal and Dr. Andy McDonald for guiding me through laser Raman spectroscopy analysis, and Dr. Joseph Petrus for his assistance with LA-ICP-MS analysis and interpretation. The close friendship and support from fellow students Craig Stewart, Taus Jorgensen and Dr. Geoff Baldwin and their assistance and advice about data collection, analysis, writing, and editing was much appreciated. Finally, I would like to thank my parents and family for their unwavering support and encouragement along the way. This study was supported by an NSERC discovery grant to Dr. Daniel Kontak.

Table of Contents

List of Tables

List of Figures

List of Appendices

Chapter 1: Introduction to Thesis

Introduction

Lithium-Cs-Ta (LCT) - type pegmatites are amongst the most evolved magmatic rocks known (London, 2008) and represent the latest stages of igneous differentiation of felsic magmatic bodies, thus they play an integral role in both the element redistribution in the upper crust and the formation of rare element mineral deposits. Despite the genetic relation of igneous melt differentiation and incompatible element (e.g., Be, Ta, Nb, Li, Cs, F, B, Sn) and volatile (H_2O, CO_2) enrichment of residual melts, the mechanism and timing of rare element mineralization and the role of pegmatite-hosted fluids in these evolved pegmatites remains poorly constrained(Roedder, 1992; Beurlen et al., 2001; London, 2008; Linnen et al., 2012).The enrichment in rare elements (e.g., Sn, Li, Ta, Nb, Rb, Cs) in evolved pegmatites is often thought to occur as a magmatic process syn-emplacement. However, field observations, such as the strong spatial association of Ta-Nb mineralization within fabric-destructive albitization alteration zones, and high-grade Sn mineralization within Ms-Qtz dominated phyllic alteration zones, suggest late stage metasomatic processes play a role (e.g., Partington et al., 1995; Webster et al., 1997; Kontak, 2006; Linnen et al., 2012). It has been known for some time that volatile enrichment lowers the granite, also the pegmatite, solidus (London et al., 1989; Thomas and Davidson, 2012;Černý et al, 2012) and this would in theory allow rare metal (Ta, Nb, Sn) enrichment to occur (Linnen 1998, London 2008; Thomas et al., 2011). Whether these melts are saturated or undersaturated in volatiles during emplacement and crystallization remains poorly constrained, with the original suggestions of Jahns and Burnham (1969) later challenged by

London (2008, 2012) and Thomas and Davidson (2012). At present there is evidence for both primary and secondary (i.e., subsolidus) rare metal mineralization, as Linnen et al. (2012) have most recently summarized, although the proportions likely vary among different pegmatite suites.

The Cretaceous (82 Ma) Little Nahanni Pegmatite Group (LNPG) presents an excellent opportunity to study the timing of melt saturation, and rare element mineralization in an LCT type pegmatite system. Excellent exposure of the dike swarm exists both along strike for 15km and vertically for 100 – 200m. In addition, broad scale mineralogical zonation is absent in the dikes, however, textural variations from fine grained aplite dikes to coarse grained pegmatitic spodumene and K-feldspar (15-35cm laths) do occur. To date, mineralogical, geochronological and lithium isotope studies by Mauthner et al. (1995), Kontak et al. (2003), Groat et al. (2003) , Černý et al. (2007) and Barnes (2010) and others have laid a strong foundation of knowledge pertaining to the geological setting, the mineralogy, mineral chemistry and geochronology of the LNPG. In addition, Barnes (2010) provided some brief comments on the nature of fluid inclusions in a single sample of pegmatite.

Through a detailed fluid inclusion study, this thesis aims to contribute to the understanding of pegmatite-exsolved aqueous fluid compositions, fluid reservoirs (i.e., external or connate to the pegmatite system), and aqueous fluid mixing within the context of a mineralized LCT-type pegmatite system. An accurate comprehension of the state of fluid saturation in aqueous and aqueous-vapor (CO_2, CH_4) pegmatitic melts is required to further understand aspects such as the timing of pegmatite formation and crystallization, mineralization and metasomatic processes.

Structure of the Thesis

This thesis is presented in the form of a manuscript (Chapter 2), which has been submitted for publication in *Geofluids*, a peer reviewed geosciences journal.

Chapter 2:

A FLUID INCLUSION STUDY OF THE LITTLE NAHANNI LCT-TYPE PEGMATITE GROUP, NWT CANADA: IMPLICATIONS FOR THE NATURE AND ORIGIN OF FLUIDS IN LCT-TYPE PEGMATITES AND PEGMATITE EVOLUTION

MICHAEL BURNS[§]
Department of Earth Sciences, Laurentian University, 935 Ramsey Lake Rd., Sudbury, Ontario, P3E 2C6

DANIEL J. KONTAK
Department of Earth Sciences, Laurentian University, 935 Ramsey Lake Rd., Sudbury, Ontario, P3E 2C6

Lee Groat
Department of Earth and Ocean Sciences, University of British Columbia, Vancouver, British Columbia, Canada

[§] *E-mail address: mg_burns@laurentian.ca*

A**BSTRACT**

The Cretaceous (82 Ma) Little Nahanni Pegmatite Group in the NWT, Canada, is a 15 km long swarm of LCT-type pegmatites that intrude Precambrian to Lower Cambrian siliciclastic metapelites and carbonate rocks. The dikes are dominated by a primary assemblage of Qtz-Spd-Kfs±Ms lacking both graphic textures and core zones, but characterized by comb-textured Spd-Kfs. Varying degrees of albitization (Ta-Nb) and lesser phyllic alteration (Sn)accompany ore-grade oxide enrichment. A detailed fluid inclusion study using a wide variety of methods (petrography, CL, microthermometry, SEM/EDS evaporate mound analysis, LA ICP-MS, laser Raman spectroscopy, $\delta^{13}C$) on minerals (Qtz, Kfs, Ab, Spd, Ms, Grt, Tur) from barren and mineralized samples suggest that most of the inclusions are secondary, thus post-dating pegmatite crystallization. The inclusions may instead represent entrapment during the late-stage metasomatic evolution of the pegmatites.

Three fluid types occur, and listed in paragenetic order are: (A) an aqueous-carbonic fluid (≤1 wt. % eq. NaCl) with varying X_{CO2}(0.1 to 0.78), purity (Tm_{CO2}= -57^o to -61^{o}C), and density; (B) a low-salinity (≤2 wt. % eq. NaCl) aqueous fluid; and (C) an aqueous-methane-nitrogen fluid. Evaporate mound analyse indicates the fluids are Na (-K) - dominant, but with significant S and enrichment in transition and chalcophile elements. Fluid inclusion extracts have $\delta^{13}C$ values (-9.7 to -27.7‰; n=7) which are consistent with the fluids having exchanged with graphite bearing wall rocks. Collectively the data indicate: (1) fluids were trapped during the late-stage evolution of the pegmatites during its metasomatic stage; (2) fluids were trapped at <2.5 kbars and <350°C with pressure fluctuating between lithostatic and hydrostatic based on isochoric calculations; (3) variable degrees of fluid:rock interaction occurred with the exocontact zone, as

recorded by variable $X_{CO2}$and CO_2:CH_4 ratios in the inclusions; and (4) metasomatism and rare-metal mineralization occurred in the presence of a low-salinity fluids, likely meteoric water. These findings indicate that the LNPG pegmatites were not a closed system during their evolution and that some, if not all, of the carbonic component of the H_2O-CO_2 fluid is exotic, and that low-salinity fluids of meteoric origin infiltrated the system during the late-stage evolution of the pegmatite.

INTRODUCTION

Lithium-Cesium-Tantalum (LCT) - type pegmatites (Černý 1991a, b) are the most chemically evolved of the pegmatites and among the most fractionated terrestrial rocks known (London 2008). However, despite the established genetic relationship between melt differentiation and rare-metal (RM) mineralization and volatile enrichment, the factors controlling mineralization (*e.g.*, Ta, Nb, Sn, W, Li, Cs, etc.) in these settings still remain unresolved (Beurlen *et al.* 2001; Linnen & Cuney 2005; London 2008; Linnen *et al*. 2012). The enrichment in both the RM and rare elements is generally attributed to primary magmatic processes (London 2008; Linnen *et al.* 2012), but field observations and supporting petrologic studies indicate that metasomatic processes are also significant, if not the dominant factor, in some cases (*e.g*., Partington *et al.* 1995; Kontak 2006; Van Lichtervelde *et al.* 2007; Van Lichtervelde *et al.* 2008; Thomas *et al.* 2011). Although it is also well established that volatiles lower the melt solidus and prolong volatile saturation (*e.g.*, London et al. 1989; Maneta and Baker 2014; Sirbescu et al. 2017), thus extending fractionation and further enhancing metal enrichment (Linnen 1998; London 2008;

Thomas *et al.* 2008a, b), timing of fluid saturation relative to melt crystallization remains unresolved (*e.g.*, Jahns & Burnham 1969; London 1986b, 2008; Roedder 1992; Kontak 2006).

At present, fluid inclusion studies of pegmatites, in particular the LCT-type, remain somewhat equivocal regarding the presence of primary inclusions related to the main stage of pegmatite crystallization (Smith 1953; London 1985b; Anderson *et al.* 2001; Sirbescu & Nabelek 2003; Sirbescu *et al.* 2008; Mulja & Williams-Jones 2018), thus precluding the nature of fluids to pegmatite evolution. Furthermore, if the guidelines governing timing of fluid inclusion entrapment are followed (i.e., Roedder1984; Bodnar, 2003a), and the concept of fluid inclusion assemblages (FIA; Goldstein & Reynolds, 1994; Bodnar, 2003a) is applied, then it is apparent that many inclusions classified as primary in these studies lack the necessary corroborating evidence (e.g., growth zones) to support their classification. Thus, evidence cited for a primary origin of inclusions – such as isolation in three-dimensional (3D) arrays, negative crystal shape, or elongation along a crystallographic axis – cannot be interpreted unequivocally as indicating such an origin without demonstrating entrapment along a crystal growth face. This distinction is critical since primary inclusions imply a fluid was present during crystal growth (Roedder 1979). An apparent lack of primary fluid inclusions does not, however, indicate volatile-undersaturation of the melt, but simply that such evidence is lacking. In addition, there is confusion as to whether some pegmatite-hosted fluid inclusions, including those from the same samples, are primary, secondary, or possibly even melt inclusions (*e.g.*, Simmons & Webber 2008); the spodumene-hosted, solid-rich inclusions from Tanco being one notable example (Anderson *et al.* 2001; Anderson 2013).

Despite uncertainty about classification and timing of fluid entrapment in LCT-type and other pegmatites, fluid compositions are well defined and generally correspond to two types: a

low-salinity (3 to 7 wt. % eq. NaCl) aqueous fluid, and a low-salinity, aqueous-carbonic fluid with variable XCO_2 (*e.g.*, London 1985b, 1986b; Thomas & Spooner 1988; Anderson *et al.* 2001; Beurlen *et al.* 2001). Fluid inclusions described as primary are mainly aqueous-carbonic (London 1985b, 1986a, Fuertes-Fuente *et al.* 1995; 2000; Nabelek & Ternes 1997; Beurlen *et al.* 2001; Sirbescu & Nabelek 2003) and imply that a H_2O-CO_2 fluid coexisted with a hydrous-silicate melt during crystallization. In addition, generation of both CO_2- and H_2O-rich fluids due to unmixing of a parental aqueous-carbonic fluid during melt crystallization has been proposed for the LCT pegmatites of the Black Hills, USA (Nabelek & Ternes 1997) and Cap de Creus, Spain (Alfonso & Melgarejo 2008). Examples of primary fluid inclusions are also cited to occur in samples from late-stage miarolitic cavities or core areas (*e.g.*, Thomas & Davidson 2012; London et al. 2012), thus indicating late-stage volatile saturation. Also relevant is whether pegmatite crystallization occurred in open or closed systems, the former implying chemical exchange between the melt, or already crystallized components, and immediate wall rock (*e.g.*, Beurlen *et al.* 2001; Kontak 2006; Martin 2013).

Fluid inclusions from the Little Nahanni Pegmatite Group (LNPG) are used herein to address many of the aforementioned issues related to LCT pegmatites: (1) timing of volatile saturation; (2) nature and origin of the fluids; (3) pressure – temperature – composition (PTX) conditions during pegmatite evolution; (4) open versus closed system evolution; and (5) relationship of fluids to RM mineralization. The analytical methods used, which include detailed petrography, cathodoluminescence (CL), microthermometry, evaporate mound SEM-EDS, in situ LA ICP-MS, laser Raman spectroscopy, and $\delta^{13}C$ of fluid inclusion extracts, represent, as far as we are aware, one of the most exhaustive studies of fluid inclusions in a pegmatite setting. The study incorporates our own field and petrological observations, past and ongoing, as well as

thtt of others (Mauthner *et al.* 1996; Groat *et al.* 2003; Kontak *et al.* 2004; Barnes 2010; Barnes *et al.* 2012) on a well characterized pegmatite setting.

GEOLOGICAL SETTING

The Cretaceous (*i.e*., 82 Ma; Mauthner *et al.* 1995; Kontak *et al.* 2016; our upubl. data) LNPG occurs along the border of the Northwest Territories and the Yukon in NW Canada (Fig. 1). Although other suites of similar age are apparently absent, the study area does lie within a part of the northern Cordillera which is characterized by regionally extensive Cretaceous felsic magmatism associated with varied mineralization *(e.g*., S, W, Au, Cu, Zn, Pb, Ag; Hart 2007). The dike swarm, which comprises hundreds of pegmatites exposed along a 15 km strike length (Fig. 1), occurs in the Northern Cordilleran Selwyn Basin which represents a deep-water setting initiated by rifting of Rodinia between the Neoproterozoic to Middle Devonian.

Within the study area the dikes are hosted by the Yusezyu and Narchilla formations of the Neoproterozoic to Lower Cambrian metasedimentary rocks of the Hyland Group (Fig. 1). The Yusezyu Formation consists of shallow water, submarine fan clastic deposits, whereas the overlying Narchilla Formation consists of deeper water, calcareous shales (Gordey & Anderson 1993; Cook *et al.* 2004). The study area experienced regional deformation and lower greenschist facies metamorphism with associated folding and development of a NW-striking penetrative cleavage during accretion of the Yukon-Tanana Terrane in the Late Permian-Early Triassic period. A later period of deformation (*i.e*., post 82 Ma) is also evident as the pegmatites are locally folded (see below). Rare examples of quartz veins, rarely with minor Fe sulfides, also occur in the study area but have not been studied in detail.

Of note and of possible relevance here is the presence of isolated, coarse biotite-cordierte-andalusite –staurolite hornfels and localized bimetasomatic skarns in the northern part of the area (see star in Fig. 1). These rocks, possibly hornfels, occur as rare outcrops, as locally abundant float and have been intersected in drilling in this area. As the hornfels record deformation, locally evidenced by rotated porphyroblasts, which may be the same event preserved by boundinaged pegmatites, it is inferred that these minerals predate this later deformation.

The area is cut by the March Fault, a major NW-trending fault that was reactivated at approximately 85 Ma (Mair *et al.* 2006). No pegmatites occur east of this fault, which thrust the host rocks (Hyland Group) over the Lower Cambrian to Ordovician Rabbitkettle and Vampire formations, respectively, which outcrop eastwards. In addition, the main dike swarm is confined to the east side of a ridge which defines the core of the Fork anticlinorium over an area of at least 15 x 2.5 km. The dike swarm post-dates the development of this structure and related axial planar fabric which locally appears to have localized the dike (Barnes 2010).

FEATURES OF THE LNPG PEGMATITES

The LNPG dike swarm consists of pegmatites and lesser fine-grained bodies (*i.e*., aplites) with a generally northwest strike. An apparent chemical uniformity across the pegmatite field exists based on uniform whole-rock (Barnes 2010) and mineral (K/Rb ratios of K-feldspar; Kontak *et al*. 2016 and our unpubl. data) chemistry; whether this indicates an underlying versus lateral source remains unknown. The dikes are best exposed in cirque faces and intervening ridges which provide excellent exposure and collecting sites.. The setting and the general textural,

mineralogical and mineral chemistry features of the pegmatites have been described previously (Groat *et al.* 1994, 2003; Kontak *et al*. 2004; Barnes 2010; Barnes *et al.* 2012), thus the following summary is focused on features relevant to this study. .

The dikes generally have variable modal mineralogy and textures and are dominated by primary K-feldspar, spodumene and quartz with much lesser albite, lepidolite and muscovite (Fig. 2a, b, c). Oriented, high-aspect ratio crystals of K-feldspar and spodumene and layered textures are common (Fig. 2a). There is a notable absence of pocket zones which characterize many pegmatite settings (*e.g.*, London 2008, 2014, 2018; Simmons & Webber 2008). Dikes range from centimetre to metre scale (<10 m) width and are traceable for 10s to 100s of metres. In the larger (>40 cm width) dikes, the elongate K-feldspar and spodumene are oriented perpendicular to wall rock contacts (Fig. 2a, c) with the intervening equigranular material consisting of quartz, spodumene and albite with minor muscovite and lepidolite (Fig. 2b). Less common is a banding or crenulate layering (Fig. 2d, e), which also includes line-rock texture. In the latter, the texture is more commonly finer grained and equigranular and where well layered lepidolite is more common (Fig. 2d).

Pocket zones, in addition to graphic textures, are conspicuously lacking but other features are present. The first are rare cases of irregularly shaped zones (<1 m sq) of aphanitic leucocratic material with penetrating acicular spodumene; such areas are interpreted as quenched melt pockets. Rarely the dikes have been seen in the highest exposed levels to change into ovoid zones of intergrown quartz and muscovite with rare calcite (Fig. 2f).

Wall zones infrequently observed are narrow (*i.e*. <1 cm), aplitic, generally lack muscovite and give way to coarser-grained pegmatite. Not uncommonly the contact zones between pegmatite and the sedimentary wall rock are characterized by the presence of pale red to

orange-red garnet, orange-brown mica and fine-grained black tourmaline. These zones may follow bedding plane horizons or fractures that penetrate for several 10s cm into the wall rock.

Of particular interest in the context of LCT pegmatites is the presence of albitization, which is prevalent throughout the pegmatite field and is fabric destructive. This is seen after primary K-feldspar and is associated with zones of rare metal mineralization (Fig. 2 g, h; Sn-W-Ta-Nb). The albite forms as either a fine-grained saccharoidal variety, which hosts the mineralization, or more rarely cleavelandite. In addition, isolated zones of high-grade, RM mineralization occur coincident with a muscovite and quartz assemblage (Fig. 2g, h).

The latest event in terms of formation of the pegmatites is represented by pocket-like features (cm to <30 cm). Their elongate shape, irregular outlines, relationship to fracturing and their fill (*i.e*. variable mixtures of quartz, bladed albite, clear mica, zeolites, carbonate, red-orange garnet and apatite; Fig. 2i, j) suggest a secondary origin and part of the post-crystallization history of the pegmatites.

As previously noted, the pegmatites are locally folded (Fig. 2k) and, in addition, can be boudinaged (Fig. 2l, m), which provides evidence for post emplacement deformation. The age of the latter event however remains unconstrained. Importantly, materials used in this study did not record this event at either the macro- or micro-scale (e.g., recrystallized quartz).

A detailed textural and paragenetic study of the pegmatites, following on the previous work of Groat *et al*. (2002) and Kontak & Groat (2008), is currently in progress (Pfister *et al*. 2018, 2019), but a few features relevant to the present study are noted. The early coarse magmatic assemblage (Qtz-Kf-Spd±Ms) is followed by a finer-grained assemblage (Qtz-Alb-Ms±Apt±RM (Ta-Nb, Sn) ores) which is overprinted by secondary albite, micas (Fe-rich muscovite, lepidolite) and additional rare metal mineralization. That albitic plagioclase (An_{0-5}) is

replaced by calcic plagioclase (An_{15-20}) in some zones suggests ingress of wall rock-derived components fluid:rock interaction (*e.g.*, Martin & De Vito 2013). Furthermore, rare cases of vermicular intergrowth of quartz and spodumene having a bulk chemistry similar to petaltie (*i.e.*, SQUI), as noted by previous workers (Groat *et al*. 2002; Barnes 2010; Pfister *et al*. 2018) and in this study, plus SQUI overgrowing earlier spodumene suggests pressure cycling accompanied pegmatite crystallization (Pfister *et al*. 2019).

ANALYTICAL METHODS

Sample preparation and petrographic study of fluid inclusion samples

Prior to microthermometry, samples were prepared as doubly polished, thick sections 300 μm thick. Sections containing clear to glassy quartz, light green translucent spodumene, and high-grade oxide mineralization typically contained the best fluid inclusions (*e.g.*, Fig. 3). All sections were studied in transmitted and reflected light using an Olympus BX51 microscope equipped with a QImaging MicroPublisher 5.0 RTV camera in the Department of Earth Sciences Fluid Inclusion Laboratory, Laurentian University, Sudbury, Ontario.

Following petrographic study, the wafers were dismounted and washed with acetone, gently polished on white paper, and cleaned again with acetone to remove any residual mounting medium, which was important for subsequent decrepitate mound analysis and laser Raman spectroscopy. Inclusion populations were classified based on the rules of Roedder (1979; see Bodnar 2003a) and areas with suitable FIA (Goldstein & Reynolds 1994) were selected for microthermometry.

Microthermometry

All heating and cooling work was performed on a Linkham TMS600 heating-freezing stage at Laurentian University. Calibration of the stage was monitored using SynFlinc fluid inclusion standards for CO_2 (Tm_{CO2} -56.6° ± 0.2°C), water (Tm_{ice} at 0° ± 0.1°C), and critical point of water (374° ± 1°C). Measurements of phase changes were made on fluid inclusions in FIA and included final ice melting (Tm_{ice}) and total homogenisation temperature (T_h) for aqueous types, and CO_2melting (Tm_{CO2}), CO_2 homogenization (Th_{CO2}), and clathrate melting (Tm_{clath}) for aqueous-carbonic types. In most cases, many observations were made during thermometric runs but only a limited amount of data recorded. Salinities (wt. % eq. NaCl) were calculated using both Tm_{ice} (Bodnar 1993, 2003b) and Tm_{clath} (Diamond (1992). Measurement of total homogenization (T_h) for aqueous-carbonic inclusions was not always possible due to decrepitation above 350°C, which is common for such inclusion types due to high internal pressures (*e.g.*, Roedder 1984).

SEM-EDS analysis of evaporate mounds

Analysis of evaporate salt mounds using energy dispersive spectroscopy attached to a scanning electron microscope (SEM-EDS) followed the protocol of Kontak (2004). Quartz chips from 8 samples, dismounted and cleaned using the method above, were overheated (450° to 500°C) on the thermometric stage to induce decrepitation and mound formation. Following carbon coating, the mounds were imaged and analyzed on a JEOL 6400 SEM with an INCA EDS detector and software system at Laurentian University. Mound analysis takes advantage of the loss of H_2O and formation of salt mounds and their relative enrichment in major (*e.g.*, Na, K, Ca) and minor or trace (*e.g.*, Fe, As, S) elements. However, as there is no control on possible loss of some of the constituents, in particular volatiles (*e.g.* F, S, B), during decrepitation. Due to the loss of the H_2O during mound formation, the contents of otherwise dilute solute components is enhanced due to

their relative increase in concentration. For example, a fluid of 2 wt. % eq. NaCl containing approximately 7800 ppm Na is enriched to approximately 400,000 ppm Na in the mound with other elements being enriched to the same degree (*i.e.*, ~50 times), assuming no loss of the solutes. Both raster and point analysis were done depending on mound size (*i.e.*, point mode for <5 μm mounds) in order to ensure homogeneity and avoid the problems of fractionation related to decrepitation (Haynes *et al.* 1988; Kontak 2004).

The detection limit for the SEM-EDS method is approximately 0.15 wt. % based on analysis of standards. As the mounds analyzed in this study were generally small, it was generally unavoidable to prevent interference with the substrate (*i.e.*, quartz) due to excitation of this material by the incident beam. Thus, taking for example a case where 30 to 50% interference of the quartz substrate occurred, this would reduce the effective minimum detection limit for elements to approximately 0.3 wt. %.

The data acquired were normalized to 100% after removing the silica component (*i.e.*, SiO_2) related to interference, as per the protocol for this method (Haynes *et al*., 1988; Kontak, 2004). Due to this latter aspect, the data are treated in relative rather than absolute proportions and results are plotted in ternary diagrams (*e.g.*, Na:K:Ca). Importantly, Haynes et al. (1988) used standards in their evaluation of the method and showed that cationic ratios in prepared solutions are retained. More recently, Tweedale et al. (2015) also validated the method using prepared standard solutions. Hence, the method, although semi-quantitative, is considered to be a good proxy for relative elemental enrichment in fluid inclusions.

For this study several additional points are further noted: (1) the low-salinity of inclusions affected both the size and production of mounds as compared to that observed in many other studies where fluid inclusions have moderate- to higher salinities (*i.e.*, >10 wt. % eq.

NaCl; *e.g.*, Kontak 2004, Kontak & Kyser 2011, Pandur *et al.* 2014); (2) it was not possible to relate inclusion types directly to mounds produced due to the abundance of inclusions in the samples, but given that the aqueous-carbonic (type A) inclusions contain little aqueous component relative to the aqueous inclusions, it is likely the majority of mounds produced represent the low-salinity aqueous (type B) inclusions; and (3) mixing of fluid chemistries for different inclusions, also a potential issue with evaporate mound analysis, is difficult to evaluate (see below). We did however analyse several mounds in each area to check for homogeneity to circumvent these problems.

Laser Raman spectroscopy

Analysis of the volatile phases within aqueous-carbonic inclusions were carried out at Laurentian University using a Horiba Scientific Jobin Yvon XploRA laser Raman operated in confocal mode with a 532 nm wavelength laser and 100X magnification lens in conjunction with LabSpec Version 5.36.11 software. Instrument calibration utilized a pure silicon wafer and analyses were performed on dismounted quartz chips with inclusions at depths ranging between 3 μm and 30 μm. Instrument settings that routinely provided the best spectra follow: 11 mW laser power, slit 100, grating 1800 over the spectrometer range of 50 $cm^{-1}$to 3000 cm^{-1}, and an acquisition time of 60 s. The relative concentrations of the gasses of interest, CO_2, CH_4, N_2 and H_2S, were calculated by integrating the peak areas of the individual spectra and using the relevant gas-scattering constants (Kiefer *et al.* 2008). Molar fractions for CO_2, CH_4 and N_2 contained within the vapor phase were determined following Frezzotti *et al.* (2012), which accounts for the band area, Raman cross-section scattering constants and the instrumental efficiency. The instrumental

efficiency was assumed to be 1 for CO_2 and N_2, and 1.5 for CH_4, as reference gas standards were unavailable. The reported accuracy for this method is within 5% (Frezzotti *et al.* 2012).

LA ICP-MS analysis of fluid inclusions

Laser-ablation ICP-MS analysis on quartz-hosted fluid inclusions was done at Laurentian University using a Resonetics RESOlution M-50 laser, ablating in ultra-pure He with a spot size of 19 μm, frequency of 10 Hz and fluence ≈ 9 J/cm^2. The ablated and subsequently ionized material was analyzed using a quadrupole Ar plasma Thermo X Series II ICP-MS. When inclusions were ablated successfully, a spike in the elements *(e.g.*, K, Na, Li) above the mineral host background occurred, thus allowing the inclusion signal to be isolated from that of the host. Data was processed with Igor Pro 6.22A and the Iolite software package using the NIST 612 standard and an internal reference of Li (see below in results section) which was present in all the inclusions analysed.

The inclusions selected for analysis had their salinities predetermined prior to ablation following normal protocol for LA ICPI-MS inclusion analysis. However, the uniformly low-salinity of these inclusions (*i.e.*, < 1-3 wt. % eq. NaCl; see below) presented challenges for the quantification of solute contents as Na was not always detected upon ablation of the selected inclusions. Thus an alternative approach was used in order to assess the chemistry of ablated inclusions which used Li as a reference element since it was detected in all inclusions and host quartz, hence it was instead used as an internal standard. Thus by using its concentration in the host quartz, as calculated with the external NIST standard, Li was used as a means to establish semi-quantitatively the content of Li in the inclusions and from this the relative concentrations of other elements. Given that the Li content of the host quartz varied, a calibration curve was

established and each chip analysed. The derived elemental concentrations are therefore only considered semi-quantitative.

$\delta^{13}C$ analyses of fluid inclusion extracts

The measurement of $\delta^{13}C$ on fluid inclusion extracts from quartz separates was conducted at the Queen's Facility for Isotope Research (QFIR), Kingston, Ontario, Canada. Samples analysed were previously assessed qualitatively for the presence of CH_4 using both thermometry (*i.e.*, Tm_{CO2} measurements) and Raman spectroscopy and only samples containing little or no methane were used. Quartz separates were hand-picked to ensure no contamination with muscovite, which contains methane-rich inclusions (see below). The CO_2 was extracted from quartz samples using an EA Elemental Analyzer interfaced to a ThermoFinnigann Delta Plus XP mass spectrometer following the methods of Vennemann & O'Neil (1993) and Köhler *et al.* (2008). The isotopic values are reported using the δ notation (‰) relative to V-PDB. Replicate $\delta^{13}C$ analyses, based on long term analyses of standards, are reproducible to ± 0.2‰.

RESULTS

Fluid inclusion petrography and types

Detailed petrographic observations complemented with limited cathodoluminescence (CL) analysis of quartz failed to identify the presence of unambiguously primary inclusions that record trapping along growth zones. However, rare isolated inclusions and 3D arrays of isolated inclusions do occur which can be considered as indeterminate type (Bodnar 2003). In general,

petrographic observations indicate that quartz, spodumene and feldspar contain abundant fluid inclusions with lesser amounts in garnet, mica and cassiterite. Given the lack of unequivocal evidence for either primary and/or pseudosecondary origins, the inclusions are considered as secondary (Figs. 3, 4). Further support for a secondary origin for most inclusions includes: (1) the presence in K-feldspar of inclusions along albite exsolution lamellae and where muscovite replacement is abundant, both of which suggest inclusion entrapment during subsolidus reactions; (2) the studied cassiterite formed as part of the hydrothermal replacement of earlier pegmatite (Fig. 2g, h); and (3) quartz-hosted inclusions are located mainly along secondary healed fracture planes, but sometimes occur in rare isolated 3D arrays of indeterminate origin.

Three types of inclusions are present: (A) aqueous-carbonic, (B) aqueous, and (C) aqueous-methane-nitrogen. These inclusion types are not equally distributed in all mineral phases and, instead, specific inclusion types are observed in different minerals (see below). All inclusion types are observed throughout the pegmatite dike swarm regardless of the wall rock and sample location.

Type A inclusions are aqueous-carbonic, typically 10 to 40 μm and contain varying levels of methane and nitrogen (Figs. 3c, 4a, b, d, f), and at room temperature (20˚C) most contain three phases (L_{CO2}, V_{CO2}, L_{H2O}). The compositions of the vapor phase, as determined by laser Raman and microthermometry, are described later. These inclusions occur in quartz, spodumene, K-feldspar, albite, tourmaline and cassiterite; those hosted in quartz and spodumene have negative crystal shapes. Due to their small size, measurements on tourmaline-hosted inclusions were not possible. The spodumene-hosted inclusions, commonly elongated parallel to the c-axis, often contain highly birefringent minerals (≤50% of the inclusion) inferred to be stepdaughter phases formed by reaction between the host mineral (spodumeme) and the fluid (Anderson *et al*. 2001).

Extended tails or wisps on elongate inclusions indicate necking occurred (Fig. 4a, b). The inclusions in quartz occur as secondary trails, along subgrain boundaries and as isolated inclusions; they lack the solid phases seen where spodumene hosted. The secondary planes of type A inclusions are commonly crosscut by secondary planes of younger inclusion types.

The X_{CO2} for type A inclusions was determined using volume fraction calculations of the carbonic phase (*i.e.*, length, width, depth at Th_{CO2}) and thermometry measurements (Th_{CO2}, Th) in conjunction with the diagram of Bakker and Diamond (2000). Results range from 0.1 to 0.78 (Fig. 5) with data for K-feldspar most uniform at 0.24 and quartz having the largest range (*i.e.*, 0.1 to 0.78). For spodumene-hosted inclusions, X_{CO2} falls into two groups at 0.2 to 0.27 and 0.42 to 0.52; the reason for this is discussed below.

Type B inclusions are aqueous and have a small vapour bubble (~10-15%; Fig. 3b), commonly exhibit a negative crystal shape and are ≤30 μm. Planes of these inclusions cross cut type A inclusion trails.

Type C aqueous-methane-nitrogen inclusions have two phases (L+V) with variable amounts of vapour (90-95% for muscovite and 75-85% for garnet). The vapor phase, as deduced from laser Raman analysis reported below, includes both methane and nitrogen. These inclusions, restricted to garnet (Fig. 4e) and muscovite (Fig. 4c), occur either in isolation or as FIA along healed fracture planes. Due to the delicate nature of muscovite and the difficulty of mounting suitable material, thermometric measurements were not made.

Microthermometry

Microthermometry measurements were made on inclusions defining FIA within which inclusions had similar phase proportions and did not exhibit obvious evidence of post-entrapment modification. Results of microthermometry for aqueous-carbonic ($Tm_{CO2,}$ Th_{CO2},Tm_{clath},Th) and aqueous (Tm_{ice}, Th) inclusions are summarized in Tables 1 and 2, which include the averages of multiple measurements for individual FIA along with the ranges for each group.

Type A inclusions measured in 26 FIA hosted by quartz have$Tm_{CO2}$from -57˚to -74˚C (Fig. 6a), with the majority close to -58 ˚C, which indicates the additional presence of minor dissolved gaseous species ($CH_{4,}$ N_2). Values of Tm_{clath} all measured in the presence of H_2O, L_{CO2}, and V_{CO2}, fall between 8.4˚ to 14˚C, with the majority>11˚C, and contrast with values in a pure CO_2-H_2O system of 10˚C. Absolute salinity determination is precluded in these inclusions because increasing salinity depresses the clathrate melting point, whereas increasing CH_4 has the opposite effect. This effect is evident in type A inclusions where inclusions with higher CH_4 concentrations, as reflected by lower Tm_{CO2}, also have elevated Tm_{clath}. The Th_{CO2} ranges from -20.1˚ to 28.0˚C, but for the same FIA the range is <1˚C (Fig. 6b; Table 1). A few Tm_{ice} values were recorded at -0.1° to -0.3°C, which equates to maximum salinities of about 0.2 to 0.5 wt. % eq. NaCl. The Th values were compromised due to inclusion decrepitation, which began at 350°C in larger inclusions, but for small ones (<5 µm) Th data record the last temperature prior to decrepitation which was from >300˚ to >323˚C.

Type A inclusions in 13 FIA hosted by spodumene have a small range for Tm_{CO2} of -57.0 ˚ to -58.2˚C, which again indicates the presence of trace amounts of other gases. The ice melting temperature range from -0.6˚ to -0.1˚C, and a Tm_{clath} of 12˚C was observed in only two FIA. The $Th_{CO2,}$ to both L_{CO2} and $V_{CO2,}$ ranged from 25˚ to 28˚C (Fig. 6b, Table 1). Values of Tm_{ice} for seven FIA ranged between -0.1° to -0.8°C, which equate to maximum salinities of about 0.2 to

1.4 wt. % eq. NaCl. Total homogenization occurred to both the vapor (Th(V)) and liquid (Th(L)) phase at temperatures of 284°C and 298° to >310°C, respectively. In the latter, decrepitation was observed at >310°C.

Type A inclusions in five FIA hosted by K-feldspar have very consistent thermometric data. The Tm_{CO2} values fell between -57.6 ºC and -57.0 ºC, which again indicates the presence of a small amount of other gases, whereas Th_{CO2} occurred via Th(V) between 26º and 27ºC. The value for Tm_{clath} between FIA ranges from 7.5° to 8.2°C ± 0.5ºC and Tm_{ice} is -0.1ºC. The Tm_{ice} for three FIA were the same at -0.1°C, which equate to maximum salinities of about 0.2 wt. % eq. NaCl. Final homogenization occurred to the vapour phase from 338ºC to 389ºC, but within individual FIA the Th(V) only varied by <7ºC.

Thermometric data for type B inclusions were only obtained for quartz-hosted inclusions and results for 40 FIAs from six samples are given in Table 2. The Tm_{ice} values ranged from -0.1° to -2.5°C with 16 of the FIA having values >1.0°C. The salinities fall into two groups at <0.4 and 1.0-3.0 wt. % NaCl eq. and in all but two of the FIA the variation of salinity is ±0.2°C or 0.5 wt. % eq. NaCl. The low-salinity of these inclusions precluded observing first melting or eutectic temperatures and better characterization of their solute chemistry (e.g., Ca, Fe). All type B inclusions exhibited homogenization to the L phase (Th(L)) with average values ranging from 167° to 312°C, but in a single FIA the variation was less than a few degrees (Table 2).

As noted above, type C inclusions are unique to garnet and mica and thermometric data was not collected on these inclusions due to fracturing and decrepitating during heating.

Evaporate mound analysis

Results for about 160 evaporate mound analyses for eight quartz chips are summarized in Table A1 and a series of diagrams in Figures 8 and 9. The data indicate the presence of three distinct fluids in terms of major cations (Fig. 8): (1) Na(-K-Ca), (2) K-Na and (3) Ca-Na-K with type 1 Na-rich the most dominant fluid. A few mounds are enriched in Fe (Fig. 8c).

The mounds deviate from ideal salt (NaCl) stoichiometry (Fig. 9) with those depleted in Cl showing enrichment in both S (Fig. 8b, 9b) and F (Fig. 8d). Furthermore, those with S enrichment have Na:Cl ratios ranging from 3:1 to 8:1 (Fig. 9a) and show marked enrichment in S when mound compositions deviate from stoichiometric NaCl (Fig. 9b). The latter is accompanied by elevated values of other elements, including Co, Ti, P, Fe, Zn, Cu, As, Mg and Mn (Fig. 10a ,b), all of which, except for F and P, are uncommon in the bulk analysis of LPNG pegmatites (Barnes 2010; Barnes *et al*. 2012). The concentrations of these elements are highly variable and not detected in all mounds. The average values (± 1σ), based on their presence in 122 analysed mounds are (in wt.% values normalized to 100 wt. %): Co = 11% (n=1),Ti = 2 ± 2 % (n=4), P = 9 ± 7 % (n=5), Fe = 9 ±10 % (n=18), Zn = 8 ± 9% (n=4), Cu = 4% (n=1), F = 14 ± 13% (n=20), As = 34% (n=1), Mg = 13 ± 5% (n=11) and Mn = 42% (n=1). The presence of these elements correlates negatively with S and occurs in the mounds with increased levels of K and Ca.

Laser Raman spectroscopy

The results of laser Raman analysis for types A and C inclusions are presented in CO_2-N_2-CH_4 ternary plots (Fig. 11a, b) with representative spectra shown in Appendices A4, 5. These show there is a dependence of gas chemistry on both the mineral host and sample. Quartz-hosted aqueous-carbonic inclusions show the large variation in chemistry with up to four gaseous

species (CO_2, CH_4, N_2, H_2S) present, but H_2S is rarely detected and only in trace amounts. The compositions for the measured FIA range from nearly pure CO_2 to mixtures of up to 50% for both CO_2-CH_4, and CO_2-N_2. Spodumene-hosted fluid inclusions contain almost pure CO_2, whereas garnet- and muscovite-hosted inclusions are dominated by CH_4, with up to 30% N_2.

When the data are examined by sample (Fig. 11b), the presence of both compositionally uniform and different fluids occurring in the same sample is apparent. In this plot the data points represent the average gas composition for an FIA, which varies little and highlights, therefore, that some variation in CH_4 and N_2 can occur in the same sample.

Finally, as noted previously, both the garnet and muscovite analyzed for their gaseous composition are inferred to represent late-stage metasomatic phase. As noted, these phases are dominated by CH_4-N_2 without detectable CO_2.

Carbon isotopes of inclusion extracts

The $\delta^{13}C$ values for fluid inclusion extracts from 7 quartz samples from across the pegmatite field and having type A inclusions with little CH_4, as determined from microthermometry and laser Raman analysis, are provided in Table 3. The data range from -9.7 to -24.7‰, but 6 of the 7 samples returned a narrower spread of -17.9 to -24.7‰. A single sample (LNPG-08-11), which was done in duplicate to assess reproducibility, returned values of -18.2 and -24.7‰, hence, some inter-sample heterogeneity is possible, as this is well outside the range of analytical error (± 0.2‰).

LA-ICP-MS analysis of quartz-hosted fluid inclusions

The quantification of the major and trace element chemistry of the fluid inclusions using LA ICP-MS was limited due to the low-salinity of the inclusions. Consequently, of the 77 ablation analyses preformed, only 39 were useful (Table 4) and all of these were for type A aqueous-carbonic inclusions as the type B inclusions did not yield detectable signals. The latter issue is attributed to a combination of both the lower salinity of the inclusions and their generally smaller size.

In addition to Na and Li which were present in most of the inclusions, other common elements detected were Al, K, Li, Na, B and Cs; in addition, the rare metals (Ta, Nb) were also detected. The results did, however, vary among the inclusions, both in terms of absolute concentration and elemental ratios. The highest values (in ppm) obtained for the petrogenetically relevant elements indicate an upper limit to the fluid inclusion solute concentrations: Na = 3100, K = 2400, Li = 670, B = 400, Sn 38, Cs = 39, Be =18, Ta = 2, Nb = 2, and W = 2. Where detected, Li, Na, and Cs all correlate positively with each other (Fig. 12a, b). Most of the results containing Li and Na also corresponded with Al anomalies, but there was no strong correlation with Al. Other trace elements detected (maximum concentrations in ppm) include Fe = 150, Mn = 30, Zn = 10 and As = 20.

DISCUSSION

The fluid inclusion microthermometry, chemistry and isotopic data is constrained by several assumptions which allow groups of inclusions to be related to each other and characterized as fluid events across the entire system: (1) the data represent FIA; (2) fluid inclusions within an FIA represent trapping of a single homogeneous fluid having similar PTX, except where

immiscible behaviour is concerned; and (3) post-entrapment modification of the fluid inclusions has not compromised the data, since care was taken to avoid using such inclusions for thermometry and PT estimations. Taking these assumptions into account, the implications of this fluid inclusion study are discussed below.

Implications of the timing of fluid inclusion entrapment

Petrographic study and the absence of CL zoning of quartz do not provide unequivocal evidence for entrapment of FIA along primary growth zones in any studied material. Instead inclusions occur along healed fracture planes with only rare cases of isolated groups of inclusions. In addition, trails of pseudosecondary fluid inclusions are also lacking. These observations relegates the studied inclusions to a secondary origin. It is noted, however, that rare examples of isolated type A inclusions (<10 μm) in quartz occur which may indicate local volatile saturation, perhaps reflecting a boundary layer liquid as suggested by others (*e.g.*, Sirbescu *et al*. 2008). Such inclusions would therefore be of primary origin.

The above observations do not preclude the infiltration of a magmatic-derived fluid(s), but it would have been generated elsewhere in the evolving pegmatite system and trapped in previously crystallized crystals as secondary inclusions. We note therefore that inclusions present in metasomatically modified K-feldspar, based on both textural and compositional (*i.e.*, Or_{100}) criteria, are late-stage with respect to the original growth of the host. This late entrapment of fluids is also consistent with the absence of early hydrous phases in the pegmatite, such as muscovite in the wall zone. The absence of primary pocket zones at LNPG also indicates that most of the pegmatite crystallized during fluid undersaturated conditions. The above evidence

suggests therefore that fluid involvement occurred late, likely toward the later stages of pegmatite crystallization or in some cases post crystallization.

The above findings are consistent with the studies of other pegmatites which reveal that few fluid inclusions can be related to an early magmatic stages (Cook 1979; London 1985a; Roedder 1984; Thomas & Spooner 1988; Thomas *et al.* 1988; 1992; Williams & Taylor 1996; Smerekanicz & Dudás 1999; Kontak *et al*. 2002). Furthermore, in other settings reports of primary, magmatic-stage fluid inclusions (*e.g.*, London 1986a) are rare and their classification might be questioned in the context of more recent criteria which are used for discriminating inclusion types. More common are reports of rare-element alteration halos around pegmatite fields and fluid infiltration into the country rocks, sometimes related to late-stage metasomatism (*e.g*., Shearer *et al.* 1984; Morgan & London 1987; Thomas & Spooner 1988; 1992; London 1990; Linnen & William-Jones 1994; Fuertes-Fuente *et al*. 1997). We also note that the large reported variance of fluid compositions in different pegmatite localities is significant in regards to the timing of fluid entrapment. Inclusions interpreted as cognate to pegmatites are reported to have salinities that vary from near 0 wt. % NaCl, as for example in this study and also see London *et al.* (2012), to hyper-saline brines with 39 wt. % eq. NaCl (*e.g*., Alfonso & Melgarejo 2008). Alternatively, the majority of fluids observed in pegmatites may be derived from wall rock reservoirs, some of which have been implicated in the replacement of K-feldspar by albite (Nijland & Touret 2001).

The apparent absence of primary fluid inclusions in samples of this study raises the potential of deformation of the host and related sub-grain development erasing such a record, as suggested by others (e.g. Johnson & Hollister 1995). However, samples used in this study did not exhibit any evidence suggestive of substantial strain, so overprinting effects cannot explain the

absence of primary inclusions. Another explanation for the absence of such inclusions in this and other studies is that the water solubility of these melts can increase significantly as they become more peralkaline (i.e., Na-enriched) through crystallization (Mustart 1972; Holtz *et al*. 1992; London 2008) or immiscibility processes (Thomas *et al*. 2012), both of which are discussed below. Thus, as volatile saturation was approached in the evolving pegmatite melt, the increase of its solubility by the melt offset fluid saturation.

Nature and origin of the different fluid types

The secondary classification of the fluid inclusions implies they post-date pegmatite crystallization and were trapped during the subsolidus stage, which has implications for fluid source(s), timing of fluid infiltration, and variable composition of the fluids. These various issues are addressed below.

Type A and B inclusions are commonly noted in LCT-type pegmatites (e.g., London 1985b, 1986a; Fuertes-Fuente *et al*. 1995, 2000; Nabelek & Ternes 1997; Beurlen *et al*. 2001; Anderson *et al.* 2001; Sirbescu & Nabelek 2003), whereas type C inclusions are rarely observed. The three inclusion types are paragenetically distinct and not related by immiscibility or fluid mixing, as supporting petrographic criteria are lacking (e.g., Diamond 1990, 2001).

Type A aqueous-carbonic inclusions have CO_2 clathrate melting temperatures (8.4^o to 14^{o}C) and Tm_{ice} values that indicate low salinities (*i.e*., near meteoric water), whereas the Tm_{CO2} values indicate the variable presence of other dissolved gases (N_2, CH_4). Inclusions with Th_{CO2} values <0^{o}C likely contain appreciable levels of CH_4, as indicated by depression of the Tm_{CO2} values down to -74^{o}C. The inclusions hosted by spodumene contrast with those in quartz in that

they lack CH_4 and N_2 and represent a more pure aqueous-carbonic end member fluid in the system. Thus, type A inclusions cover a large range in CO_2:CH_4:N_2, X_{CO2}, and also density based on their Th_{CO2}. The first of these is discussed below, with the other two aspects addressed in the subsequent section.

The highly variable CH_4:N_2 ratios of the carbonic phase (Fig. 11) suggest that fluid:rock interaction may have influenced the fluid chemistry in the absence of an internal buffer in the pegmatite. Whereas the production of CH_4 is possible due to fluid:rock interaction and reduction of a CO_2-rich fluid, generation of N_2 requires a source of nitrogen. Nitrogen is both a common component in carbonic fluids and an important constituent of sedimentary rocks where it is thought to originate from breakdown of NH^+_4 bearing feldspars and mica (e.g., Van den Kerkhof & Thiéry 2001). Pure N_2 inclusions and N_2 as a component of carbonic and aqueous-carbonic fluid inclusions have been noted in a range of studies, including mantle-derived high-temperature ultramafic xenoliths (e.g., Anderson & Newmann 2001; Anderson *et al.* 1995) to low temperature (*i.e.*, 250°C) barite veins associated with intense bleaching of wall-rock siltstones (Kontak *et al*. 2006). However, rarely has N_2 been recognized as a component of fluids in rare-element pegmatites, but this may also reflect the variable use of Raman spectroscopy applied to these systems. A possible source for N_2 at LNPG is the immediate wall rocks, which include locally graphitic and sulphidic mudstones. Other studies have also documented a dependence of the N_2 content of fluid inclusions on the immediate wall rock (Bottrell *et al*. 1988; Kontak *et al.* 2006). In pegmatite settings, Linnen & Williams-Jones (1994) identified N_2 in rare-metal pegmatites cutting psammitic metasedimentary country rocks and Alfonso & Melgarejo (2008) report up to 15 mol% N_2 in carbonic inclusions hosted in RM pegmatites cutting metapelites with minor limestone and felsic volcanic rocks. Thus, the coincidence of N_2 within

fluid inclusions and proximity to an available sedimentary reservoir favours such a source for the N_2 within the inclusions at LNPG.

Fluid inclusion extracts from quartz yielded $\delta^{13}C$ values from –9.7 to -24.7‰ which indicate a biogenic source for some of the carbon in type A inclusions, which is tentatively suggested to involve the subgreenschist facies metapelitic and calcareous wallrocks in the area. Reduced carbon in the form of graphite is observed marginal to some pegmatites at LNPG and could potentially be a source for the reduced volatiles. Other potential sources to be considered are calcareous wall rocks via decarbonisation reactions, decomposition of organic matter, or redox reactions involving graphite (Van den Kerkhof & Thiéry 2001). It is unlikely that Fischer-Tropsch hydrocarbon synthesis occurred (e.g., Salvi and Williams-Jones 1997) as only minor amounts of H_2 are present according to Raman results, and hydrocarbon species larger than CH_4 were not detected. Given that the redox state of the infiltrating fluid will be buffered by wall rocks, binary compositions of both oxidizing (CO_2-N_2) and reducing (CO_2-CH_4) mixtures are expected (Van den Kerkhof & Thiéry 2001), both of which are observed in type A inclusions hosted in quartz and consistent with the host rocks. The reduced component is also reflected by the rare presence of type C inclusions, which are methane dominant. Hydrocarbon volatile contamination of pegmatite-hosted fluid inclusions has been described elsewhere, most notably at the Tanco pegmatite where Thomas & Spooner (1992) suggested assimilation of the graphitic wall rocks, or fluid interaction with the wall rocks, may be the source. These authors also noted that if contamination occurred, the hydrocarbons did not re-equilibrate at the expected temperature of pegmatite crystallization.

Further support for wall rock interaction of the fluid is found in the decrepitate mound data. Enrichment of some mounds in sulphur and both chalcophile- and transition elements (Fig. 10) is consistent with interaction of the pegmatite-hosted fluids with the shale component of the host rocks (*e.g.*, Gromet *et al*. 1984). Enrichment of the mounds in Ca, an element typically depleted in pegmatites, also indicates exchange of the fluids with the wall rocks. Similar evidence for either exchange of pegmatite-hosted fluids with wall rocks or ingress of external fluids has been encountered in a variety of other pegmatite settings (e.g., Kontak 2006; Salvi & Williams-Jones 1997& 1990; Martin & De Vito 2013).

Type B inclusions have a very narrow range of salinity (0 to 2.0 wt. % eq. NaCl) with only one FIA of 4.5 wt. % eq. NaCl. The origin of such fluids may include: (1) mixing of two end member fluids of different salinities; (2) a single fluid evolving with the addition of fluid:rock interaction; or (3) evolution of a single magmatic fluid. In the first case, the relatively saline fluid component may represent the remnant of a more saline fluid which mixed with a low-salinity fluid, possibly meteoric water. Alternatively, the range in salinity of the aqueous inclusions may be due to an increase in salinity via fluid:rock interaction, but this would have been very restricted. The third model, based on models presented in Cline & Bodnar (1991), involves a low-salinity fluid (<2 wt. % eq. NaCl) fluid being generated at low pressure (0.5 to 1 kbar) due to melt fractionation. In this model, fluids become less saline due to the partitioning of Cl into the melt, the lower solubility of H_2O in melts at low pressures, and mass balance between the fluids and melt during second boiling. Application of this model to LNPG would imply that the fluids may represent the end product of crystallization of the melt rather than mixing with another fluid. Relevant to these models are the following: (1) presence of F in the decrepitate mounds (Fig. 8a) and detection of B in the fluids via LA ICP-MS analysis (Table 4), both of

which are common magmatic source fluids (Partey *et al*. 2009); and (2) stable isotopic data for LNPG (O, D; Burns *et al.* 2013) which indicate the late-stage evolution of the LNPG pegmatites occurred in the presence of an ^{18}O-depleted fluid of likely meteoric origin. Thus, the data suggest at least two sources for the aqueous fluid, one magmatic and the other meteoric. It is also noted that decrepitate mound analysis, in particular the antithetic relationship between Cl and S (Fig. 9b), suggest that type B fluids record some interaction with the wall rocks. The timing of the fluid inclusion entrapment also suggests that fluid saturation occurred either very late after most of the pegmatite had crystallized. Finally, the presence of a surficial-derived fluid is important as it suggests a high-level setting which is a structurally favourable environment for emplacement of the pegmatite dikes.

Variation of X_{CO2} and fluid density in type A inclusions

Variation in both the density of CO_2 and X_{CO2} are common in type A inclusions, both of which are relevant to the source(s) of CO_2 and conditions during fluid trapping. It is first noted that variability in X_{CO2} and proportions of phases (i.e., H_2O versus CO_2) between FIA cannot be explained by fluid unmixing, as the expected inclusion pairs are not present *(e.g.*, Diamond 1990). For example, only a weak positive correlation exists between X_{CO2} and Tm_{CO2}, whereas a much stronger correlation is expected if immiscibility had occurred as the vapour phase should be enriched in CH_4 relative to the liquid phase, which would be seen by depressed Tm_{CO2} values.

The first case considered is post-entrapment modification, as suggested by decrepitate-textured inclusions in quartz and alignment of vapour-rich (CO_2) inclusions along sub-grain boundaries. Such CO_2-rich inclusions may represent residues trapped along grain-boundaries

formed via loss of the aqueous component and subsequent migration of the CO_2-rich fluid during deformation-induced strain (*e.g.*, Johnson & Hollister 1995). Although the density and X_{CO2} of these modified inclusions may vary in some FIA, their salinities and CO_2 purity (Tm_{CO2}) are similar. Although this explanation may account for some variation in $X_{CO2,}$ in general the pegmatites lack textural evidence for extensive in samples studied. Furthermore, the effects of grain boundary fluid migration only seem to affect inclusions at the intersections between grain boundaries and secondary fluid inclusion planes, leaving inclusions elsewhere unaffected. Thus, a more viable explanation for variable X_{CO2} may instead be interaction of fluids with the carbonaceous wall rock, for which supporting evidence has been noted both in the $\delta^{13}C$ data and evaporate mound chemistry. An important aspect of this conclusion is that it is difficult, therefore, to assess the primary signature of the type A inclusions, perhaps the most common fluid type reported in LCT-type pegmatites, versus what may have resulted from fluid:wall rock interaction. The results of LA ICP-MS analysis indicates that type A inclusions are enriched to some extent in Na, Li, B, Be, Cs and rare metals, thus this fluid clearly has the fingerprint of the LCT suite.

The large range in density for type A inclusions can be accounted for instead by transient fluctuations in pressure at constant X_{CO2}. This density variation, reflected inTh_{CO2} values from -20.9^o to 28.5^{o}C, is also seen as variable proportions of phases in inclusions at room temperature (*e.g.*, see Figs. 8, 9 of Sterner & Bodnar (1989)). Thus, such density variation for the carbonic phase of these inclusions can be related to changing pressures, rather than separate fluid events or fluid unmixing.

P-T conditions of entrapment

The P-T conditions inferred for crystallization of LCT-type pegmatites are in part based on interpreting observed mineral assemblages (i.e., spodumene-quartz-petalite) and textures (e.g., skeletal, graphic) in the context of experimental work on the relevant systems (*e.g.*, London 1984a, 2000; Maneta and Baker 2014; Sirbescu et al. 2017). In addition, fluid and melt inclusions are also used to constrain the evolution of such pegmatite systems (e.g., Sirbescu et al. 2008). Although the fluid inclusions examined herein are noted to most likely post-date the growth of the hosts, at least the aqueous-carbonic inclusions are considered to represent entrapment during the subsolidus stage of the system during its cooling and metasomatism.

Fundamental to the above is the presence of fluid inclusions in secondary (i.e., metasomatic) K-feldspar and albite. As noted already, the coarse K-feldspar records albitization due to coupled dissolution precipitation processes (e.g., Plumper & Putnis 2009). As such, fluid inclusions trapped in this neomorphic feldspar can be used to constrain the P-T conditions during this metasomatic event. Unfortunately, inclusions hosted by albite were not suitable for thermometric study due to the cloudiness of the host. As noted, however, inclusions observed in K-feldspar along the albitization reaction fronts, hence paragenetically related to this process, were studied (see above). In this context, the inclusions hosted in this secondary feldspar, both surrounding and within zones of albitization, may be considered primary in relation to the time of albitization. These fluids are dominantly aqueous-carbonic and similar to the type A inclusions in quartz and spodumene.

The thermometric data were used to construct isochores for the two dominant fluid inclusion types (A, B) and integrated with the stability fields for the relevant mineral

assemblages in the pegmatites to constrain its evolutionary path in P-T space (Fig. 13). In this context the following aspect are used to constrain the initial conditions of pegmatite evolution in P-T space: 1) the intergrowth of petalite, SQUI and spodumene, as discussed previously and noted by others (Barnes 2010; Pfister et al. 2018, 2919); 2) lack of eucryptite; and 3) the maximum undercooling condition of ca. 450°C (see above).Thus, the aforementioned is use to constrain initial conditons of pegmatite formation to $P \geq 2.5$ kbars and $T \geq 450$°C. Furthermore, that Pfister et al. (2019) noted rare petalite rimming SQUI suggests that pressure must have fluctuated during pegmatite evolution. The presence of type A and B inclusions are used below to further constrain the conditions of crystallization and metasomatism (*i.e.*, alteration).

Given these constraints and suggestion that variable densities of type A inclusions reflect pressure cycling, then the different isochoric trajectories for the fluid inclusions can be interpreted in the context of fluctuating P as T decreased from a maximum of 500ºC. Furthermore, the trajectory for the low-density, low X_{CO2} (0.2) fluid in quartz and K-feldspar is consistent with this fluid being secondary and trapped during subsolidus cooling rather than primary and requiring these phases to coexist with primary petaltite. Furthermore, the lack of evidence for fluid immiscibility constrains P to $\geq$ 0.9 kbars (i.e., intersection of $X_{CO2} = 0.2$ with H_2O-CO_2 solvus). Thus, using type A inclusions it is suggested that P changed during fluid entrapment. If the aqueous inclusions (type B) are considered, then P may have at times been lower, but only if they were trapped at the same time and not sometime later .

The interpretation that the range of densities for type A inclusions is due to fluctuations in P is not unusual for either magmatic-hydrothermal or metamorphic fluids. A possible analogy is found in porphyry settings where changes from lithostatic to hydrostatic conditions are

recorded by FIA, some of which reflect fluid unmixing (e.g., Redmond *et al*. 1986; Rusk *et al*. 2008). A second more relevant analogue is represented in the work of Linnen & Williams-Jones (1995) who documented pressure fluctuations from 0.5 to 2.5 kbars for aqueous-carbonic inclusions in a pegmatite setting. The low salinities documented here for both type A and B fluids (i.e., to near 0 wt. % eq. NaCl), which are generally uncommon for pegmatitic systems, provide compelling evidence that the dike swarm may have penetrated to shallower depths. In this model, the setting for the LNPG dikes is considered to have permitted ingress of meteoric fluids when the system reverted to hydrostatic rather than lithostatic conditions.

In summary, the properties of type A fluid inclusions suggest transient pressure fluctuations (i.e., lithostatic to hydrostatic) occurred during the late-stage evolution of the pegmatites , the former of which had a maximum near 3 kbars and thus providing the best estimate for depth of pegmatite emplacement and subsequent metasomatism at ≤8 km to 10 km. A temperature of 400° to 450°C is proposed for the metasomatic stage of the pegmatite based on the spodumene stability field and intersecting quartz-hosted type A isochores.

Relationship between fluids and Sn-Ta-Nb oxide mineralization

Field observations and supporting petrographic study, albeit of a limited number of samples in this study, do provide convincing evidence for a relationship between alteration and rare-metal (Sn-W-Ta-Nb) mineralization at LNPG. This association is exemplified by the spatial association between the oxides and fluid-mediated albitization, both cleavelanditic and saccharoidal varieties, and quartz-muscovite assemblages (Fig. 2; also see Groat *et al*. 2003). Importantly, others have noted similar associations of rare-metal oxide mineralization and albitization hosted

by LCT pegmatites (e.g., Černý 1982; Černý & Ercit 1989; Chakoumakos & Lumpkin 1990; Partington *et al.* 1995; Suwimonprecha *et al.* 1995; Ahmad 1995; Linnen 1998; Fuertes-Fuente & Martin-Izard 1998; Tindle *et al.*1998; Sweetapple & Collins 2002; Alfonso *et al.* 2003; Kontak 2006; Stilling *et al.* 2006). In rare cases hypersaline fluids are sometimes implicated in this process (Alfonso & Melgarejo 2008), although this is not always the case (London 1986a; Kontak *et al*. 2011). Although this study did not focus specifically on the mineralization, the limited data collected do provide the basis for some interpretation about the relationship of the fluid chemistry noted and origin of the oxide mineralization, The following discussion focuses therefore on the nature of the fluids associated with the rare-metal mineralization at LNPG.

Both albite and micaceous alteration types at LNPG are spatially and temporally related to oxide mineralization, but there is a distinct difference in the volatile chemistry of these fluids in the cassiterite zones hosted in muscovite-quartz versus the Ta-Nb oxides hosted by quartz-albite. This association of oxide mineralization with specific alteration types has been noted in other rare-element pegmatites (e.g., Linnen & Williams-Jones 1994). In terms of volatile chemistry, the coarse euhedral muscovite (1-3 cm) in contact with cassiterite (1-2 cm) contains abundant type C inclusions (Fig. 4c). As noted before, we are unaware of comparable inclusions in mica from other rare-element pegmatites. In contrast, quartz from both the muscovite- and albite-alteration zones contains type A inclusions with CH_4 concentrations of up to 25% of the vapour phase (i.e., CO_2).Whereas the type C CH_4-rich inclusions are restricted to the cassiterite mineralized zones, $CO_2 \pm CH_4$-N_2inclusions are pervasive throughout the dike swarm and have been reported, albeit rarely, in other LCT-type systems (Ahmad 1995). The difference in volatile chemistry for contrasting alteration zones associated with variable rare-metal mineralization indicates that varying oxidation conditions may have prevailed, correlating with the type of oxide

mineralization. Since there is evidence that these fluids likely obtained their relative redox states from interaction with the wall rocks, it follows that this exchange may, therefore, have influenced what oxide type precipitated.

The nature of the oxide mineralization at LNPG is also at odds with the constitutional zone refining model of London (2008). According to London, such mineralization forms through saturation of a flux-rich boundary layer in undercooled melts but, as already noted, the nature of the oxide mineralization at LNPG is paragenetically late, thus post-dating pegmatite crystallization at the current level of exposure, but not necessarily at depth. In contrast, Thomas & Davidson (2012) suggest that rare metals are enriched in a fluid-rich melt produced during melt-melt-fluid immiscibility; the combined bulk H_2O composition for such a melt estimated at 20 wt. %. The peralkaline nature of the water-rich immiscible melt fraction in the latter study, equivalent to the B-type inclusions of Thomas *et al.* (2000), has high rare-element concentrations and offers an alternative explanation to the formation of hydrous, alkali-rich assemblages associated with HFSE oxide mineralization. This latter model is more consistent with observations at LNPG, but does preclude more than one model being possible.

The above conclusions raise the issue of the origin of the fluid phase present in the pegmatites at LNPG if such a free fluid phase is absent during the onset of crystallization, and what is the genetic link between the fluids, pervasive sodic-metasomatism, and rare-element oxide mineralization? These questions are compounded by the suggestion from current models that fluid saturation of a melt is not a necessary feature of pegmatite formation. Further work on this important question is required.

Implication of fluid chemistry for the origin of pervasive albite metasomatism

Albite in LCT-type pegmatites is near end member $NaAlSi_3O_8$ and occurs either as a minor part of the primary assemblage or locally as more abundant saccharoidal and cleavelandite types which replace earlier magmatic, blocky K-feldspar of Or_{60-80} composition (Groat *et al.* 1994; 2003; Nijland & Touret 1999; Kontak 2006; Alfonso & Melgarejo 2008). It has been argued by Kontak (2006) that late-stage albite replacement of K-feldspar was facilitated via coupled dissolution precipitation due to the ingress of a late-stage Na-rich melt. The latter replaced the already crystallized K-feldspar, part of the earlier K-feldspar, spodumene and quartz (± muscovite) assemblage. In this latter model, a low-density and mobile, hydrous sodic-rich melt is generated in a contiguous part of the magmatic system through fractionation (London 2008). The latter is thus exotic to the site where albitization occurs, but is petrogenetically related to it. Whereas others have suggested, based on fluid inclusion studies, that albite metasomatism occurs in the presence of saline brines (25-35 wt. % eq. NaCl) at 350^o to 450^{o}C and 2 kbar (Nijland & Touret 1999; Alfonso & Melgarejo 2008), this study finds otherwise. Our results for fluid inclusions hosted in the re-equilibrated K-feldspar (Or_{100} composition) and albite at LNPG have a uniform of low-salinity (<0.2 wt. % eq. NaCl) chemistry. These low-salinity fluids in K-feldspar, in addition to similar data for quartz-hosted inclusions, occur throughout LNPG and are unlikely to have been capable, thus not responsible, for the development of the observed pervasive sodic metasomatism. Thus, we also favour a model whereby this alteration is instead related to infiltration of a low-density, sodic-rich melt which facilitated dissolution of K-feldspar and precipitation of secondary albite. As discussed by Kontak (2006), the source of this melt in LCT pegmatite systems is inferred to originate from the deeper, unexposed parts of the pegmatite

swarm. This model is wholly consistent with the 3D, continuous connectivity model of pegmatite melts and bodies which has been discussed in detail by London (2008, 2014)

SUMMARY AND CONCLUSIONS

A detailed fluid inclusion study incorporating a wide variety of analytical methods (detailed petrography and quartz CL, SEM-EDS evaporate mound analysis, laser Raman spectroscopy, LA ICP-MS, $\delta^{13}C$ of inclusion extracts) addressed the nature and origin of fluids present during the late-stage evolution of a rare-metal mineralized LCT pegmatite. The results suggest that the evolution the rare-metal mineralized LNPG suite is more complex than for pegmatites in general and most importantly, involved chemical exchange with their host rocks. This latter aspect is not generally integrated into current models for pegmatite evolution. The main conclusions of this study are:

1) No unambiguous evidence for entrapment of primary fluid inclusions was found. Thus, the dominant fluid present, an aqueous-carbonic type, was likely introduced and trapped during post-crystallization, late-stage metasomatism of the pegmatite.

2) The two main fluid types present, an earlier aqueous-carbonic (type A) and later aqueous (type B), have very low-salinities (i.e., $\leq$2 wt. % eq. NaCl), which is interpreted to reflect mixing of a magmatic-derived fluid with an externally derived fluid of probable meteoric origin. Type C inclusions, also of secondary origin, are late-stage and occur in hydrothermal garnet and muscovite near wall-rock contacts, and are considered to be in large part wall-rock derived fluids.

3) The presence of type A and B inclusions in secondary feldspar phases and the rare-metal (Sn-W-Ta-Nb) oxide mineralization stage indicates these fluids were part of the extended, sub-solidus evolution of the pegmatite.

4) The nature and origin of the carbonic component of the fluids, which is common in LCT pegmatites, may likely reflects interaction of the pegmatite-derived fluids with the wall rocks, as inferred from the low $\delta^{13}C$ values of fluid inclusion extracts (to -24.7‰) and the presence of S and transition and chalcophile elements in the fluids (i.e., decrepitate mound analyses). Further similar work on other suites is needed to address the global relevance of this suggestion.

5) The association of rare-metal oxide mineralization with zones of albitization and more rarely phyllic alteration, both fluid mediated, indicates such mineralization is related to hydrothermal processes rather than the crystallization of the host pegmatitic melt, hence not a product of constitutional zone refinement (cf., London 2008).

6) The nature of the dominant fluid type (i.e., aqueous-carbonic) is similar to fluids observed in many other LCT-type pegmatites. Results of this study suggest that some of this carbonic component relates to fluid:rock interaction. If this study can be extrapolated to other pegmatite settings where similar fluids are present, then a reassessment of the nature and origin of such fluids in rare-metal pegmatites is warranted.

7) The large range of Th_{CO2} for the aqueous-carbonic-rich inclusions indicates transient pressure variation accompanied pegmatite metasomatism, a process not generally considered as part of the overall model for pegmatite emplacement and subsequent evolution, and which may relate to the structural setting of these systems.

ACKNOWLEDGEMENTS

The analytical data presented in this paper was supported by NSERC research and equipment grants to D.J. Kontak, whereas field logistics and sample collection were supported in part by Eagle Hill Exploration Corporation. We thank Drs. Dan Marshall, Simon Fraser, and Andrew McDonald, Laurentian University, for assistance with Raman spectroscopy analysis and methods, Joe Petrus, Laurentian University, for assistance with the LA ICP-MS analysis and data reduction, and Queens' University Isotope Facility for the isotopic data. We particularly acknowledge numerous discussions over the years with Bob Bodnar, Alan Anderson, Rob Linnen, Jim Reynolds, Robert F. Martin and David London about aspects of both fluid inclusions and pegmatites, but any errors of fact or omissions are the responsibility of the authors.

REFERENCES

Ahmad M (1995) Genesis of tin and tantalum mineralization in pegmatites from the Bynoe area, Pine Creek Geosyncline, Northern Territory. *Australian Journal of Earth Sciences*, **42**, 519-534.

Alfonso P, Melgarejo JC, Yusta I, Velasco F (2003) Geochemistry of feldspar and muscovite in granitic pegmatite from the Cap de Creus field, Catalonia, Spain. *Canadian Mineralogist*, **41**, 103-116.

Alfonso P, Melgarejo JC (2008) Fluid evolution in the zoned rare-element pegmatite field at Cap de Creus, Catalonia, Spain. *Canadian Mineralogist*, **46**, 597-617.

Andersen T, Burke EAJ, Neumann E (1995) Nitrogen-rich fluid in the upper mantle: fluid inclusions in spinel dunite from Lanzarote, Canary Islands. *Contributions to Mineralogy and Petrology*, **120**, 20-28.

Andersen T, Neumann E (2001) Fluid inclusions in mantle xenoliths. *Lithos*, **55**, 301-320.

Anderson AJ (2013) Are silicate-rich inclusions in spodumene crystallized aliquots of boundary layer melt? *Geofluids*, **13**, 460-466.

Anderson AJ, Clark AH, Gray S (2001) The occurrence and origin of zabuyelite (Li_2CO_3) in spodumene-hosted fluid inclusions: implications for the internal evolution of rare-element granitic pegmatites. *Canadian Mineralogist*, **39**, 1513-1527.

Bakker RJ, Diamond LW (2000) Determination of the composition and molar volume of H_2O-CO_2 fluid inclusions by microthermometry. *Geochimica et Cosmochimica Acta*,**64**, 1753-1764.

Barnes EM (2010) *Emplacement and Geological Setting of the Little Nahanni Pegmatite Group,Northwest Territories and its Geochemical and Lithium Isotopic Evolution*. Unpubl. Ph.D thesis, University of British Columbia, Vancouver, British Columbia, 236 p.

Barnes EM, Weis D, Groat LA (2012) Significant Li isotope fractionation in geochemically evolved rare element-bearing pegmatites from the Little Nahanni Pegmatite Group, NWT, Canada. *Lithos*, **132-133**, 21-36.

Beurlen H, da Silva MRR, de Castro C (2001) Fluid inclusion microthermometry in Be-Ta-(Li-Sn)-bearing pegmatites from the Borborema Province,Northeast Brazil. *Chemical Geology*, **173**, 107-123.

Bodnar RJ (1993) Revised equation and table for determining the freezing point depression of H_2O–NaCl solutions. *Geochimica et Cosmochimica Acta*, **57**, 683–684.

Bodnar RJ (2003a) Introduction to fluid inclusions. In: *Fluid Inclusions*: *Analysis and Interpretation*, (eds Samson I, Anderson AF, Marshall D), Mineralogical Association of Canada, Short Course Series **32**, pp. 1-8.

Bodnar RJ (2003b) Interpretation of data from aqueous-electrolyte fluid inclusions. In: *Fluid Inclusions*: *Analysis and Interpretation*, (eds Samson I, Anderson AJ, Marshall D), Mineralogical Association of Canada, Short Course Series **32**, pp. 81-100.

Bottrell SH, Carr LP, Dubessy J (1988) A nitrogen-rich metamorphic fluid and coexisting minerals in slates from North Wales. *Mineralogical Magazine*, **52**, 451-457.

Brown, PE (1989) FLINCOR: A microcomputer program for the reduction of and investigation of fluid inclusion data. *American Mineralogist*, **74** 1390-1393.

Brown, PE, Lamb WM (1986) Mixing of H2O-CO2 in fluid inclusions: Geobarometry and Archean gold deposit. *Geochimica et Cosmochimica Acta***, 50**, 847-852.

Burnham CW (1979) Magmas and hydrothermal fluids. In: *Geochemistry of Hydrothermal Ore Deposits*, 2nd edn (ed Barnes HL), pp.71-136. John Wiley & Sons, New York.

Burnham CW, Nekvasil H (1986) Equilibrium properties of granite pegmatite magmas. *American Mineralogist*, **71**, 239-263.

Burns M, Kontak D, Barrett TJ (2012) Fluids in the Montclerg Archean mesothermal gold system: an SEM-EDS evaporate mound approach to unravelling the chemistry and origin of different fluids. *Pan-American Current Research on Fluid Inclusions (PACROFI-XI), University of Windsor, Windsor, Ontario, Canada, June 18-20, 2012, Abstract Volume*, 13-14.

Burns MGG, Kontak DJ, McDonald A, Groat LA, Kyser TK (2013) Implications of stable isotopes ($\delta^{18}O$, δD, $\delta^{13}C$) for magma and fluid sources in an LCT pegmatite swarm in the NWT, Canada: Evidence for involvement of multiple fluid reservoirs. *GAC-MAC Joint Annual Meeting, Winnipeg, Manitoba, Canada, May 21-24, 2013, Abstract Volume*, 36.

Černý P (1982) The Tanco pegmatite at Bernic Lake, Manitoba. In: *Granitic Pegmatites in Science and Industry* (ed Černý P). *Mineralogical Association of Canada, Short Course Handbook*, **8**,527-543.

Černý P (1991a) Rare-element granitic pegmatites. Part I: anatomy and internal evolution of pegmatitic deposits. *Journal of the Geological Association of Canada*, **18**, 49-67.

Černý P (1991b) Rare-element granitic pegmatites. Part II: regional to global environments and petrogenesis. *Journal of the Geological Association of Canada*, **18**, 68-81.

Černý P, Ercit S (1989) Mineralogy of niobium and tantalum: crystal chemical relationships, paragenetic aspects and their economic implications. In: *Lanthanides, Tantalum and Niobium* (eds Möller P, Černý P, Saupé F), pp. 27-29. SGA Special Publications 7, Springer-Verlag, New York.

Černý P, London D, Novák M (2012) Granitic pegmatites as reflections of their sources. *Elements*, **8,** 289-294.

Chakoumakos BC, Lumpkin GR (1990) Pressure-temperature constraints on the crystallization of the Harding pegmatite, Taos County, New Mexico. *Canadian Mineralogist*, **28**, 287-298.

Cline JS, Bodnar RJ (1991) Can economic porphyry copper mineralization be generated by a typical calc-alkaline melt? *Journal of Geophysical Research*, **96**, 8113-8126.

Cook FA, Clowes RM, Snyder DB, van der Velden AJ, Hall KW,Erdmer P, Evenchick CA (2004) Precambrian crust beneath the Mesozoicnorthern Canadian Cordillera discovered

by Lithoprobe seismic reflection profiling.*Tectonics*, **23**, TC2010, DOI:10.1029/2002TC001412.

Diamond, LW (1990) Fluid inclusion evidence for P-V-T-X evolution of hydrothermal solutions in late-Alpine gold -quartz veins at Brusson, Val D'Ayas, northwest Italian Alps. *American Journal Science*, **290**, 912-958.

Diamond, LW (2001) Review of the systematics of CO_2 –H_2O fluid inclusions. *Lithos*, **55**, 69-99.

Frezzoti ML, Tecce F, Casagli A (2012) Raman spectroscopy for fluid inclusion analysis. *Journal of Geochemical Exploration*, **112**, 1-20.

Fuertes-Fuente M, Martin-Izard A, Moreiras D (1995) The Forcarei Sur zoned pegmatitic field, Galicia, northwestern Spain. In: Mineral Deposit (eds Pašava J, Kribek B, Žák K), pp. 439-442. Balkema, Rotterdam, Netherlands.

Fuertes-Fuente M, Martin-Izard A (1998) The Forcarei Sur rare element (Sn, Ta, Nb, Li, Be, Rband P) pegmatite field and its associated mineralization, Galicia, Spain. *Canadian Mineralogist*,**36**, 303-325.

Fuertes-Fuente M, Martin-Izard A, Boiron MC, Vinuela JM (2000) P-T path and fluid evolution in the Franqueira granitic pegmatite, Central Galicia, Northwestern Spain. *The Canadian Mineralogist*, **38**, 1163-1175.

Goldstein RH, Reynolds TJ (1994) Systematics of fluid inclusions in diagenetic minerals. *SEPM (Society for Sedimentary Geology) Short Course*, **31**, 1–199.

Gordey SP, Anderson RG (1993) Evolution of the northern cordilleran miogeocline, Nahanni map area [105I], Yukon and Northwest Territories. *Geological Survey of Canada*, Memoir 428.

Groat LA, Ercit TS, Raudsepp M, Mauthner MHF (1994) Geology and mineralogy of the Little Nahanni Pegmatite Group, part of NTS area 105 I/02. Department of Indian Affairs and Northern Development, NWT Geology Division, Yellowknife, Northwest Territories, Economic Geological Survey, Open File report 1994-14.

Groat LA, Mulja T, Mauthner MHF, Ercit TS, Raudsepp M, Gault RA, Rollo HA (2003) Geology and mineralogy of the Little Nahanni rare-element granitic pegmatites, Northwest Territories. *Canadian Mineralogist*, **41**, 139-160.

Gromet PL, Dymek, RF, Haskin, LA, Korotev, RL (1984) The "North American shale composite": Its compilation,major and trace element characteristics. *Geochimica et Cosmochimica Acta*, **48**, 25469-2482.

Hart, CRJ (2007) Reduced intrusion-related gold systems. In: *Goodfellow, W.D., ed. Mineral Deposits of Canada: A Synthesis of Major Deposit Types, District Metallogeny, the Evolution of Geological Provinces, and Exploration Methods:Geological Asociation of Canada, Mineral Deposits Division, Special Publication,* No.5, 95-112.

Haynes FM, Sterner, SM, Bodnar, RJ (1988) Synthetic fluid inclusions in natural quartz. IV. Chemical analysis of fluid inclusions by SEM/EDA: Evaluation of method. *Geichemica et Cosmochimica Acta,***52**, 969-977.

Holtz F, Behrens H, Dingwell DB, Taylor RP (1992) Water solubility in aluminosilicate melts of haplogranite composition at 2kbar. *Chemical Geology*, **96**, 289-302.

Jahns RH (1982) Internal evolution of pegmatite bodies. In: *Granitic Pegmatites in Science and Industry* (ed Černý P), *Mineralogical Association of Canada, Short-Course Handbook*, **8**,293-327.

Jahns RH, Burnham CW (1969) Experimental studies of pegmatite genesis: I. A model for the derivation and crystallization of granitic pegmatites. *Economic Geology*, **64**, 843-864.

Johnson EL, Hollister LS (1995) Syn-deformational fluid trapping in quartz: determining the pressure-temperature conditions of deformation from fluid inclusions and the formation of pure CO_2 fluid inclusions during grain-boundary migration. *Journal of Metamorphic Geology*, **13**, 239-249.

Kiefer J, Seeger T, Steuer S, Schorsch S, Weikl MC, Leipertz A (2008) Design and characterization of a Raman-scattering-based sensor system and its application in a gas turbine power plant. *Measurement Science and Technology*. **19**, 1-9.

Köhler J, Konnerup-Madsen J, Markl G (2008) Fluid geochemistry in the Ivigtut cryolite deposit, South Greenland. *Lithos*, **103**, 369-392.

Kontak DJ (2004) Analysis of evaporate mounds as a complement to fluid-inclusion thermometric data: case studies from granitic environments in Nova Scotia and Peru. *Canadian Mineralogist*, **42**, 1315-1329.

Kontak DJ (2006) Nature and origin of an LCT-suite pegmatite with late-stage sodium enrichment, Brazil Lake, Yarmouth County, Nova Scotia. I. Geological setting and petrology. *Canadian Mineralogist*, **44**, 563-598.

Kontak DJ, Dostal J, KyserTK, Archibald DA (2002) A petrological, geochemical, isotopic and fluid inclusion study of 370 Ma Pegmatite-Aplite Sheets, Peggy's Cove, Nova Scotia, Canada. *Canadian Mineralogist*, **40**, 1249-1286.

Kontak DJ, Groat LA, Barnes E (2004) A visit to the Little Nahanni rare-element pegmatites, N.W.T., and other curiosities along the way. In:*Mineralogical Association of Canada Newsletter*, **73**, 1-22.

Kontak, DJ., Groat L, Burns MG, Archibald DA, Creaser R. (2016) Documenting the complex evolution of a rare-metal pegmatite swarm: The Little Nahanni Pegmatite Group, NWT, Canada. Geological Association of Canada, Mineralogical Association of Canada, Whitehorse, YK, Canada, Program with Abstracts, v. 39.

Kontak DJ, Kyzer TK (2002) Preliminary fluid inclusion and oxygen isotope studies of Flinstone Rock (NTS 11E/13) silica-clay deposit, Yarmouth County, Nova Scotia. In: *Mines and Minerals Branch Report of Activities 2000* (ed MacDonald DR), pp. 37-48. Nova Scotia Department of Natural Resources, Report 2001-1.

Kontak, DJ, Kyser, TK, Gize, A, Marshall, D (2006) Structurally controlled vein barite mineralization, Maritimes Basin of Eastern Canada: geological setting, stable isotopes and fluid inclusions. *Economic Geology*, **101**, 407-430.

Kontak DJ, Kyser TK (2009) Nature and origin of an LCT-suite pegmatite with late-stage sodium enrichment, Brazil Lake, Yarmouth County, Nova Scotia. II. Implications of stable isotopes ($\delta^{18}O$, δD) for magma source, internal crystallization and nature of sodium metasomatism. *Canadian Mineralogist*, **47**, 745-764.

Kontak DJ, Kyser TK (2011) Fingerprinting multiple fluid reservoirs in a 380 Ma Intrusion-Related Gold (IRG) setting, Nova Scotia, Canada: Implications for the nature and origin of IRG deposits. *Mineralium Deposita*, **46**, 337-363.

Kontak DJ, Cao Y, Ulrich T, Kyser TK (2011) The significance of sodic metasomatism in rare-element pegmatites: a petrological and fluid inclusion study of the Brazil Lake LCT-type pegmatite, Nova Scotia. *GAC-MAC Joint Annual Meeting Abstracts Volume*, Ottawa 2011, **34,** 110-111.

Linnen RL (1998) The solubility of Nb-Ta-Zr-Hf-W in granitic melts with Li and Li + F: constraints for mineralization in rare metal granites and pegmatites. *Economic Geology*, **93**, 1013-1025.

Linnen RL, Williams-Jones AE (1994) The evolution of pegmatite-hosted Sn-W mineralization at Nong Sua, Thailand: evidence from fluid inclusions and stable isotopes. *Geochimica et Cosmochimica Acta*, **58**, 735-747.

Linnen RL, Williams-Jones AE (1995) Genesis of a magmatic metamorphic hydrothermal system: The Sn-W polymetallic deposits at Pilok, Thailand. *Economic Geology*, **90**, 1148-1166.

Linnen RL, Cuney M (2005) Granite-related rare-element deposits and experimental constraints on Ta-Nb-W-Sn-Zr-Hf mineralization. In: *Rare Element Geochemistry and Mineral Deposits* (eds Linnen RL, Samson IM), *Geological Association of Canada Short Course Notes***17**, 45-68.

Linnen RL, Van Lichtervelde M, Černý P (2012) Granitic pegmatites as sources of strategic metals. *Elements*, **8**, 275-280.

London D (1984) Experimental phase equilibria in the system $LiAlSi0_4$-SiO_2-H_2O: a petrogenetic grid for lithium-rich pegmatites. *American Mineralogist*, **69**, 995-1004.

London D (1986b) Formation of tourmaline-rich gem pockets in miarolitic pegmatites. *American Mineralogist*, **71**, 396-405.

London D (1985b) Origin and significance of inclusion in quartz: a cautionary example from the Tanco pegmatite, Manitoba. *Economic Geology*, **80**, 1988-1995.

London D (1985a) Pegmatites of the Middletown district, Connecticut. *New England Intercollegiate Geological Conference, 77th Annual Meeting*. *Connecticut Geological and Natural History Survey, Guidebook*, **6**, 509-533.

London D (1986a) The magmatic-hydrothermal transition in the Tanco rare-element pegmatite: evidence from fluid inclusions and phase equilibrium experiments. *American Mineralogist*, **71**, 376-395.

London D (1990) Internal differentiations of rare-element pegmatites: a synthesis of recent research. In: *Ore-Bearing Granite Systems; Petrogenesis and MineralizingProcesses* (eds Stein HJ, Hannah JL). *Geological Society of America, Special Paper*,**246**, 35-50.

London D (2008) *Pegmatites*. Mineralogical Association of Canada, Special Publication 10, 347 p.

London D (2009) The origin of primary textures in granitic pegmatites. *Canadian Mineralogist*, **47**, 697-724.

London D (2014) A petrologic assessment of internal zonation in granitic pegmatites. *Lithos*,**184**, 74-104.

London D (2018) Ore-forming processes within granitic pegmatites. *Ore Geology Reviews*, **101**, 349-383.

Mair JL, HartCJR, StephensJR (2006) Deformation history of the northwestern Selwyn Basin, Yukon, Canada; implications for orogen evolution and Mid-Cretaceous magmatism. *Geological Society of America Bulletin*, **118**, 304-323.

Martin RF, De Vito C (2013) The fall and rise of calcium in a granitic pegmatite, and the explanation of mixed NYF–LCT assemblages at Anjanabonoina, Madagascar, *GAC-MAC Joint Annual Meeting Abstracts Volume*, Winnipeg 2013, **36,** 138.

Maneta V, Baker DR (2014) Exploring the effect of lithium on pegmatitic textures: An experimental study. *American Mineralogis*t, **99**, 1383-1403.

Masoudi F, Mehrabi M, Rezai Aghdam M, Yardley BWD (2009) The nature of fluids during pegmatite development in metamorphic terrains: evidence from Hamadan Complex, Sanandaj-Sirjan metamorphic zone, Iran. *Journal of Geological Society of India*, **73**, 407-418.

Mauthner MHF, Mortensen JK, Groat LA, Ercit TS (1995) Geochronology of the Little Nahanni Pegmatite Group, Selwyn Mountains, southwestern Northwest Territories. *Canadian Journal of Earth Sciences*, **32**, 2090-2097.

Morgan GB, VI, London, D (1987) Alteration of amphibolitic wall rocks around the Tanco rare-element pegmatite, Bernic Lake, Manitoba. *American Mineralogist*, **72**, 1097-1121.

Mulja T, Williams-Jones AE (2018) The physical and chemical evolution of fluids in rare-element granitic pegmatites associated with the Lacorne pluton, Québec, Canada. *Chemical Geology*, **403**, 281-307.

Murphy DC and Héon D (1996) Geological map of the Seattle Creek map area (115 P/16), western Selwyn Basin, Yukon [1:50 000 scale]. Exploration and Geological Services Division, Yukon, Indian and Northern Affairs Canada, Open File report 1996-3(G).

Mustart DA (1972) Phase relations in the peralkaline portion of the system Na_2O-Al_2O_3-SiO_2-H_2O. Unpubl. Ph.D thesis, Stanford University, Stanford, California.

Nabelek PI, Ternes K (1997) Fluid inclusions in the Harney Peak granite and associated pegmatites, Black Hills, South Dakota, USA: implications for solubility and evolution of magmatic volatiles and crystallization of leucogranite magmas. *Geochimica et Cosmochimica Acta*, **61**, 1447-1465.

Nabelek PI, Whittington AG, Sirbescu MC (2010) The role of H_2O in rapid emplacement and crystallization of granite pegmatites: resolving the paradox of large crystals in highly undercooled melts. *Contributions to Mineralogy and Petrology*, **160**, 313-325.

Nijland TG, Touret JLR (2001) Replacement of graphic pegmatite by graphic albite-actinolite-clinopyroxene intergrowths (Mjåvatn, southern Norway). *European Journal of Mineralogy*, **13**, 41-50.

Pandur K, Kontak DJ, Ansdell KM (2014) Hydrothermal evolution in the Hoidas Lake vein-type REE deposit, Saskatchewan, Canada: Constraints from fluid inclusion microthermometry and evaporate mound analysis. *Canadian Mineralogist*, **52**, 717–744

Partey F, Lev S, Casey R, Widom E, Lueth VW, Rakovan J (2009) Source of fluorine and petrogenesis of the Rio Grande Rift-Type barite-fluorite-galena deposits. *Economic Geology*, **104**, 505-520.

Partington GA, McNaughton NJ (1995) A review of the geology, mineralization, and geochronology of the Greenbushes pegmatite, Western Australia. *Economic Geology*, **90**, 616-635.

Pfister J, Kontak DJ, Groat L. (2018) An integrated stable isotopic and textural study of the Little Nahanni LCT-type rare-metal pegmatite system, NWT. RFG Meeting, Vancouver, BC, Program with Abstracts, June 2018.

Pfister J, Kontak DJ, Groat L, Fayek M (2019) Textural and isotopic studies of the Cretaceous Little Nahanni Pegmatite Group (NWT, Canada) suggest mixed fluid reservoirs during its evolution. PEG 2019 - 9th International Symposium on Granitic Pegmatites, Pala, California.

Plumper O, Putnis A (2009) The complex hydrothermal history of granitic rocks: Multiple feldspar replacement reactions under subsolidus conditions. *Journal of Petrology*, **50**, 967-987.

Redmond PB, Einaudi MT, Inan EE, Landtwing MR, Heinrich CA (1986) Copper deposition by fluid cooling in intrusion-centered systems: New insights from the Bingham porphyry ore deposit, Utah. *Geology*, **32**, 217-220.

Roedder E (1979) Fluid inclusions as samples of ore fluids. In: *Geochemistry of Hydrothermal Ore Deposits*, 2nd edn (ed Barnes HL), pp. 684-737. John Wiley & Sons, New York.

Roedder E (1984) *Fluid Inclusions*. *Reviews in Mineralogy12*, 644 p. (ed. Ribbe PH), Mineralogical Society of America.

Roedder E (1992) Fluid inclusion evidence for immiscibility in magmatic differentiation. *Geochimica et Cosmochimica Acta*, **56**, 5-20.

Rusk B, Reed M, Dilles JH (2008) Fluid inclusion evidence for magmatic-hydrothermal fluid evolution in the porphyry copper-molybdenum deposit, Butte, Montana*: Economic Geology*, **103**, 307-334.

Salvi S, Williams-Jones AE (1997) Fischer-Tropsch synthesis of hydrocarbons during sub-solidus alteration of the Strange Lake peralkaline granite, Quebec/Labrador, Canada. *Geochimica et Cosmochimica Acta*, **61**, 83-99.

Salvi S, Williams-Jones AE (1990) The role of hydrothermal processes in the granite hosted Zr, Y, REE deposit at Strange Lake, Quebec/Labrador: Evidence from fluid inclusions. *Geochim. Cosmochim. Acta*, **54**, 2403-2418.

Shearer CK, Papike JJ, Simon SB, Laul JC (1984a) Pegmatite-wall rock interactions, Black Hills, South Dakota: interaction between pegmatite-derived fluids and quartz-mica schist wall rock. *American Mineralogist*, **71**, 518-539.

Simmons WB, Webber KL (2008) Pegmatite genesis: state of the art. *European Journal of Mineralogy*, **20**, 421-438.

Sirbescu MC, Nabelek PI (2003a) Crystallization conditions and evolution of magmatic fluids in the Harney Peak granite and associated pegmatites, Black Hills, South Dakota – evidence from fluid inclusions. *Geochimica et Cosmochimica Acta*, **67**, 2443-2465.

Sirbescu MC, Nabelek PI (2003b) Crustal melts below 400°C. *Geology*, **31**, 685-688.

Sirbescu, M-LC, Hartwick, EE, Student, JJ (2008) Rapid crystallization of the Animikie Red Ace Pegmatite, Florence county, northeastern Wisconsin: inclusion thermometry and conductive-cooling modeling. *Contributions Mineralogy & Petrology*, **156**, 289-305.

Sirbescu, M-LC, Schmidt, C, Veksler, IV, Whittington, AC, Wilke, M (2017) Experimental crystallization of undercooled felsic liquids: Generation of pegmatitic texture. *Journal of Petrology*, **58**, 53-568.

Smerekanicz JR, Dudas FO (1999) Reconnaissance fluid inclusion study of the Morefield pegmatite, Amelia County, Virginia. *American Mineralogist*, **84**, 746-753.

Smith FG (1953) Complex inclusions in pegmatitic minerals. *American Mineralogist*, **38**, 559-560.

Sterner SM, Bodnar RJ (1989) Synthetic fluid inclusions – VII. Re-equilibration of fluid inclusions in quartz during laboratory-simulated metamorphic burial and uplift. *Journal of Metamorphic Geology*, **7**, 243-260.

Stilling A, Černý P, Vanstone PJ (2006) The Tanco pegmatite at Bernic Lake, Manitoba. XVI. Zonal and bulk compositions and their petrogenetic significance. *Canadian Mineralogist*, **44**, 599-623.

Suwimonprecha P, Černý P, Friedrich G (1995) Rare metal mineralization related to granites and pegmatites, Phuket, Thailand. *Economic Geology*, **90**, 603-615.

Sweetapple MT, Collins PLF (2002) Genetic framework for the classification and distribution of Archean rare metal pegmatites in the North Pilbara Craton, Western Australia. *Economic Geology*, **97,** 873-895.

Thomas AV, Spooner ETC (1988) Fluid inclusions in the system H_20-CH_4-NaCl-CO_2 from metasomatic tourmaline within the border unit of the Tanco zoned granitic pegmatite, S.E. Manitoba. *Geochimica et Cosmochimica Acta*, **52**, 1065-1075.

Thomas AV, Bray CJ, Spooner ETC (1988) A discussion of the Jahns-Bumham proposal for the formation of zoned granitic pegmatites using solid-liquid-vapour inclusions from the Tancogranitic pegmatite, S.E. Manitoba, Canada. *Transactions of the Royal Society of Edinburgh*, **79**, 299-3 15.

Thomas AV, Spooner ETC (1992) The volatile geochemistry of magmatic H_2O-CO_2 fluid inclusions from the Tanco zoned granitic pegmatite, southeastern Manitoba, Canada. *Geochimica et Cosmochimica Acta*, **56**, 49-65.

Thomas R, Webster JD, Heinrich W (2000) Melt inclusions in pegmatite quartz: complete miscibility between silicate melts and hydrous fluids at low pressure. *Contributions to Mineralogy and Petrology*, **139**, 394-401.

Thomas R, Davidson P, Hahn A (2008) Ramanite-(Cs) and ramanite-(Rb): new cesium and rubidium pentaborate tetrahydrate minerals identified with Raman spectroscopy. *American Mineralogist*, **93**, 1034-1042.

Thomas R, Davidson P, Hartmut B (2011) Tantalite-(Mn) fromt he Borborema Pegmatite Province, northeastern Brazil: conditions of formation and melt-and fluid-inclusion constraints on experimental studies. *Mineralium Deposita,***46**, 749-759.

Thomas R, Davidson P (2012) Water in granite and pegmatite-forming melts. *Ore Geology Reviews*, **46**, 32-46.

Thomas SM, Thomas R, Davidson P, Reichard P, Koch-Müller M, Dollinger G (2008b) Application of Raman spectroscopy to quantify trace water concentrations in glasses and garnets. *American Mineralogist*, **93**, 1550-1557.

Tindle AG, Breaks FW, Webb PC (1998) Wodginite-group minerals from the Separation Rapids rare-element granitic pegmatite group, northwestern Ontario. *Canadian Mineralogist*, **36**, 637–658

Tweedale F, Hanley J, Kontak DJ, and Rogers N (2013) Evaporate analysis of quartz-hosted fluid inclusions by SEM/EDS: Evaluation and application of the method to assess granite metal fertility. *Geological Association of Canada-Mineralogical Association of Canada Annual Meeting, Program with Abstracts*, **37**.

Tweedale F, Hanley JJ, Kontak DJ, Rogers N (2015) Petrographic observations and evaporate mound analysis of quartz-hosted fluid inclusions hosted by granitoid samples from the South Mountain Batholith, Nova Scotia: An exploration tool for vectoring towards mineralised areas in intrusive rocks; in TGI4 – Intrusion Related Mineralisation Project: New Vectors to Buried Porphyry-Style Mineralisation, (ed.) N. Rogers; *Geological Survey of Canada, Open File* **7843**, p. 79-9

Van den Kerkhof A, Thiéry R (2001) Carbonic inclusions. *Lithos*, **55**, 49-68.

Van Lichtervelde M, Salvi S, Beziat D, Linnen RL (2007) Textural features and chemical evolution in tantalum oxides: magmatic versus hydrothermal origins for Ta mineralization in the Tanco lower pegmatite, Manitoba, Canada. *Economic Geology*, **102**, 257-276.

Van Lichtervelde M, Grégoire M, Linnen RL, Béziat D, Salvi S (2008) Trace element geochemistry by laser ablation ICP-MS of micas associated with Ta mineralization in the Tancopegmatite, Manitoba, Canada. *Contributions to Mineralogy and Petrology*, **155**, 791-806.

Vennemann T, O'Neil JR (1993) A simple and inexpensive method of hydrogen isotope and water analysis of minerals and rocks based on zinc reagent. *Chemical Geology*, **103**, 227-234.

Williams AE, Taylor MC (1996) Mass spectrometric identification of boric acid in fluid inclusions in pegmatite minerals. *Geochimica et Cosmochimica Acta*, **60**, 3435-3443.

Webster JD, Thomas R, Rhede D, Forster HJ, Seltmann R (1997) Melt inclusions in quartz from an evolved peraluminous pegmatite: Geochemical evidence for strong tin enrichment in fluorine-rich and phosphorus-rich residual liquids. *Geochimica et Cosmochimica Acta*, **61**, 2589-2604.

List of Figures:

well-developed layering parallel to the wall-rock contact. The irregular-shaped dark spots are moss coatings. (f) Close up of part of a rare, vug-like feature containing an intergrowth of euhedral quartz and muscovite (left side) surrounded by a coarser-grained intergrowth of quartz-feldspar. (g, h) Example of quartz-rich zone in a quartz-K-feldspar-spodumene pegmatite that is host to coarse-grained phases of Sn, Ta and Nb oxides. Note that in image (h) the sample is also rich in muscovite. (i) Late vug in pegmatite that is lined with an assemblage of clear zeolite, carbonate are rare quartz. (j) Irregular shaped openings in pegmatite lined with carbonate and zeolites. Area of pegmatite is outlined by the dashed white line. (k) Section of deformed metasedimentary rocks with steeply dipping pegmatite dikes, as indicate by arrows. View is facing southeast. (l, m) Two steeply dipping pegmatite dikes with the thinner dike showing boudinage features. In detail (image m) note the fabric wraps around the pods and in once case (lower pod) its termination is tapered like a tear shape.

Figure 3. Photomicrographs of fluid inclusions hosted by cassiterite (a) and quartz (b, c) in LNPG pegmatites; all photos taken in plain polarized light. (a) Vapour-rich inclusions hosted by cassiterite. Note that some of the inclusions contain a tadpole-shaped tail of an orange phase extending from the inclusions which is possibly tantalite as noted from SEM-EDS analysis of similar textures. (b) Typical secondary, type B aqueous fluid inclusions in quartz comprising a fluid inclusion assemblage (FIA); note the shapes suggest the inclusions were produced form necking. These inclusions within the FIA are homogeneous in terms of their salinity and liquid:vapour ratios, hence their density. Inset shows an enlargement of one of the inclusions. (c) A plane of typical type A, three-phase (LH_2O, LCO_2, VCO_2) fluid inclusions in quartz that comprise an FIA. Again the shapes suggest the inclusions are a product of necking.

Figure 4. Photomicrographs of fluid inclusions, in plain polarized (PL) and crossed nicols (XN) conditions, from different mineral phases and samples from the LNPG pegmatites. (a) A PL image of a four-phase (LH_2O, LCO_2, VCO_2, solid) fluid inclusion hosted in spodumene. Note the inclusion is elongated parallel to the c axis of the host and displays wisps or tails extending from the ends of the inclusion, which suggests necking. (b) Small, equant-shaped, three-phase aqueous-carbonic (LH_2O, LCO_2, VCO_2) inclusions with uniform phase proportions that occur along a healed fracture plane in spodumene. One of these inclusions is shown enlarged in the inset. Both images are taken in PL. (c; top and bottom) PL images of negative-shaped, mixed H_2O-CH_4 inclusions hosted in muscovite. (d) A PL image of representative, three-phase aqueous-carbonic (LH_2O, LCO_2, VCO_2) inclusions hosted in K-feldspar. One of these inclusions is shown enlarged in the inset. (e) An example of methane inclusions that contain unknown, highly birefringent solid phases hosted by garnet (photo in XN). (f) A rare example of CO_2-rich aqueous-carbonic inclusions hosted in tourmaline; photo taken in PL.

Figure 5. Histogram plots for mole % CO_2 (X_{CO2}) for aqueous-carbonic inclusions hosted in different phases. (a) Spodumene with values for bins from left to right falling at: 0.15; 0.22-0.3; 0.36; 0.45-0.48; 0.58, (b) Quartz, with bin values at: 0.1; 0.18-0.2; 0.22-0.3; 0.42-0.5; 0.55; 0.66; 0.75-0.78. (c) K-feldspar with bin values at 0.22-0.26. The data are plotted as FIA with each FIA containing several ($n = \geq 3$) analyzed inclusions. The bar width represents the range in XCO_2 values.

Figure 6. Histogram plots summarizing the microthermometric data for CO_2 in type A fluid inclusions. Note that the bar widths in figures (a) and (b) are proportional to the ranges in temperature within each bin. (a) Measurements for $TmCO_2$for type A inclusions in quartz, spodumene and K-feldspar. Note that the values are depressed relative to pure CO_2 (i.e., -56.6°C). (b) Measurements of $ThCO_2$ for type A inclusions. Note that the populations with $ThCO_2 > 24^oC$ are from spodumene and K-feldspar-hosted inclusions whereas the data for $ThCO_2 < 24^oC$ are from quartz-hosted inclusions. The large population at 26ºC is due to K-feldspar hosted inclusions and these all homogenize to the vapour phase.

Figure 7. Histogram plot summarizing the salinity (wt. % eq. NaCl) for FIA of type B aqueous inclusions. The variation of the salinity for individual FIA is relatively homogeneous and varies less than 0.5 wt. %. The FIAs hosted in K-feldspar contain consistently low salinities (i.e., 0.2 wt. % eq. NaCl), whereas quartz and spodumene hosted inclusions account for the larger range in salinity (i.e., from 0.9 to 3.0 wt. % eq. NaCl), and the highest salinity inclusions (at 4.2 wt. % eq. NaCl) are hosted in quartz.

Figure 8. Ternary plots (in wt. %) showing the composition, as determined from SEM-EDS analysis, of decrepitate mounds for quartz-hosted fluid inclusions. In each plot the data include both individual spot and raster analyses, the use of which depended on the size of the mound, as discussed in the text (i.e., < 5 μm >). (a) Na-Ca-K, (b) Na-S-Cl, (c) Na-Fe-K, and (d) Na-F-Cl. The data circled in (b) and (d) are the same group of data circled in Figure 9. Note that the F enriched mounds in (d) are relatively enriched in S (b). The composition of the mounds cannot be equated to specific fluid inclusion types because the inclusions, dominantly type A and B, are

mixed together in the chips which were used for decrepitation. See text for further discussion of the data.

Figure 9. A summary of the evaporate mound data produced from SEM-EDS analysis. (a) Plot of Cl versus Na (atomic %) for evaporate mounds showing that the majority of mound data define, as expected, a generally positive correlation between Na and Cl. Note however that in this plot there is a group of samples (circled) that are Na rich (ca. 70 atomic % Na) and Cl poor (< 20 atomic % Cl) with Na:Cl ratios between 3:1 and 8:1. This latter group of samples, which are circled, are also enriched in S and F (see Fig. 8). (b) Plot of S (atomic %) versus Na/Cl (using atomic %) for evaporate mounds to show the strong correlation of increasing S content with decreasing Cl.

Figure 10. A summary of the minor- and trace-element chemistry for evaporate mounds determined by SEM-EDS analysis. (a) Plot of frequency (i.e., number of mounds containing said element) versus the minor or trace element detected in the mound. (b) A plot of the Na/Cl ratio (atomic) versus the sum (in atomic %) of additional elements in the evaporate mounds. The data show that the deviation from an ideal Na:Cl ratio (atomic) of 1:1 coincides with an increased elemental abundance in the mounds of metals. The trend line is set at 1:1 for the relationship between the X and Y axis which shows that the change in NaCl ratios is not proportional to the addition of other elements.

Figure 11. Ternary plots summarizing the volatile compositions (CO_2 -N_2-CH_4) of fluid inclusions contained within groups of FIA that have consistent compositions, thus each dot

represents the average for an FIA. The types and proportions of the volatile species were determined by laser Raman spectroscopy analysis, as discussed in the text. (a) Data plotted according to the host phase. (b) Data plotted according to sample.

Figure 12. Binary element plots for trace element data (Li, Cs) vs. Na for quartz-hosted fluid inclusions which were determined using LA ICP-MS. Note the correlations of the data for plots of (a) Na versus Li, and (b) Na versus Cs.

Figure 13. The petrogenetic P-T grid for the system SiO_2-Al_2O_3-Li_2O-H_2O showing the stability fields and phase relationships for spodumene-quartz-petalite-eucryptite (after London 1984) with the CO_2 -H_2O solvus projected at 10 mole % CO_2 and 0 wt. % NaCl (from Diamond 2003); note that the solvus moves to the right with the addition of NaCl and CH_4. Also shown are the isochores for type A fluid inclusions (long dashes; calculated using FLINCOR (Brown 1986) and the equation of Brown & Lamb (1989)) for representative compositions (X_{CO2} = 0.2, 0.5, 0.6, 0.75) in different host minerals (quartz, spodumene, K-feldspar) and isochores for type B fluid inclusions (dotted lines; also calculated with FLINCOR). Note that for the latter type B inclusions, the minimum and maximum homogenization temperatures of 240^{o}C to 310^{o}C were used. In addition the 0.2 X_{CO2} isochore for type A inclusions hosted in quartz is noted to represent the highest PT boundary for the system and that the isochore for the 0.75 X_{CO2} crosses into the spodumene stability field at about 2.3 kbar and 420^{o}C; the significance of these latter observations is discussed in the text.

List of Tables:

Figures:

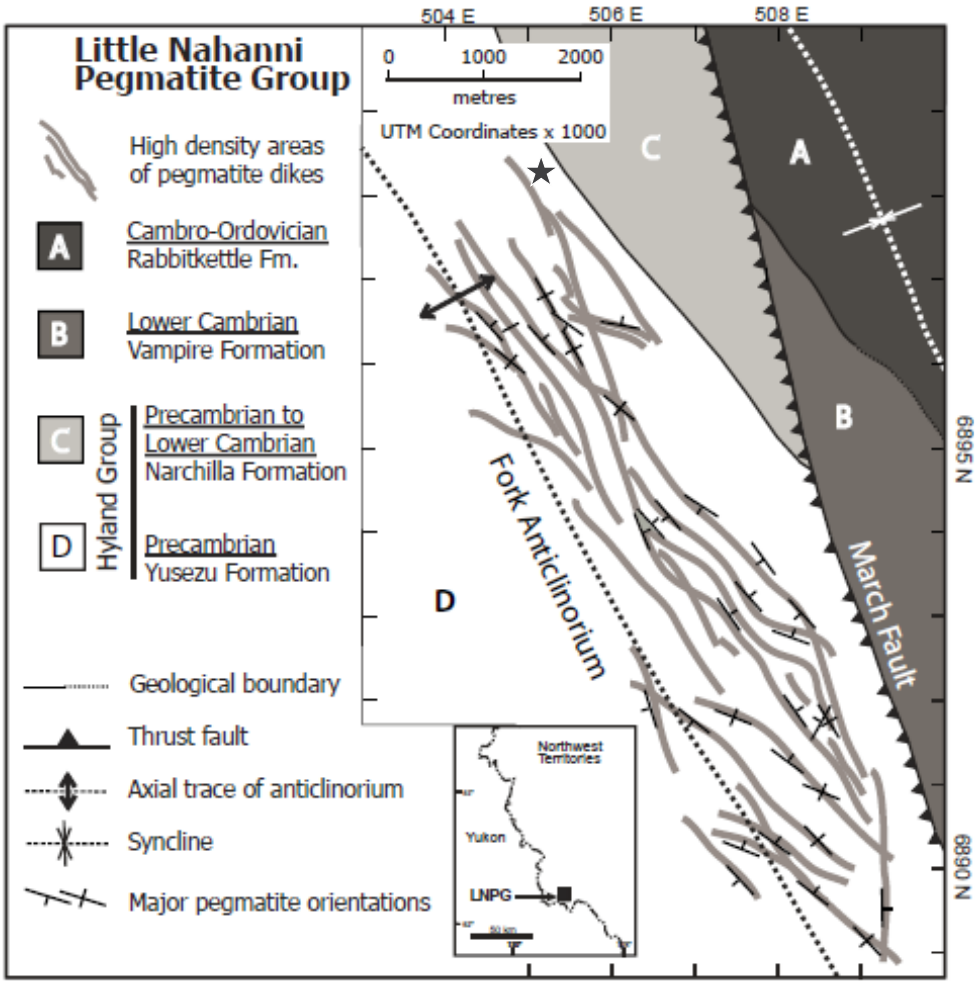

Figure 1: Location and Regional Geology

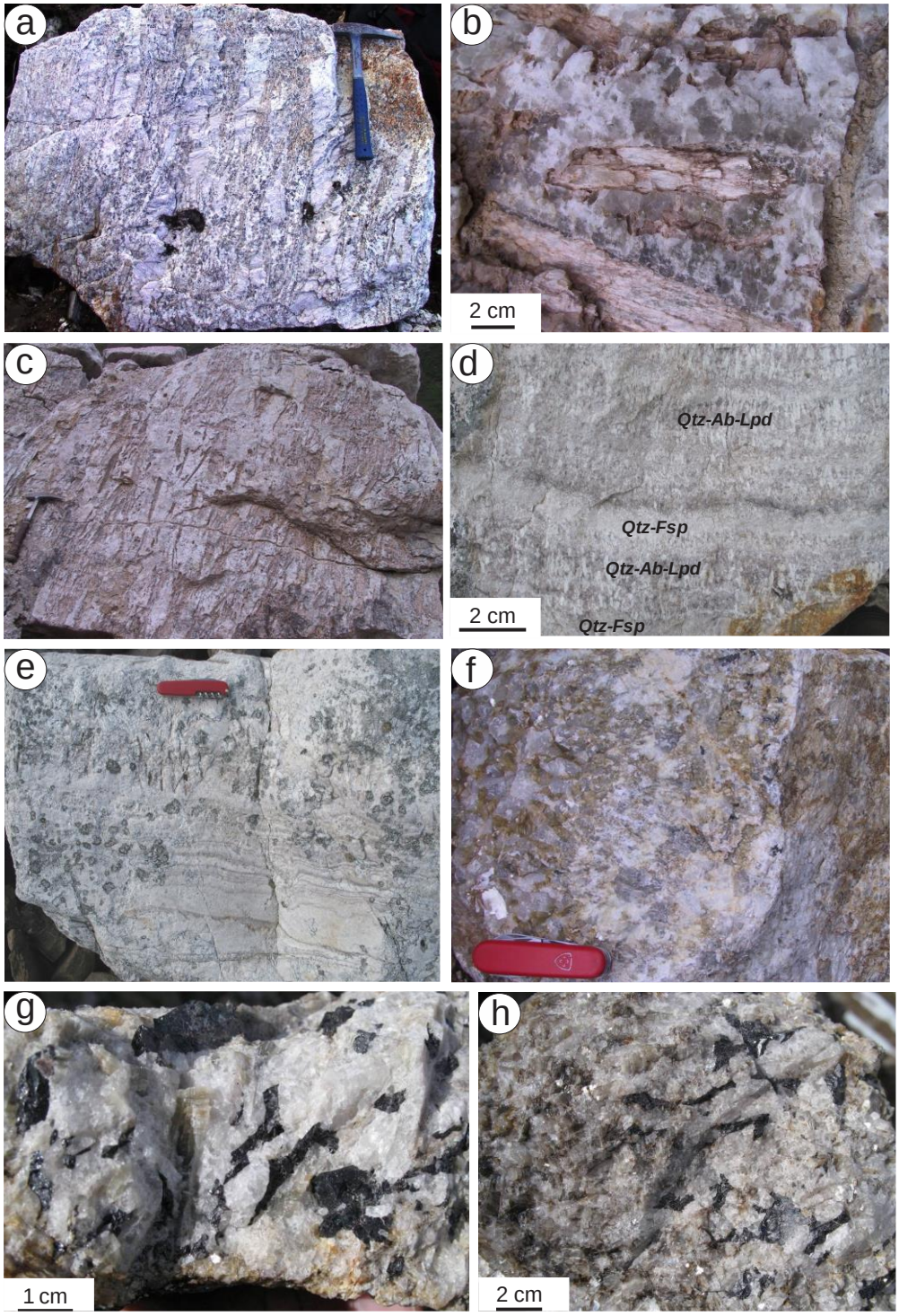
a
b
2 cm
c
d
Qtz-Ab-Lpd
Qtz-Fsp
Qtz-Ab-Lpd
2 cm
Qtz-Fsp
e
f
g
1 cm
h
2 cm

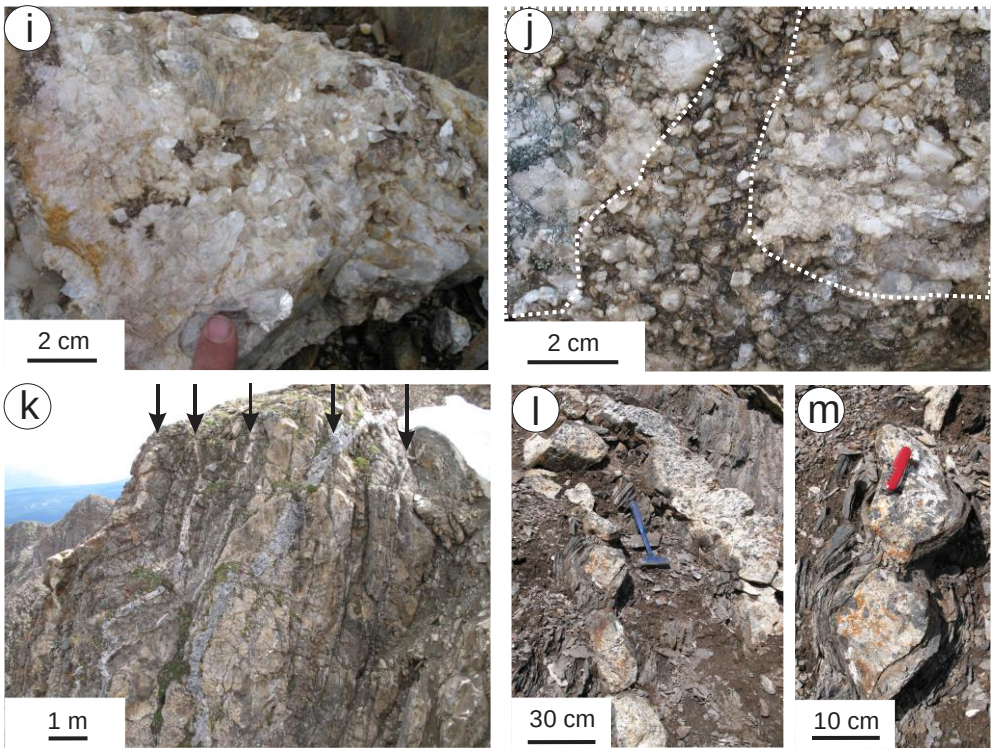

Figure 2: Outcrop Photographs

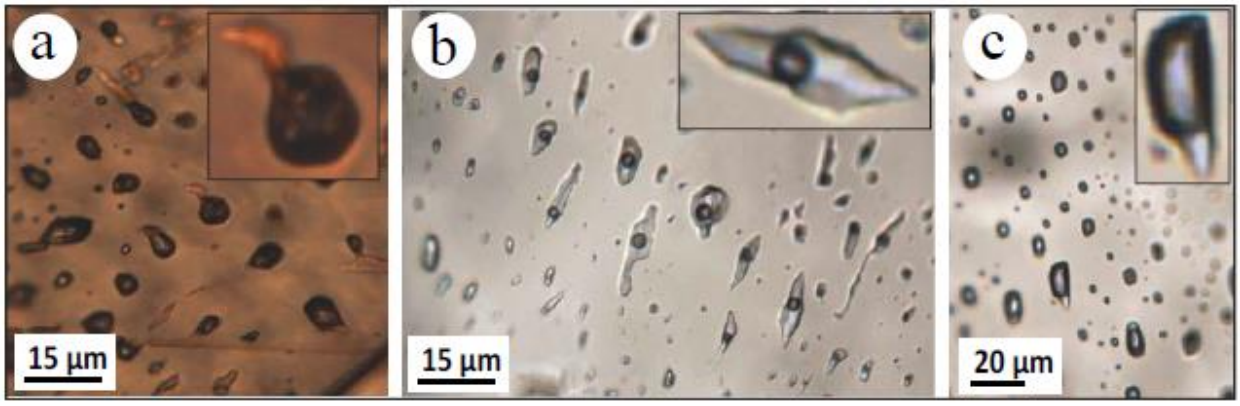

Figure 3: Photomicrographs of Fluid Inclusions

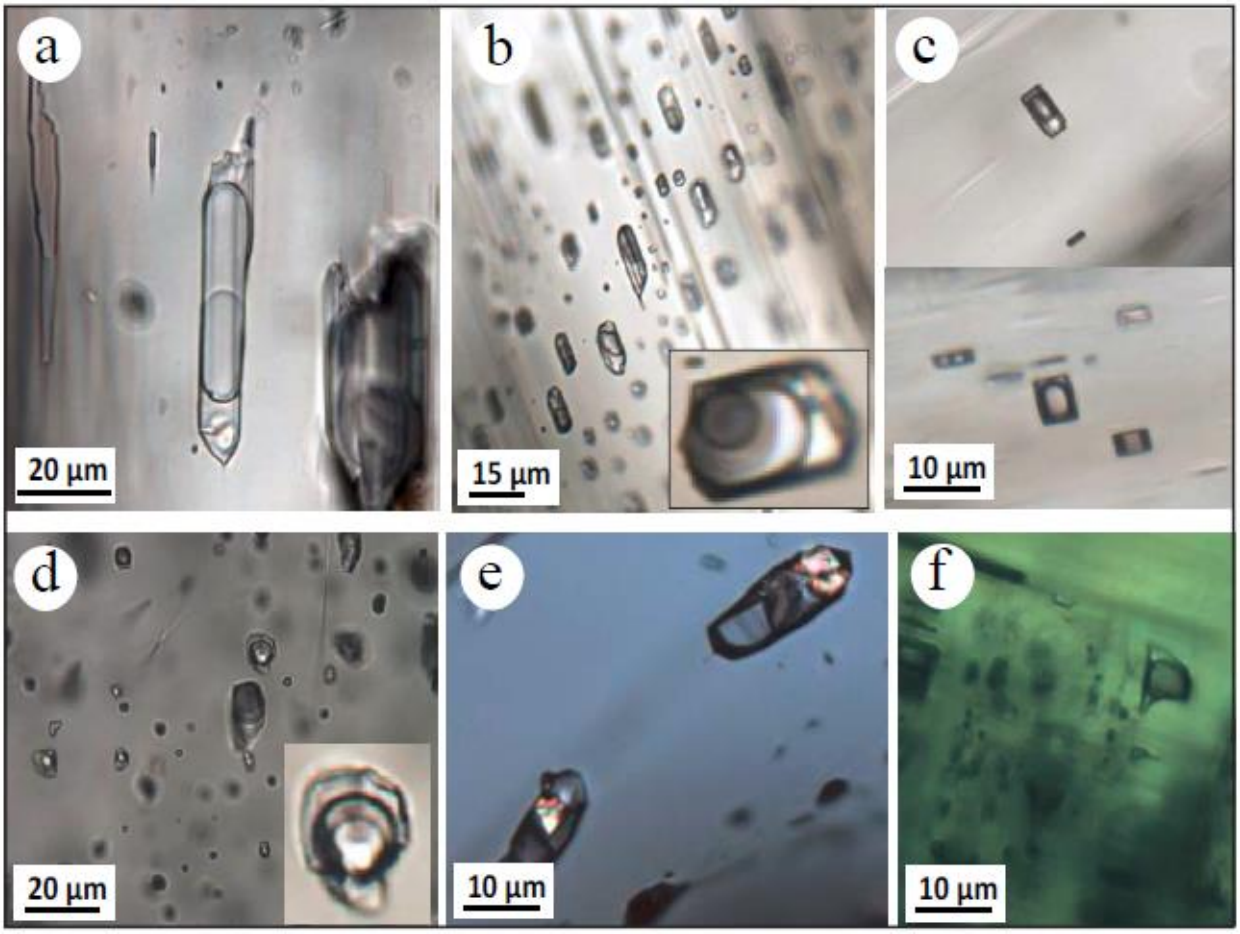

Figure 4: Photomicrographs of Fluid Inclusions

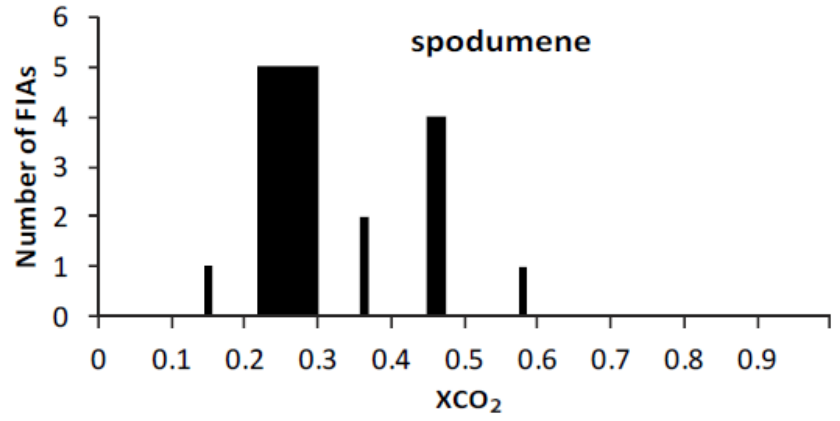

Figure 5a: Histogram plots for mole % CO_2 (XCO_2) for aqueous-carbonic inclusions in spodumene

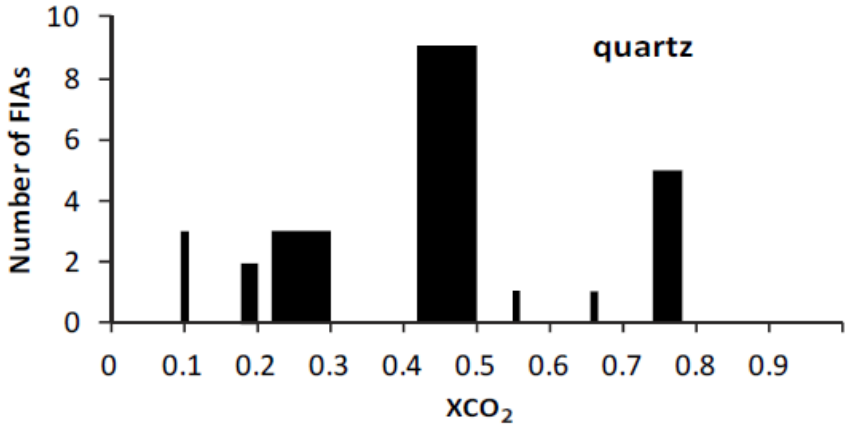

Figure 5b: Histogram plots for mole % CO_2 (XCO_2) for aqueous-carbonic inclusions in quartz

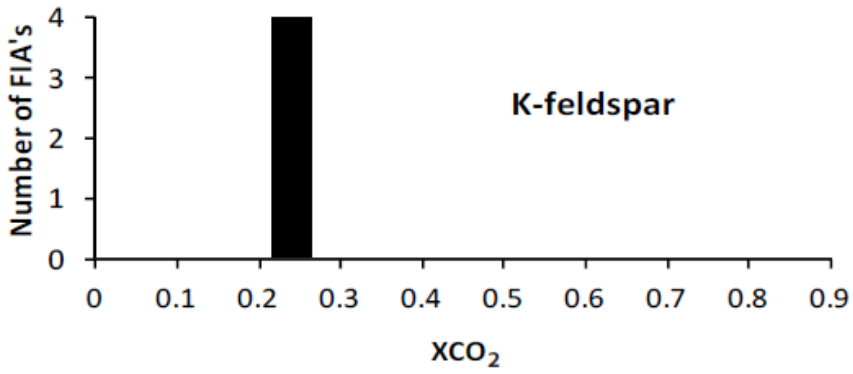

Figure 5c: Histogram plots for mole % CO_2 (XCO_2) for aqueous-carbonic inclusions in K-feldspar

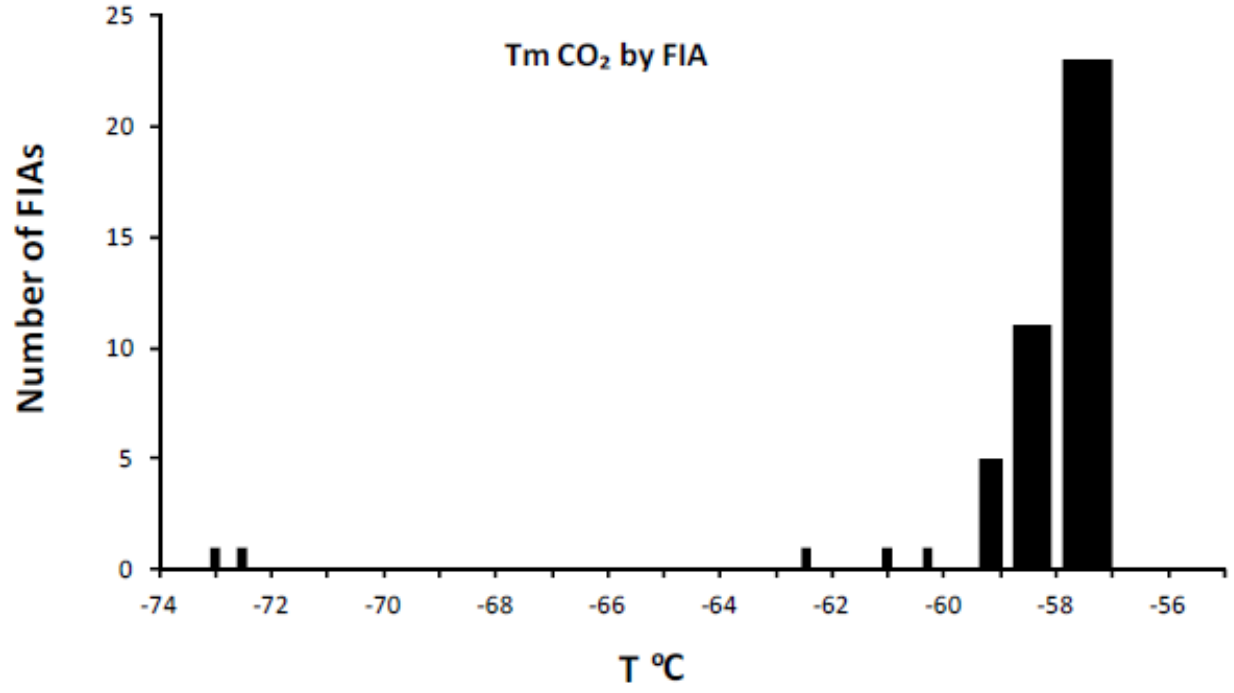

Figure 6a: Histogram of CO_2 melting temperature by Fluid Inclusion Assemblage

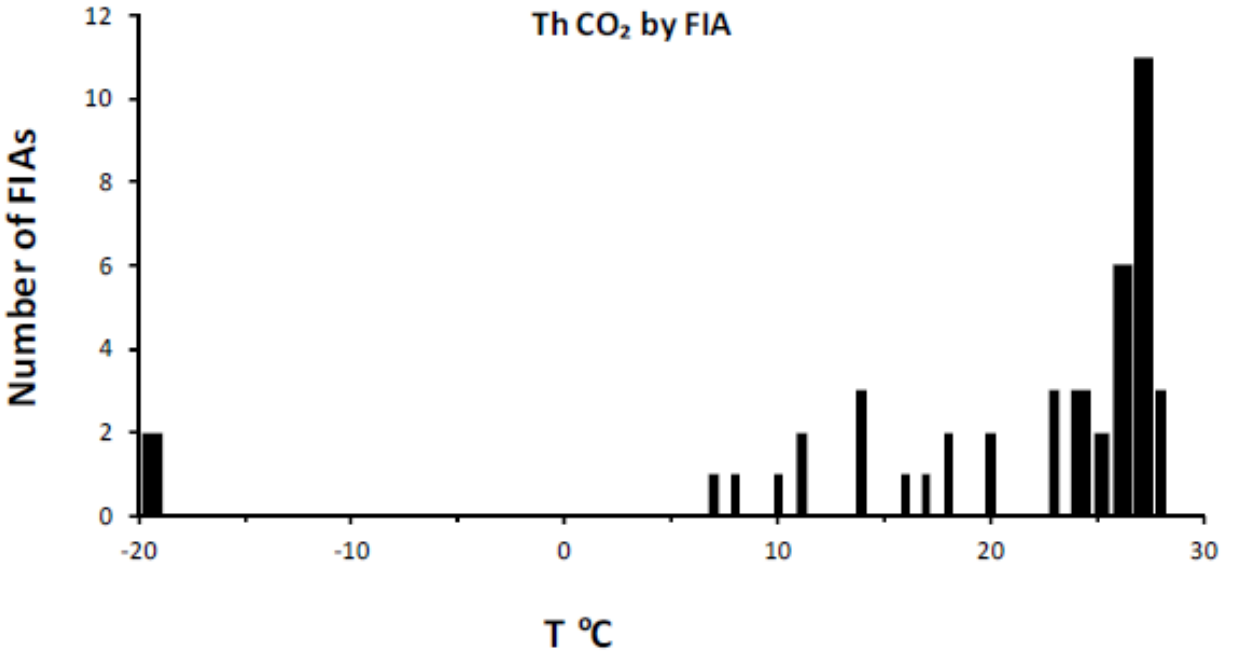

Figure 6b: Histogram of CO_2 homogenization temperature by Fluid Inclusion Assemblage

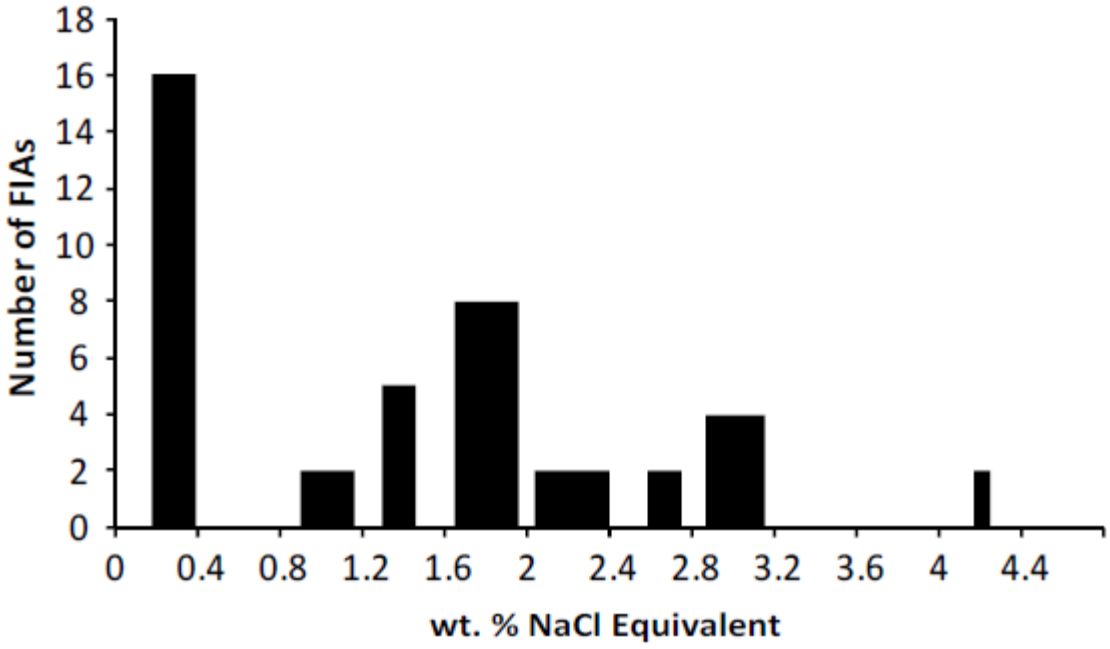

Figure 7: Salinity histogram for type A inclusions

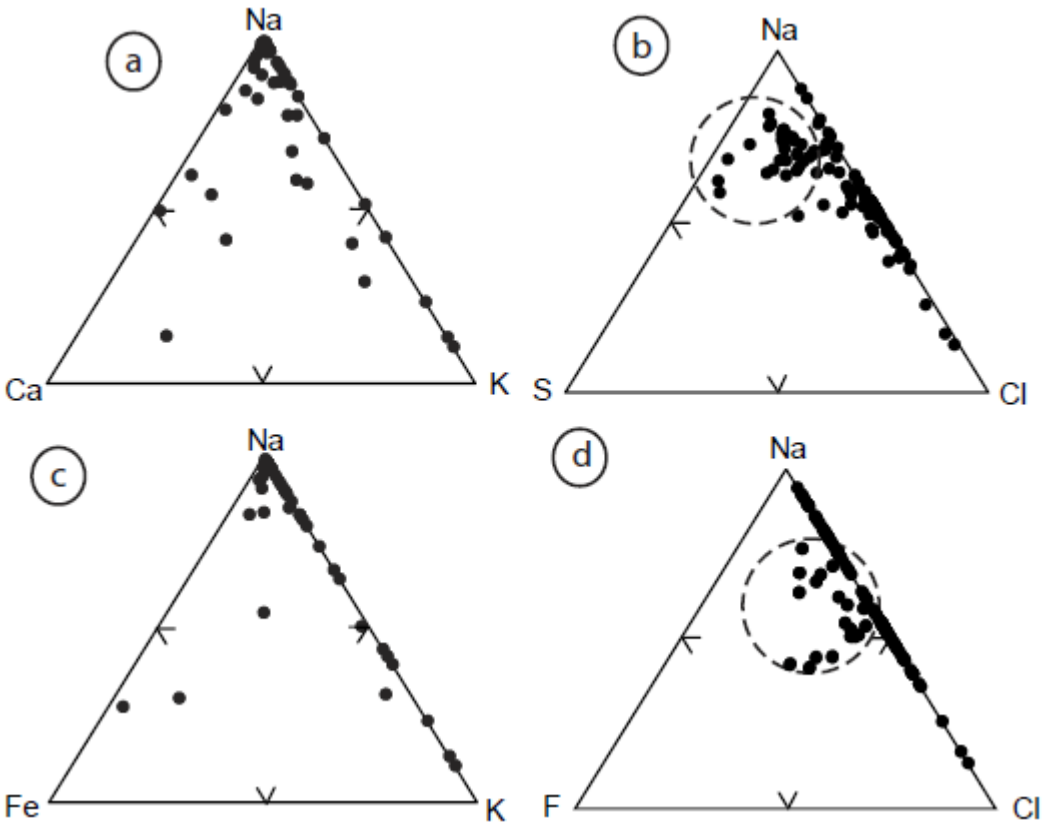

Figure 8: Ternary plots in wt. % showing results of SEM-EDS analysis of evaporate mounds

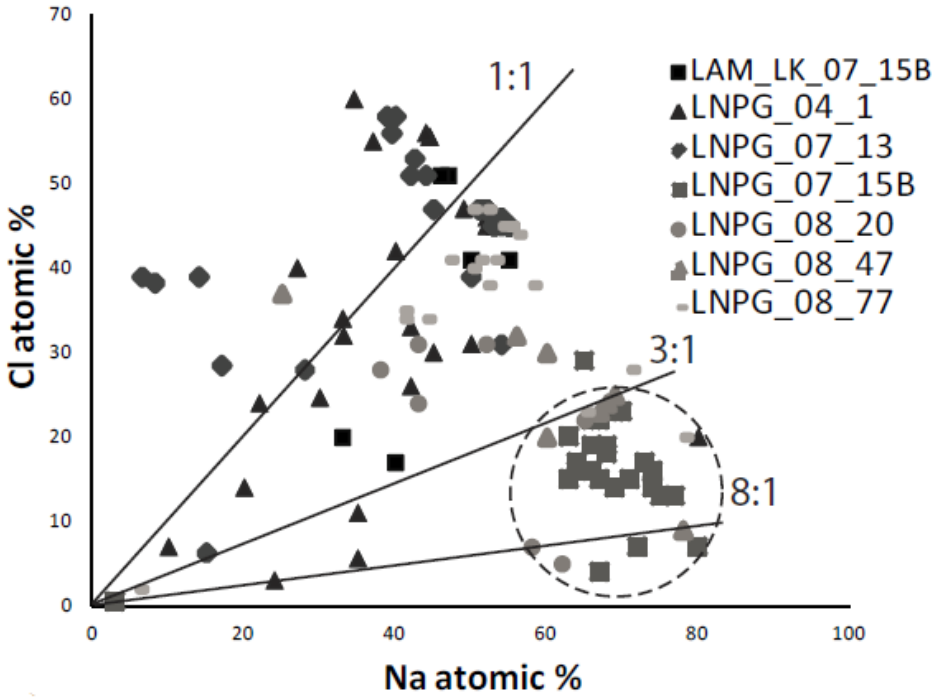

Figure 9a: Na vs. Cl in atomic % for evaporate mounds analyzed by SEM-EDS

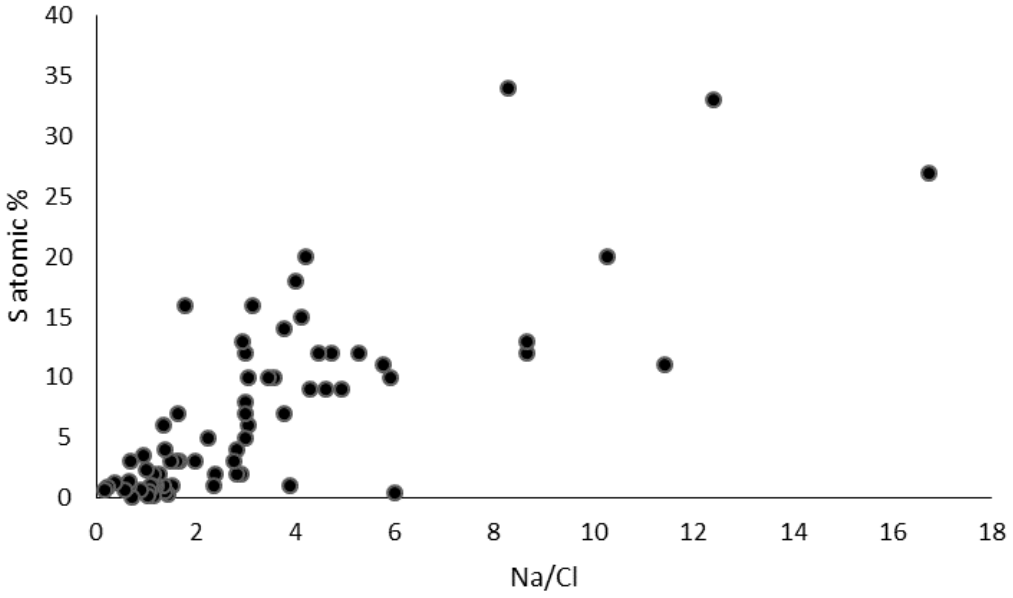

Figure 9b: Na/Cl vs S in atomic % for evaporate mounds analyzed by SEM-EDS

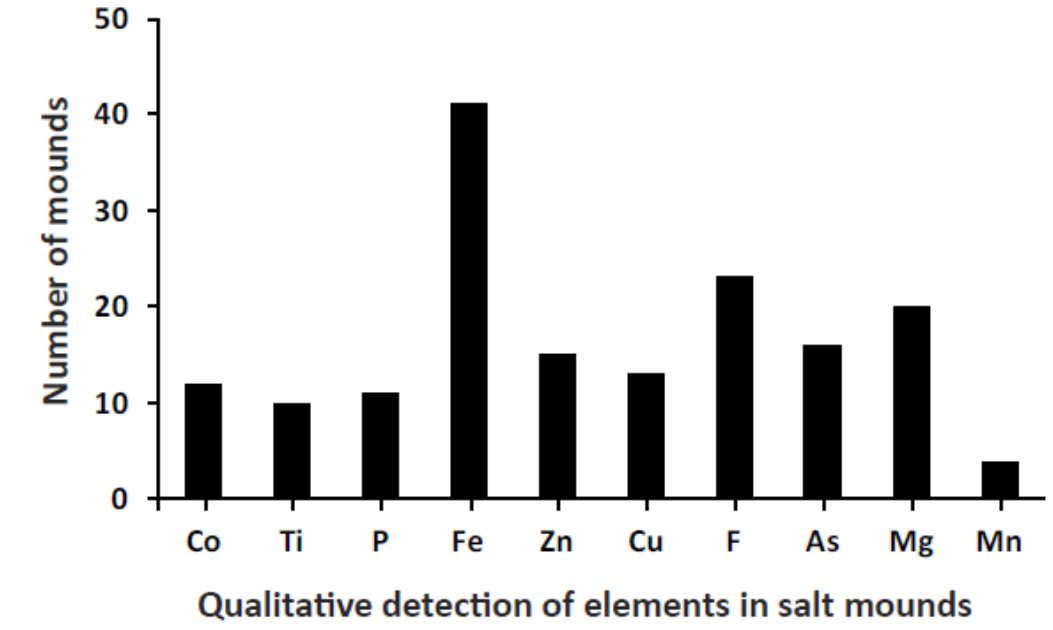

Figure 10a: Minor and Trace element presence in evaporate mounds analyzed by SEM-EDS

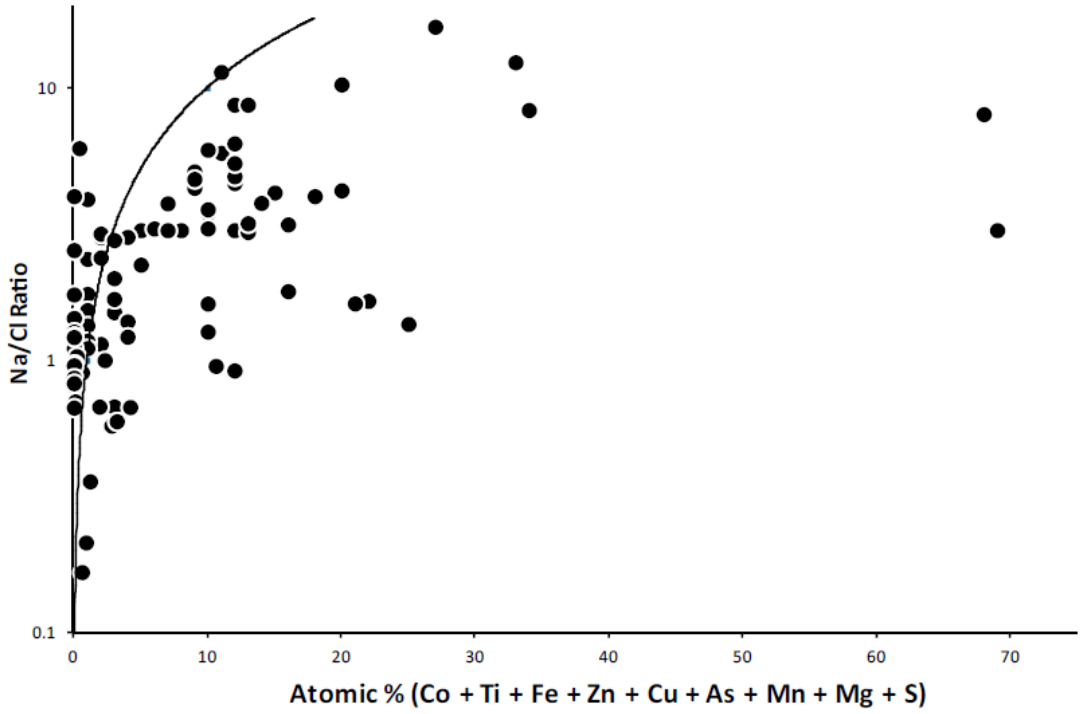

Figure 10b: Plot of Na/Cl ratio vs. combined atomic % of trace elements present in evaporate mounds analyzed by SEM-EDS

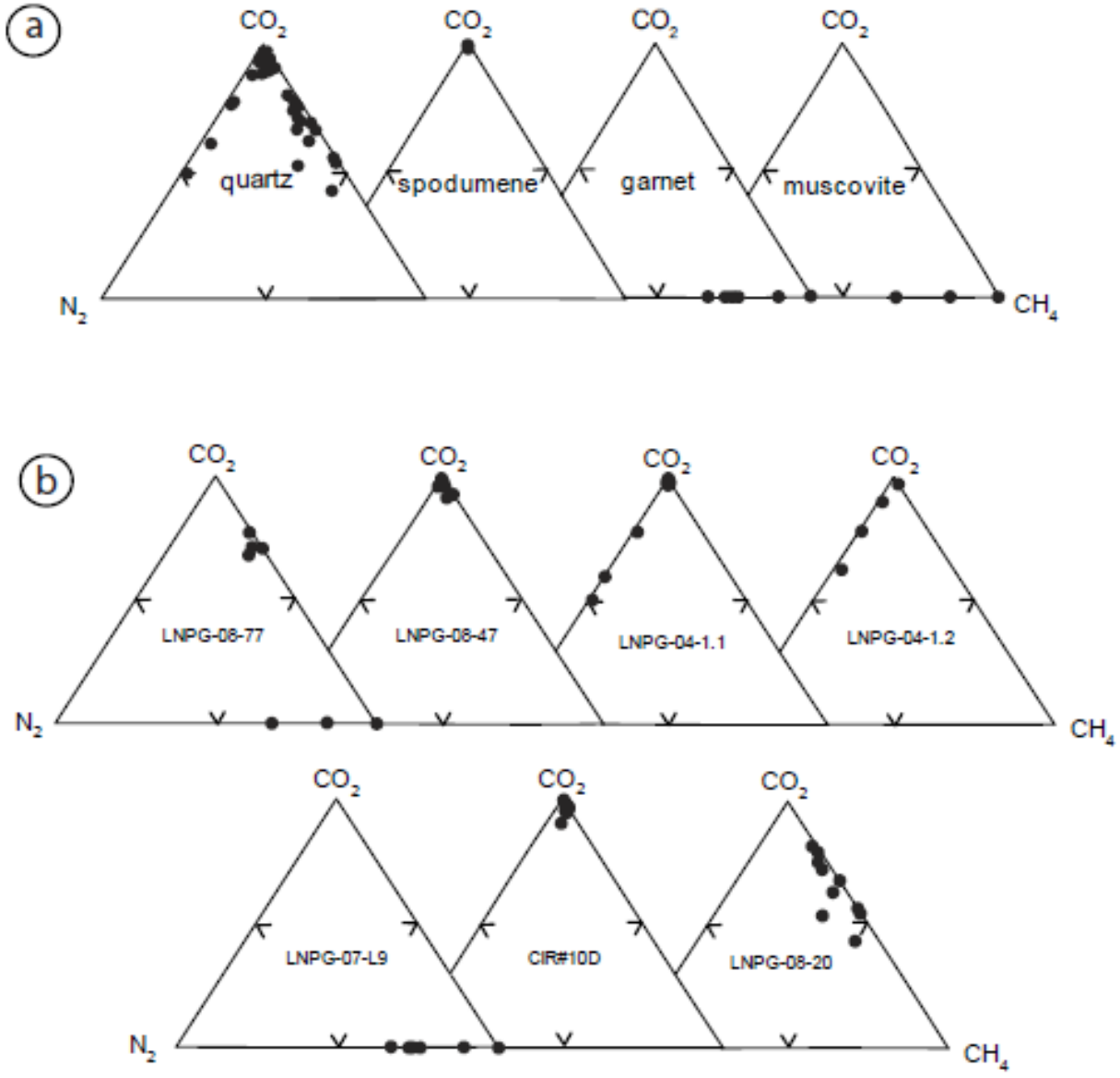

Figure 11: Ternary plots of the volatile composition of fluid inclusions analyzed by Raman spectroscopy

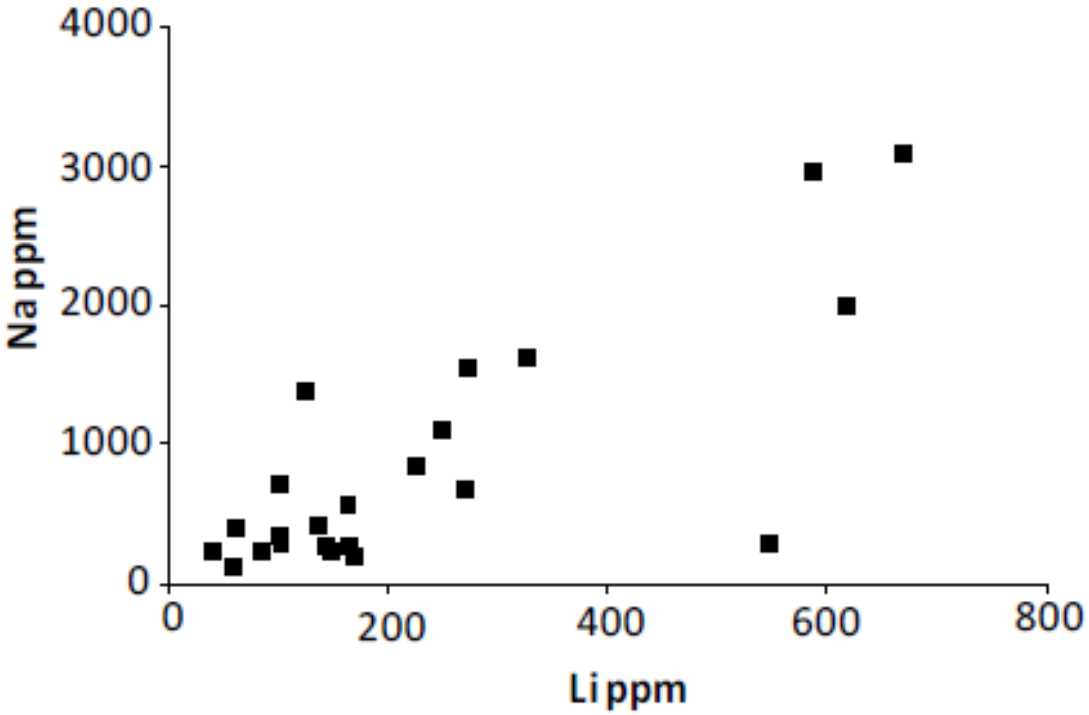

Figure 12a: Na-Li binary plots of LA ICP-MS data from fluid inclusions

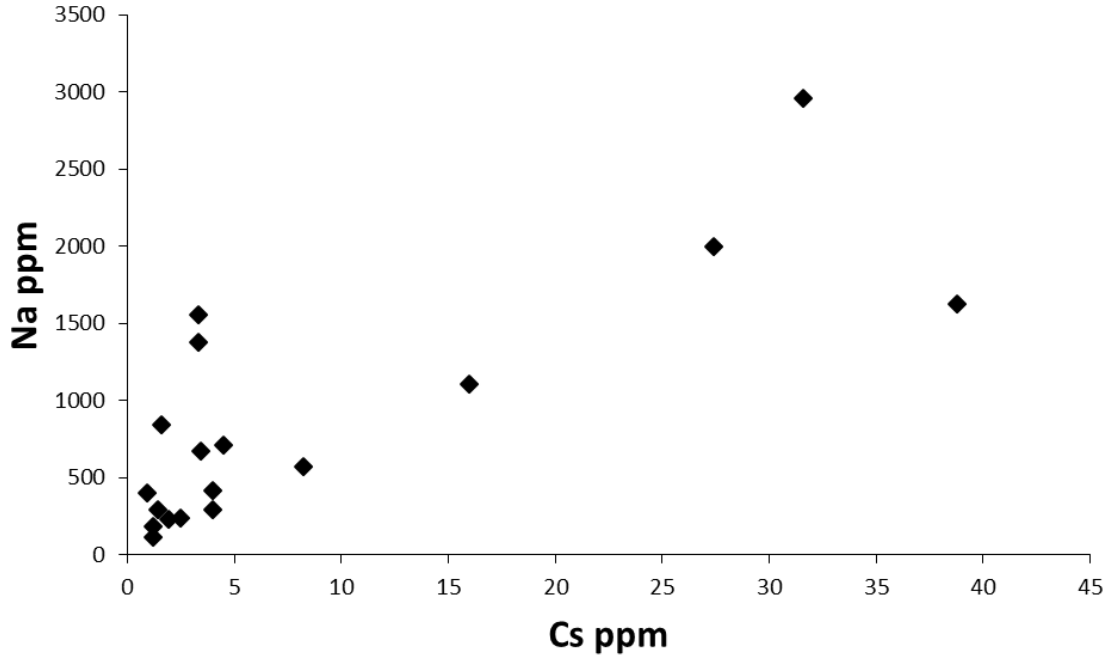

Figure 12b: Na-Cs binary plots for La ICP-MS data from fluid inclusions

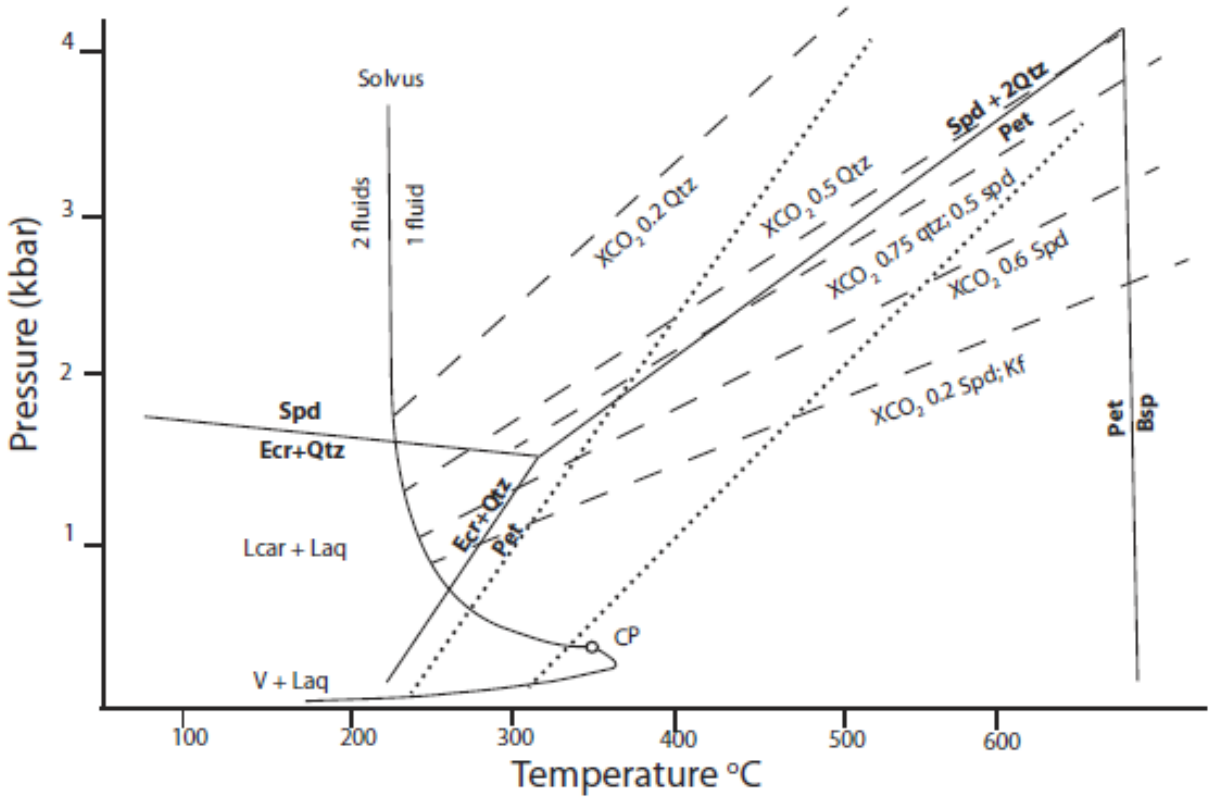

Figure 13: Stability diagram for Spd, Qtz, Pet, Ecr pegmatites with superimposed isochores determined from fluid inclusion analysis.

Sample	Chip	Host	FIA (n=x)	Vol. % CO2	TmCO2	±	Tm clath	±	Th CO2 (L,V)		±	Th(L,V) [Decrep]	±	Tm ice
LNPG-07-13	1	Quartz	1(3)	25.0	-57.1	0.1	10.0	0.1	27.8	(L)	0.7	-	-	-
		Quartz	2(4)	25.0	-57.0	0.1	10.0	0.1	27.0	(L)	0.5	-	-	-
		Quartz	3(2)	75.0	-57.0	0.1	10.0	0.1	17.9	(V)	1.3	-	-	-
	3	Quartz	4(3)	70.0	-57.0	0.1	10.5	0.5	7.5	(L)	0.5	-	-	-
		Quartz	5(4)	70.0	-57.0	0.1	10.5	0.6	7.0	(L)	1.0	-	-	-
	4	Quartz	1(3)	85-95	-61.0	1.0	10.3	0.5	10.6	(L)	1.3	-	-	-
		Quartz	2(3)	85-95	-60.3	2.1	10.6	0.5	9.5	(L)	1.8	-	-	-
		Quartz	3(4)	85-95	-62.5	3.1	10.0	0.1	10.5	(L)	4.0	-	-	-
		Quartz	4(3)	70.0	-58.8	0.1	11.3	0.1	16.5	(L)	0.7	-	-	-
		Quartz	5(4)	70.0	-58.8	0.1	11.3	0.1	15.2	(L)	0.1	-	-	-
	5	Quartz	1(3)	70.0	-59.2	0.1	11.0	0.1	14.0	(L)	1.6	-	-	-
		Quartz	2(3)	70.0	-59.2	0.1	10.9	0.1	13.8	(L)	2.1	-	-	-
	6	Quartz	1(3)	85.0	-59.2	0.1	12.0	0.1	13.9	(L)	0.0	[323]	-	-
LNPG-07-15A	3	Quartz	1(4)	67.0	-57.0	0.1	8.7	0.4	23.1	(L)	0.1	>320	-	-0.3
LNPG-07-15B	2	Quartz	1(4)	90.0	-59.0	0.1	-10.0	0.1	19.5	(V)	0.1	-	-	-
		Quartz	2(3)	90.0	-59.0	0.1	-10.0	0.1	19.4	(L)	0.2	-	-	-
		Quartz	3(3)	90.0	-59.0	0.1	-10.0	0.1	17.7	(L)	0.8	-	-	-
	3	Quartz	1(3)	50.0	-58.2	0.1	9.9	0.1	23.8	L,V)	0.5	[300]	-	-
		Quartz	2(4)	50.0	-58.2	0.1	9.9	0.1	24.0	(L)	0.2	-	-	-
		Quartz	3(3)	80.0	-57.7	0.1	9.9	0.1	24.3	(L)	0.1	-	-	-
CIR 10D	1	Quartz	1(4)	35.0	-57.9	0.0	8.4	0.0	22.5	(L)	0.1	>300	-	-
		Quartz	2(5)	50.0	-57.8	0.6	9.2	0.1	25.3	(V)	0.2	>300	-	-
		Quartz	3(3)	75.0	-59.0	0.2	14.0	0.1	23.0	(L)	0.1	-	-	-
		Quartz	4(3)	55.0	-59.3	1.2	13.0	0.1	23.0	(L)	1.1	>300	-	-0.1
LNPG-08-20	4	Quartz	1(4)	90.0	-73.0	0.7	-	-	-19.0	(L)	1.3	-	-	-
		Quartz	1(3)	90.0	-72.6	0.5	-	-	-20.1	(L)	0.6	-	-	-
LAM Lk(1)	1	Spodumene	1(3)	75.0	-57.5	0.0	12.0	0.1	26.2	(L)	0.1	-	-	-
		Spodumene	2(3)	75.0	-57.5	0.0	12.0	0.1	26.1	(L)	0.1	-	-	-
LNPG-07-15B	4	Spodumene	1(3)	82.0	-58.2	0.1	-	-	28.0	(L)	1.4	>310	-	-0.1
		Spodumene	2(3)	70.0	-58.2	0.1	-	-	26.5	(L)	0.8	-	-	-
		Spodumene	3(3)	75.0	-58.1	0.1	-	-	26.6	(L)	0.4	-	-	-
	5	Spodumene	1(4)	75.0	-58.2	0.1	-	-	25.2	(V)	1.8	-	-	0.8
LNPG-07-15A	1	Spodumene	1(4)	56.0	-57.8	0.2	-	-	27.0	(L)	0.1	298(L)	1.0	-0.5
		Spodumene	2(3)	52.0	-57.5	0.2	-	-	28.0	(L)	1.0	298(L)	1.0	-0.5
		Spodumene	3(3)	64.0	-57.0	0.1	-	-	25.0	(V)	0.1	284(V)	25.0	-
		Spodumene	4(3)	71.0	-57.0	0.1	-	-	26.0	(V)	0.1	284(V)	20.8	-0.5
	2	Spodumene	1(4)	56.0	-57.7	0.1	-	-	26.5	(L)	0.1	-	-	-0.2
		Spodumene	2(4)	65.0	-57.3	0.1	-	-	25.4	(L)	0.1	-	-	-0.6
		Spodumene	3(3)	65.0	-57.0	0.1	-	-	25.5	(L)	0.2	-	-	-
LNPG-08-13	1	K-feldspar	1(4)	74.0	-57.1	0.2	7.5	0.3	27.0	(V)	0.1	338(V)	9.0	-0.1
		K-feldspar	2(3)	73.0	-57.1	0.2	8.2	0.5	27.0	(V)	0.1	350(V)	2.0	-
		K-feldspar	2(6)	72.0	-57.6	0.0	8.1	0.8	26.0	(V)	0.2	389(V)	7.0	-
LNPG-04-1.2	1	K-feldspar	1(5)	71.0	-57.0	0.0	7.9	0.3	26.5	(V)	0.1	372(V)	2.0	-0.1
LNPG-04-1.2		K-feldspar	2(4)	73.0	-57.1	0.1	8.0	0.1	27.0	(V)	0.1	345(V)	1.0	-0.1

Table 1: Thermometric data for type B aqueous carbonic inclusions

sample	Chip	Host	FIA (n=x)	Volume % of bubble	Th(L)	±	Tdecrep	Tm ice	±
LNPG-07-13	2	Quartz	1(2)	10-15	-	-		-0.7	0.1
		Quartz	2(4)	10-15	-	-		-0.8	0.1
		Quartz	3(4)	10-15	-	-		-1.0	0.1
		Quartz	4(2)	10-15	-	-		-1.4	0.1
	3	Quartz	1(4)	15	-	-		-0.8	0.3
		Quartz	2(4)	15	-	-		-1.0	0.2
		Quartz	3(4)	15-20	-	-		-1.2	0.2
		Quartz	4(3)	15-20	-	-		1.1	0.2
	4	Quartz	1(3)	25	222.0	14.1	410.0	-1.0	0.1
		Quartz	2(5)	25	242.0	9.8		-1.0	0.1
		Quartz	3(2)	25	234.5	0.6		-1.0	0.1
		Quartz	4(3)	25	239.5	4.9		-0.5	0.1
	5	Quartz	1(4)	25	245.8	0.5	425.0	-1.1	0.1
	6	Quartz	1(4)	20	312.0	11.0		-0.8	0.2
		Quartz	2(5)	20	307.0	11.5		-0.1	0.1
		Quartz	2(5)	20	309.7	10.5		-0.1	0.1
LNPG-07-15B	1	Quartz	1(5)	20	215.7	18.6	460.0	-0.1	0.2
		Quartz	2(4)	20	229.0	4.8		-0.1	0.2
		Quartz	3(3)	20	225.9	1.6		-0.1	0.1
		Quartz	4(4)	20	225.8	2.7		-0.1	0.1
		Quartz	5(5)	20	226.0	5.3		-0.6	0.1
		Quartz	6(4)	20	262.0	9.7		-1.6	0.6
		Quartz	7(4)	20	257.5	24.4		-2.5	0.1
		Quartz	8(5)	20	272.8	3.9		-2.5	0.1
	3	Quartz	1(4)	18	204.6	36.8		-1.5	0.3
LNPG_08_20	1	Quartz	1(3)	25	227.6	24.0	435.0	-0.1	0.1
		Quartz	2(3)	25	202.6	11.5		-0.1	0.1
	2	Quartz	1(3)	20	217.0	8.0		-0.1	0.1
		Quartz	2(4)	20	215.0	5.4)		-0.1	0.1
	3	Quartz	1(3)	15	205.0	5.0		-0.1	0.1
		Quartz	2(3)	15	214.0	18.3		-0.1	0.1
LNPG_08_20b	1	Quartz	1(4)	20	224.8	4.7	445.0	-1.1	0.2
		Quartz	2(5)	15	208.2	18.0		-0.8	0.2
	2	Quartz	3(4)	15	217.0	9.0		-0.1	0.1
		Quartz	4(4)	15	229.3	16.0		-0.1	0.1
		Quartz	5(5)	15	230.6	6.4		-0.1	0.1
		Quartz	6(4)	15	228.0	6.7		-0.1	0.1
LNPG_08_20	4	Quartz	1(4)	10	225.0	1.4	400.0	-1.7	0.1
		Quartz	2(4)	10	224.0	1.7		-1.7	0.2
CIR10D	1	Quartz	3(3)	15-30	202.7	20.1		-1.7	0.1
		Quartz	4(3)	15-31	166.7	41.3		-1.8	0.2

Table 2: Thermometric data for type A aqueous inclusions

Sample #	Description	$\delta^{13}C$(VPDB)
LNPG-07-1	Qtz-Spd-Kf pegmatite	-9.7
LNPG-07-2	thin Qtz-Kf-Ms pegmatite	-20.2
LNPG-07-3	Qtz-Spd-Kf pegmatite	-17.9
LNPG-07-45	Qtz-Spd peg with secondary albite	-22.2
LNPG-08-42	Qtz from Ms-rich Ta-Sn mineralized zone in altered pegmatite	-21.0
LNPG-08-11	Qt-Kf-Spd peg	-18.2
LNPG-08-11	see above	-24.7
LNPG-08-12	Qtz-Spd-Kf pegmatite at contact with wall rock sedimentary rocks	-15.6

Spd = spodumene, Qtz= quartz, Kf = K-feldspar, Ms = muscovite

Table 3: δ13C analysis of fluid inclusion extracts from quartz

Sample	Site	Flinc	Li	Be	B	Na	Al	K	Fe	Mn	Zn	As	Rb	Sr	Nb	Sn	Sb	Cs	Ta	W
LNPG-08-43	1	2	617	-	291	2000	-	222	-	-	-	22.6	2.5	1.2	0.3	-	0.4	27.4	0.1	1.3
LNPG-08-43	1	3	249	-	188	1107	-	-	-	-	-	20	1	-	-	-	0.6	16	0.1	0.9
LNPG-08-43	1	4a	587	-	400	2955	224	-	-	-	-	23.2	2.2	0.6	-	-	-	31.6	-	0.94
LNPG-08-43	1	4b	326	-	235	1624	116	-	-	-	-	12.7	1.8	-	-	-	-	38.8	-	0.6
LNPG-08-43	1	5	548	1.8	-	292	-	101	-	-	9.3	4	-	0.6	-	3.8	-	1.4	0.1	0.3
LNPG-08-43	1	7	-	-	-	-	-	-	-	-	-	-	-	0.5	0.3	-	-	2.3	2.8	-
LNPG-08-43	3a	2	101.8	-	-	709	-	-	-	-	-	-	-	1.8	0.3	-	0.4	4.5	1.5	-
LNPG-08-43	3a	3	669	1.7	173	3090	779	182	-	-	5.2	5.5	-	-	-	16.2	-	-	-	-
LNPG-08-43	3a	5a	169	-	-	201	364	-	-	-	-	-	-	-	-	8.6	-	-	-	-
LNPG-08-43	3a	5b	100	-	-	346	773	-	-	-	-	-	-	-	-	-	-	-	-	-
LNPG-08-43	3b	1a	61.9	-	-	401	-	192	-	-	-	-	9.6	-	0.7	-	-	0.9	1.6	-
LNPG-08-43	3b	1b	39.6	-	-	231	-	-	-	-	-	-	-	-	-	-	-	1.9	-	-
LNPG-08-43	3b	1c	26	-	-	-	-	-	-	-	-	-	-	-	-	-	-	1.2	-	-
LNPG-08-43	3b	4	273	-	-	1555	-	-	-	-	-	-	-	-	-	-	-	3.3	-	-
LNPG-08-43	3b	5a	163	-	-	570	-	-	-	-	-	-	-	-	-	-	-	8.2	-	-
LNPG-08-43	3b	5b	102	-	-	292	-	-	-	-	-	-	-	-	-	-	-	4	-	-
LNPG-08-43	3b	5c	59	-	-	114	-	-	-	-	-	-	-	-	-	-	-	1.2	-	-
LNPG-08-43	3b	7a	84	-	-	239	-	-	-	-	-	-	-	-	-	-	-	2.5	-	-
LNPG-08-43	3b	7b	135	-	-	414	-	-	-	-	-	-	-	-	-	-	-	4	-	-
LNPG-08-43	4a	3	114	-	-	-	1122	380	-	-	-	-	-	-	-	-	-	-	-	-
LNPG-08-43	4a	3a	508	-	-	-	-	-	-	-	-	-	-	-	-	23	-	-	-	-
LNPG-08-43	4a	6	148	18	-	240	6485	2426	-	34	-	-	-	-	-	37.5	-	-	-	-
LNPG-08-43	4b	2a	420	-	-	-	-	-	-	-	-	-	-	-	1.7	-	-	-	2.2	-
LNPG-08-43	4b	2b	364	-	-	-	-	-	-	-	-	-	-	-	0.7	-	-	-	1.4	-
LNPG-08-33	1a	4a	150	-	-	205	-	-	-	-	-	-	-	-	-	-	-	-	-	-
LNPG-08-33	1a	4b	142	-	-	268	-	-	-	-	-	-	-	-	-	-	-	-	-	-
LNPG-08-33	2	6	232	-	-	-	1013	-	-	-	-	-	-	-	-	-	-	-	-	-
LNPG-08-33	2	3a	107	-	-	-	322	-	-	-	-	-	-	-	-	-	-	-	-	-
LNPG-08-33	2	3b	93	-	-	-	362	-	-	-	-	-	-	-	-	-	-	-	-	-
LNPG-08-33	2	7	124	2.9	63.7	1377	915	255	-	-	-	5	5	-	0.12	-	-	3.3	-	1.2
LNPG-08-33	2	8	271	-	237	674	193	-	-	-	-	2.7	-	-	-	-	-	3.4	-	1.8
LNPG-08-33	3	1	115	-	-	-	361	-	-	-	-	-	-	-	-	-	-	-	-	-
LNPG-08-33	3	3	225	-	-	840	7310	250	145	-	-	-	-	-	0.5	3.7	-	1.6	0.2	-
LNPG-08-33	3	4a	336	-	-	-	420	-	-	-	-	-	-	-	-	-	-	-	-	-
LNPG-08-33	3	4b	257	-	-	-	373	-	-	-	-	-	-	-	-	-	-	-	-	-
LNPG-08-33	3	4c	259	-	-	-	407	-	-	-	-	-	-	-	-	-	-	-	-	-
LNPG-08-13	1	2	128	-	-	504	-	-	-	-	-	-	-	-	-	-	-	2.2	0.1	0.9
LNPG-08-13	1	3	164	-	-	266	-	-	-	-	-	-	-	-	-	-	-	-	0.1	0.6
LNPG-08-13	2	2	-	-	-	182	-	-	-	-	-	-	-	-	-	-	-	1.2	-	-

* All data is in ppm, and of inclusions hosted in quartz.

Table 4: Results of LA ICP-MS analysis of quartz-hosted, aqueous-carbonic fluid inclusions.

Appendix

Table A 1: $\delta^{13}C$ data from quartz hosted fluid inclusion extracts processed at Queen's University, Kingston, ON.

Sample #	d 13C/12C	d 18O/16O
LNPG5	0.158	14.839
LNPG5	0.133	14.825
LNPG5	0.135	14.894
LNPG5	0.184	14.811
LNPG5	0.184	14.634
LNPG5	0.113	14.764
LNPG5	0.1498	14.7856

Table A 2: Decrepitate mound data from SEM-EDS analysis at Laurentian University's Central Analytical Facilities. Results are reported in atomic %. Unreported values were not detected.

Sample	Co	Ti	Na	K	Ca	P	Fe	Zn	Cu	Ni	Cl	S	F	As	Mg	Mn
LNPG-07-15B_2	-	-	1	-	15	-	-	-	-	-	-	1	82	-	-	-
LNPG-08-77	-	-	42	-	-	-	-	-	-	-	29	0.3	27	-	-	-
LNPG-08-77	-	-	41	-	-	-	-	-	-	-	34	-	23	-	-	-
LNPG-08-77	-	-	44	-	-	-	-	-	-	-	34	-	20	-	-	-
LNPG-08-77	-	-	41	5	1	-	-	-	-	-	35	1	15	-	-	-
LNPG-08-47	-	-	60	2	-	-	-	-	-	-	20	5	14	-	-	-
LNPG-07-15B_2	-	-	64	-	-	-	-	-	-	-	17	7	11	-	-	-
LNPG-08-77	-	-	65	1	-	-	-	-	-	-	23	2	9	-	-	-
LNPG-07-13	-	-	50	-	-	-	-	-	-	-	39	-	9	-	-	-

LNPG-08-77	-	-	50	-	-	-	-	-	-	-	40	-	8	-	-	-
LNPG-08-77	-	-	52	0.5	-	-	-	-	-	-	38	0.5	8	-	-	-
LNPG-07-15B_2	-	-	69	-	-	-	-	-	-	-	14	9	7	-	-	-
LNPG-04-1.1	-	-	45	10	3	-	-	-	-	-	30	3	7	-	-	-
LNPG-08-77	-	-	51	-	-	-	-	-	-	-	41	-	7	-	-	-
LNPG-08-47	-	-	67	1	-	-	-	-	-	-	23	2	7	-	-	-
LNPG-08-47	-	-	60	1	-	-	-	-	-	-	30	3	6	-	-	-
LNPG-08-47	-	-	56	1	-	1	-	-	-	-	32	-	5	-	-	-
LNPG-08-77	-	-	53	-	-	-	-	-	-	-	41	-	4	-	-	-
LNPG-08-47	-	-	68	1	-	-	-	-	-	-	24	4	3	-	-	-
LNPG-08-77	-	-	58	-	-	-	-	-	-	-	38	1	2	-	-	-
LNPG-07-15B_1	-	-	3	-	-	-	-	-	-	-	0.5	0.4	-	-	-	-
LNPG-07-15B_1	- dd	-	63	-	-	-	-	-	-	-	20	16	-	-	-	-
LNPG-07-15B_1	-	-	67	-	-	-	-	-	-	-	4	27	-	-	-	-
LNPG-07-15B_1	-	-	72	-	-	-	-	-	-	-	7	20	-	-	-	-
LNPG-07-15B_1	-	-	67	-	-	-	-	-	-	-	-	30	-	-	-	-
LNPG-07-15B_1	-	-	63	-	-	-	-	-	-	-	15	20	-	-	-	-
LNPG-07-15B_1	-	-	62	-	-	-	-	-	-	-	-	35	-	-	-	-
LNPG-07-15B_1	-	-	66	-	-	-	-	-	-	-	16	15	-	-	-	-
LNPG-07-15B_1	-	-	64	-	-	-	-	-	-	-	16	18	-	-	-	-
LNPG-07-15B_1	-	-	75	1	-	-	-	-	-	-	-	23	-	-	-	-
LNPG-07-15B_1	-	-	68	-	-	-	-	-	-	-	-	31	-	-	-	-
LNPG-07-15B_1	-	-	67	-	-	-	-	-	-	-	-	32	-	-	-	-

LNPG-07-15B_1	-	-	63	-	-	-	-	-	-	-	-	36	-	-	-	-
LNPG-07-15B_1	-	-	6	-	-	-	-	-	-	-	-	1	-	-	-	-
LNPG-07-15B_2	-	-	84	-	-	-	-	-	-	-	-	15	-	-	-	-
LNPG-07-15B_2	-	-	84	-	-	-	-	-	-	-	-	16	-	-	-	-
LNPG-07-15B_2	11	-	10	5	9	-	18	-	-	-	-	11	-	34	-	-
LNPG-07-15B_2	-	-	90	-	-	-	-	-	-	-	-	10	-	-	-	-
LNPG-07-15B_2	-	-	84	-	-	-	-	-	-	-	-	16	-	-	-	-
LNPG-07-15B_2	-	-	67	6	-	-	-	-	-	-	15	12	-	-	-	-
LNPG-07-15B_2	-	-	66	5	-	-	-	-	-	-	19	10	-	-	-	-
LNPG-07-15B_2	-	-	82	-	-	-	-	-	-	-	-	18	-	-	-	-
LNPG-07-15B_2	-	-	89	-	-	-	-	-	-	-	-	10	-	-	-	-
LNPG-07-15B_2	-	-	89	-	-	-	-	-	-	-	-	10	-	-	-	-
LNPG-07-15B_2	-	-	67	-	-	-	-	-	-	-	-	33	-	-	-	-
LNPG-07-15B_2	-	-	75	-	-	-	-	-	-	-	-	25	-	-	-	-
LNPG-07-15B_2	-	-	-	9	4	-	20	17	4	-	-	17	-	-	23	-
LNPG-07-15B_2	-	-	86	-	-	-	-	-	-	-	-	13	-	-	-	-
LNPG-07-15B_2	-	-	79	-	-	-	-	-	-	-	-	20	-	-	-	-
LNPG-07-15B_2	-	-	79	-	-	-	-	-	-	-	-	20	-	-	-	-
LNPG-07-15B_2	-	-	80	-	-	-	-	-	-	-	7	11	-	-	-	-
LNPG-07-15B_2	-	-	84	-	-	-	-	-	-	-	-	16	-	-	-	-
LNPG-07-15B_2	-	-	75	-	-	-	-	-	-	-	13	11	-	-	-	-
LNPG-07-15B_2	-	-	68	-	-	-	-	-	-	-	18	14	-	-	-	-
LNPG-07-15B_2	-	-	70	-	-	-	-	-	-	-	23	6	-	-	-	-
LNPG-07-15B_2	-	-	72	-	-	-	-	-	-	-	-	27	-	-	-	-

LNPG-07-15B_2	-	-	69	-	-	-	-	-	-	-	23	8	-	-	-	-
LNPG-07-15B_2	-	-	71	-	-	-	-	-	-	-	15	12	-	-	-	-
LNPG-07-15B_2	-	-	77	-	-	-	-	-	-	-	13	10	-	-	-	-
LNPG-07-15B_2	-	-	73	-	-	-	-	-	-	-	17	9	-	-	-	-
LNPG-07-15B_2	-	-	69	-	-	-	-	-	-	-	23	7	-	-	-	-
LNPG-07-15B_2	-	-	68	2	-	-	-	-	-	-	19	10	-	-	-	-
LNPG-07-15B_2	-	-	67	-	-	-	-	-	-	-	22	10	-	-	-	-
LNPG-07-15B_2	-	-	74	-	-	-	-	-	-	-	14	12	-	-	-	-
LNPG-07-15B_2	-	-	74	-	-	-	-	-	-	-	16	9	-	-	-	-
LNPG-07-15B_2	-	-	65	-	-	-	-	-	-	-	29	5	-	-	-	-
LNPG-07-15B_2	-	-	85	-	-	-	-	-	-	-	-	15	-	-	-	-
LNPG-07-15B_2	-	-	66	-	-	-	-	-	-	-	22	12	-	-	-	-
LNPG-07-15B_2	-	-	81	-	-	-	-	-	-	-	-	19	-	-	-	-
LNPG-07-15B_2	-	-	79	-	-	-	-	-	-	-	-	21	-	-	-	-
LNPG-08-20	-	-	27	-	40	16	-	-	-	-	-	16	-	-	-	-
LNPG-08-20	-	-	61	-	-	-	-	-	-	-	-	39	-	-	-	-
LNPG-08-20	-	-	58	-	-	-	-	-	-	-	-	41	-	-	-	-
LNPG-08-20	-	-	54	11	-	-	-	-	-	-	-	35	-	-	-	-
LNPG-08-20	-	-	68	-	-	-	-	-	-	-	-	32	-	-	-	-
LNPG-08-20	-	-	43	-	17	-	-	-	-	-	24	16	-	-	-	-
LNPG-08-20	-	-	58	-	-	-	-	-	-	-	7	34	-	-	-	-
LNPG-08-20	-	-	62	-	-	-	-	-	-	-	5	33	-	-	-	-
LNPG-08-20	-	-	43	15	6	-	-	-	-	-	31	4	-	-	-	-
LNPG-08-20	-	-	52	13	2	-	-	-	-	-	31	3	-	-	-	-

LNPG-08-20_b	-	-	65	-	-	-	-	-	-	-	22	13	-	-	-	-
LNPG-08-20_b	-	4	38	-	9	-	8	7	-	-	28	6	-	-	-	-
LAM_LK_07_15B_3spd	-	-	53	0.8	-	-	-	-	-	-	45	-	-	-	-	-
LAM_LK_07_15B_3spd	-	-	10	15	47	13	-	-	-	-	-	14	-	-	-	-
LAM_LK_07_15B_3spd	-	-	33	18	6	15	-	-	-	-	20	7	-	-	-	-
LAM_LK_07_15B_3spd	-	-	50	1	3	-	-	-	-	-	41	1	-	-	3	-
LAM_LK_07_15B_3spd	-	-	40	1	39	-	-	-	-	-	17	1	-	-	-	-
LAM_LK_07_15B_3spd	-	-	47	1	-	-	-	-	-	-	51	-	-	-	-	-
LAM_LK_07_15B_3spd	-	-	46	1	-	-	-	-	-	-	51	0.6	-	-	-	-
LAM_LK_07_15B_3spd	-	-	53	1	-	-	-	-	-	-	45	1	-	-	-	-
LAM_LK_07_15B_3spd	-	-	55	1	1	-	-	-	-	-	41	1	-	-	-	-
LNPG-04-1.1	-	-	49	2	-	-	-	-	-	-	47	-	-	-	-	-
LNPG-04-1.1	-	-	52	0.6	0.7	-	0.3	-	-	-	45	0.2	-	-	-	-
LNPG-04-1.1	-	-	52	-	-	1	-	-	-	-	46	1	-	-	-	-
LNPG-04-1.1	-	-	20	-	-	-	-	-	-	-	14	-	-	-	-	-
LNPG-04-1.1	-	-	10	-	-	-	-	-	-	-	7	-	-	-	-	-
LNPG-04-1.1	-	-	24	-	6	-	6	-	-	-	3	-	-	-	17	42
LNPG-04-1.1	-	1	42	1	10	-	2	-	-	-	33	2	-	-	5	-
LNPG-04-1.1	-		50	3	3	-	7	-	-	-	31	3	-	-	-	-
LNPG-04-1.1	-	3	42	4	5	-	4	-	-	-	26	-	-	-	14	-
LNPG-08-77	-	-	55	-	-	-	-	-	-	-	45	-	-	-	-	-
LNPG-08-77	-	-	52	-	-	-	-	-	-	-	47	-	-	-	-	-
LNPG-08-77	-	-	54	1	-	-	-	-	-	-	45	-	-	-	-	-
LNPG-08-77	-	-	47	5	2	-	-	-	-	-	41	2	-	-	-	-

LNPG-08-77	-	1	6	-	21	-	20	-	-	-	2	-	-	-	48	-
LNPG-08-77	-	-	71	-	-	-	-	-	-	-	28	-	-	-	-	-
LNPG-08-77	-	-	55	-	-	-	-	-	-	-	45	-	-	-	-	-
LNPG-08-77	-	-	56	-	-	-	-	-	-	-	44	-	-	-	-	-
LNPG-08-77	-	-	55	-	-	-	-	-	-	-	45	-	-	-	-	-
LNPG-08-77	-	-	58	9	-	-	1	4	-	-	-	27	-	-	-	-
LNPG-08-77	-	-	61	1	-	-	1	4	-	-	-	30	-	-	-	-
LNPG-08-77	-	-	50	1	-	-	-	-	-	-	47	0.5	-	-	-	-
LNPG-08-77	-	-	78	-	-	-	-	-	-	-	20	1	-	-	-	-
LNPG-07-13	-	-	54	8	-	-	-	-	-	-	31	-	-	-	-	-
LNPG-07-13	-	-	55	-	-	-	-	-	-	-	45	-	-	-	-	-
LNPG-07-13	-	-	25	3	-	-	62	-	-	-	-	9	-	-	-	-
LNPG-07-13	-	-	53	-	-	-	-	-	-	-	46	-	-	-	-	-
LNPG-07-13	-	-	55	-	-	-	-	-	-	-	45	-	-	-	-	-
LNPG-07-13	-	-	51	1	-	-	-	-	-	-	47	-	-	-	-	-
LNPG-07-13	-	-	53	1	-	-	-	-	-	-	45	-	-	-	-	-
LNPG-07-13	-	-	53	-	-	-	-	-	-	-	46	-	-	-	-	-
LNPG-07-13	-	-	52	-	-	-	-	-	-	-	47	-	-	-	-	-
LNPG-07-13	-	-	51	1	-	-	-	-	-	-	47	-	-	-	-	-
LNPG-07-13	-	-	55	-	-	-	-	-	-	-	45	-	-	-	-	-
LNPG-07-13	-	-	55	-	-	-	-	-	-	-	45	-	-	-	-	-
LNPG-07-13	-	-	54	1	-	-	-	-	-	-	45	-	-	-	-	-
LNPG-07-13	-	-	53	2	-	-	-	-	-	-	45	-	-	-	-	-
LNPG-07-13	-	-	52	1	-	-	-	-	-	-	47	-	-	-	-	-

LNPG-07-13	-	-	53	1	-	-	-	-	-	-	45	1	-	-	-	-
LNPG-07-13	-	-	55	-	-	-	-	-	-	-	45	-	-	-	-	-
LNPG-07-13	-	-	54	-	-	-	-	-	-	-	46	-	-	-	-	-
LNPG-07-13	-	-	52	-	-	-	-	-	-	-	47	1	-	-	-	-
LNPG-07-13	-	-	52	1	-	-	-	-	-	-	47	-	-	-	-	-
LNPG-08-47	-	-	25	34	-	-	-	-	-	-	37	3	-	-	-	-
LNPG-08-47	-	-	69	1	-	-	-	-	-	-	25	3	-	-	-	-
LNPG-08-47	-	-	78	-	-	-	-	-	-	-	9	12	-	-	-	-
LNPG-08-47	-	-	78	-	-	-	-	-	-	-	9	13	-	-	-	-
LNPG-04-1.1-1	-	-	80	-	-	-	-	-	-	-	20	-	-	-	-	-
LNPG-04-1.1-1	-	-	40	1.8	5.4	-	2.2	-	-	-	42	3.5	-	-	5.1	-
LNPG-04-1.1-1	-	-	33.1	-	0.2	-	-	-	-	-	32	0.2	-	-	-	-
LNPG-04-1.1-1	-	-	29.9	-	-	-	-	-	-	-	24.65	-	-	-	-	-
LNPG-04-1.1-1	-	-	27	25	-	-	0.9	-	-	-	40	1	-	-	-	-
LNPG-04-1.1-2	-	-	33	16	7	-	-	-	-	-	34	-	-	-	-	-
LNPG-04-1.1-6	-	-	44.5	-	-	-	-	-	-	-	55.5	-	-	-	-	-
LNPG-04-1.1-6	-	-	44.4	-	-	-	-	-	-	-	55.55	-	-	-	-	-
LNPG-04-1.1-6	-	-	44	-	0.5	-	-	-	-	-	56	-	-	-	-	-
LNPG-04-1.1-6	-	-	37	1	2.5	-	1.3	-	-	-	55	1.4	-	-	1.5	-
LNPG-04-1.1-6	-	-	34.5	0.5	1.5	-	0.6	-	-	-	60	0.7	-	-	-	-
LNPG-04-1.1-6	-	-	22	9	-	-	9	-	-	-	24	-	-	-	3	-
LNPG-07-13-3	-	-	28	35	6	-	-	-	-	-	28	2.3	-	-	-	-
LNPG-07-13-3	-	-	17	34	6.5	-	3.2	-	-	-	28.5	-	-	-	-	-
LNPG-07-13-4	-	-	42.5	0.3	0.4	-	-	-	-	-	53	-	-	-	-	-

LNPG-07-13-5	-	-	45	5	-	-	-	-	-	-	47	-	-	-	-	-
LNPG-07-13-5	-	-	44	-	-	-	-	-	-	-	51	-	-	-	-	-
LNPG-07-13-5	-	-	42	1.4	-	-	-	-	-	-	51	-	-	-	-	-
LNPG-07-13-5	-	-	40	-	0.6	-	-	-	-	-	58	-	-	-	-	-
LNPG-07-13-5	-	-	39.5	1.4	0.4	-	-	-	-	-	56	0.1	-	-	-	-
LNPG-07-13-5	-	-	38.8	-	-	-	-	-	-	-	58	-	-	-	-	-
LNPG-07-13-5	-	-	14	45	-	-	-	-	-	-	39	1.2	-	-	-	-
LNPG-07-13-5	-	-	8.2	52.5	-	-	-	-	-	-	38.3	0.9	-	-	-	-
LNPG-07-13-5	-	-	6.5	54	-	-	-	-	-	-	39	0.6	-	-	-	-
LNPG-04-1.1-2	-	-	35	2	21	-	-	-	-	-	5.6	-	-	-	12	-
LNPG-04-1.1-2	-	-	35	7	22	-	-	-	-	-	11	-	-	-	13	-
LNPG-07-13-3	-	-	15	-	77	-	-	-	-	-	6.3	2	-	-	-	-

Table A 3: LA ICP-MS data reported in ppm from ablated fluid inclusions in quartz. Unreported values were not detected.

Sample	Li	Be	B	Na	Al	K	Fe	Mn	Zn	As	Rb	Sr	Y	Nb	Sn	Sb	Cs	Ta	W
LNPG-08-43	617	-	291	2000	-	222	-	-	-	22.6	2.5	1.2	-	0.3	-	0.4	27.4	0.1	1.3
LNPG-08-43	249	-	188	1107	-	-	-	-	-	20	1	-	-	-	-	0.6	16	0.1	0.9
LNPG-08-43	587	-	400	2955	224	-	-	-	-	23.2	2.2	0.6	-	-	-	-	31.6	-	0.94
LNPG-08-43	326	-	235	1624	116	-	-	-	-	12.7	1.8	-	-	-	-	-	38.8	-	0.6
LNPG-08-43	548	1.8	-	292	-	101	-	-	9.3	4	-	0.6	-	-	3.8	-	1.4	0.1	0.3
LNPG-08-43	-	-	-	-	-	-	-	-	-	-	-	0.5	-	0.3	-	-	2.3	2.8	-
LNPG-08-43	101.8	-	-	709	-	-	-	-	-	-	-	1.8	-	0.3	-	0.4	4.5	1.5	-
LNPG-08-43	669	1.7	173	3090	779	182	-	-	5.2	5.5	-	-	-	-	16.2	-	-	-	-
LNPG-08-43	169	-	-	201	364	-	-	-	-	-	-	-	-	-	8.6	-	-	-	-
LNPG-08-43	100	-	-	346	773	-	-	-	-	-	-	-	-	-	-	-	-	-	-
LNPG-08-43	61.9	-	-	401	-	192	-	-	-	-	9.6	-	-	0.7	-	-	0.9	1.6	-
LNPG-08-43	39.6	-	-	231	-	-	-	-	-	-	-	-	-	-	-	-	1.9	-	-
LNPG-08-43	26	-	-	-	-	-	-	-	-	-	-	-	-	-	-	-	1.2	-	-
LNPG-	273	-	-	1555	-	-	-	-	-	-	-	-	-	-	-	-	3.3	-	-

08-43																			
LNPG-08-43	163	-	-	570	-	-	-	-	-	-	-	-	-	-	-	-	8.2	-	-
LNPG-08-43	102	-	-	292	-	-	-	-	-	-	-	-	-	-	-	-	4	-	-
LNPG-08-43	59	-	-	114	-	-	-	-	-	-	-	-	-	-	-	-	1.2	-	-
LNPG-08-43	84	-	-	239	-	-	-	-	-	-	-	-	-	-	-	-	2.5	-	-
LNPG-08-43	135	-	-	414	-	-	-	-	-	-	-	-	-	-	-	-	4	-	-
LNPG-08-43	114	-	-	-	1122	380	-	-	-	-	-	-	-	-	-	-	-	-	-
LNPG-08-43	508	-	-	-	-	-	-	-	-	-	-	-	-	-	23	-	-	-	-
LNPG-08-43	148	18	-	240	6485	2426	-	34	-	-	-	-	-	-	37.5	-	-	-	-
LNPG-08-43	420	-	-	-	-	-	-	-	-	-	-	-	-	1.7	-	-	-	2.2	-
LNPG-08-43	364	-	-	-	-	-	-	-	-	-	-	-	-	0.7	-	-	-	1.4	-
LNPG-08-33	150	-	-	205	-	-	-	-	-	-	-	-	-	-	-	-	-	-	-
LNPG-08-33	142	-	-	268	-	-	-	-	-	-	-	-	-	-	-	-	-	-	-
LNPG-08-33	232	-	-	-	1013	-	-	-	-	-	-	-	-	-	-	-	-	-	-
LNPG-08-33	107	-	-	-	322	-	-	-	-	-	-	-	-	-	-	-	-	-	-
LNPG-	93	-	-	-	362	-	-	-	-	-	-	-	-	-	-	-	-	-	-

08-33																			
LNPG-08-33	124	2.9	63.7	1377	915	255	-	-	-	5	5	-	-	0.12	-	-	3.3	-	1.2
LNPG-08-33	271	-	237	674	193	-	-	-	-	2.7	-	-	-	-	-	-	3.4	-	1.8
LNPG-08-33	115	-	-	-	361	-	-	-	-	-	-	-	-	-	-	-	-	-	-
LNPG-08-33	225	-	-	840	7310	250	145	-	-	-	-	-	-	0.5	3.7	-	1.6	0.2	-
LNPG-08-33	336	-	-	-	420	-	-	-	-	-	-	-	-	-	-	-	-	-	-
LNPG-08-33	257	-	-	-	373	-	-	-	-	-	-	-	-	-	-	-	-	-	-
LNPG-08-33	259	-	-	-	407	-	-	-	-	-	-	-	-	-	-	-	-	-	-
LNPG-08-13	128	-	-	504	-	-	-	-	-	-	-	-	-	-	-	-	2.2	0.1	0.9
LNPG-08-13	164	-	-	266	-	-	-	-	-	-	-	-	-	-	-	-	-	0.1	0.6
LNPG-08-13	-	-	-	182	-	-	-	-	-	-	-	-	-	-	-	-	1.2	-	-

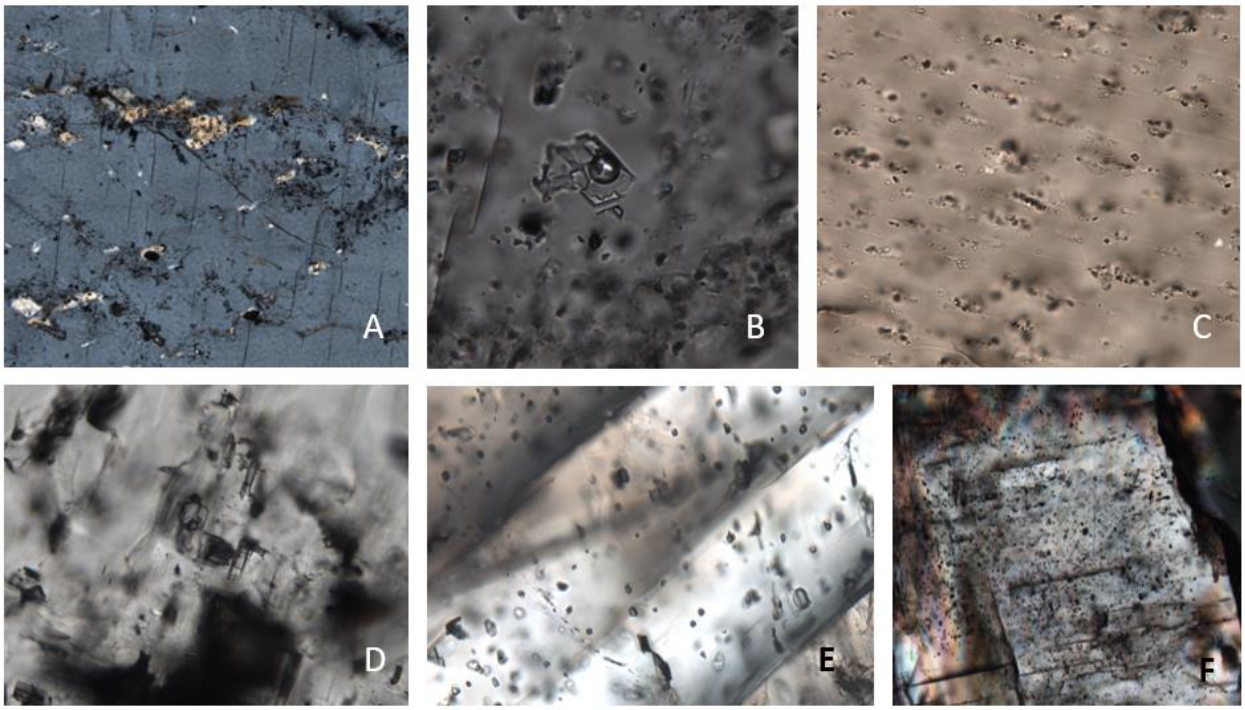

Figure A-1. Photomicrographs of fluid inclusions in samples from the LNPG pegmatites. A) Cirqure 10D, 10x: Fluid inclusions along fractures in altered K-feldspar. B) LNPG-07-11, 40X: Aqueous carbonic fluid inclusion hosted in K-feldspar. C) LNPG-07-11, 10x: Secondary fluid inclusions aligned along cleavage planes in K-feldspar. D) LNPG-08-13, 50x: Irregular arrays of aqueous carbonic inclusions hosted in K-feldspar. E) LNPG-08-13, 40x: Negative crystal shape of 3 phase aqueous carbonic fluid inclusions hosted in K-feldspar from the same sample as “F”. F) LNPG-08-13, 10x: K-feldspar inundated with secondary three phase aqueous carbonic fluid inclusions.

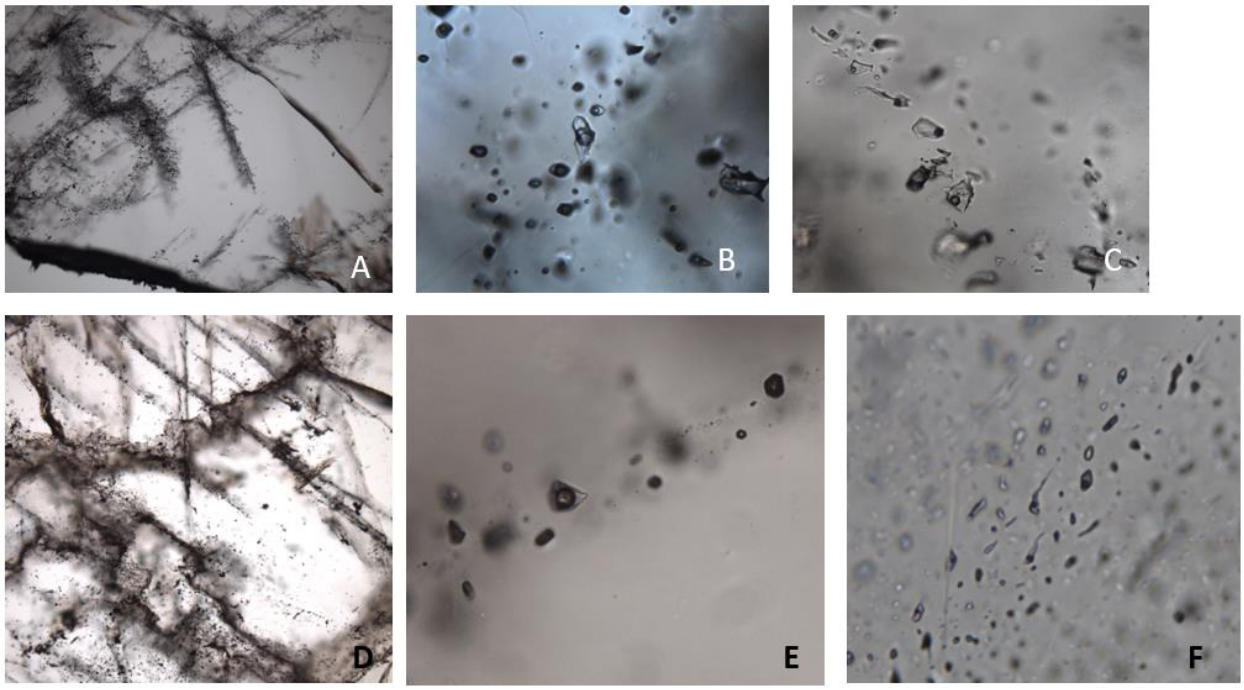

Figure A-2: Photomicrographs of fluid inclusions in samples from the LNPG pegmatites . A) Cirque 10D, 2x: Sample of aqueous carbonic - type secondary fluid inclusions in quartz showing fluids along secondary fractures in otherwise clean quartz. B) Close up of previous image at 40x: Aqueous carbonic inclusions showing irregular and negative crystal habits. C) Close up of image in A again, 40x: A L-V type FIA in quartz showing irregular inclusion shapes, yet consistent L:V ratios in the inclusions. D) LNPG-07-15B, 2x: FIA's showing secondary aqueous carbonic inclusions along fractures and grain boundaries in quartz. Note that the quartz matrix hosts few irregular arrays of L-V type inclusions. E) LNPG-07-15B, 40x: Aqueous carbonic inclusions with variable L:V ratios along a secondary fracture in quartz. F) LNPG-08-73, 80x: Secondary L-V fluid inclusions in fine-grained quartz within an apalite layer. Note the inclusions exhibitg necking and inconsistent phase ratios.

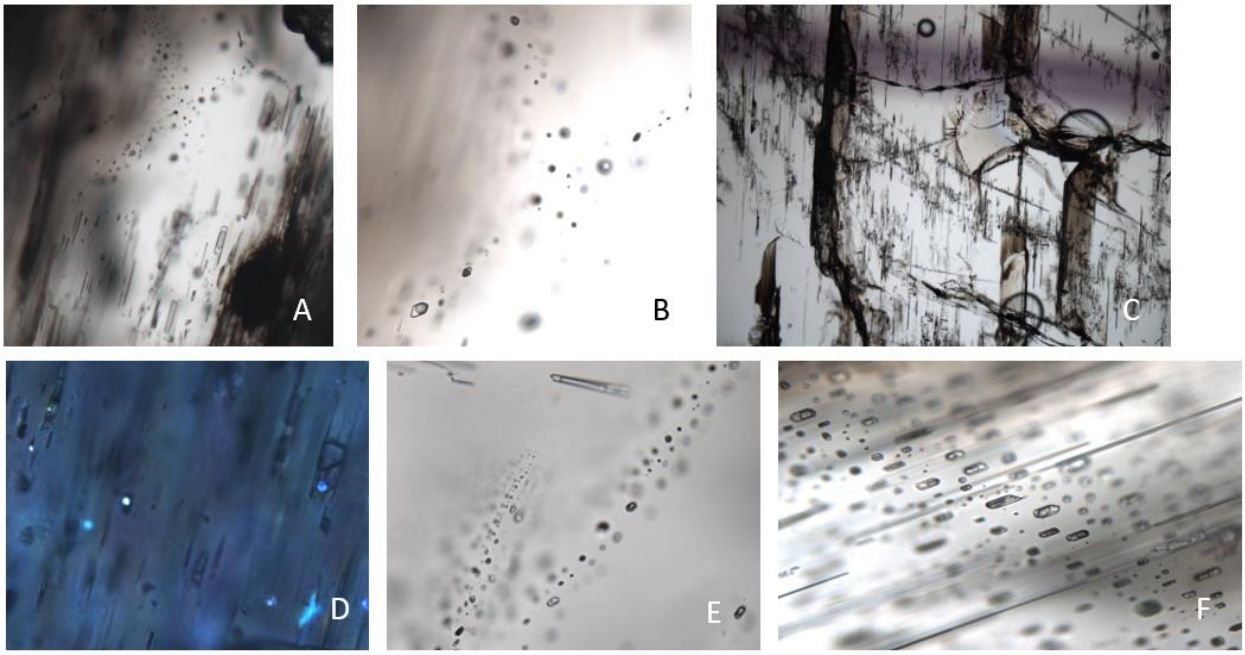

Figure A-3: Photomicrographs of fluid inclusions in samples from the LNPG pegmatites. A) LNPG-07-15B, 20x: Spodumene hosting elongate secondary aqueous carbonic fluid inclusions. B) LNPG-07-15B, 40x: Secondary aqueous carbonic fluid inclusions which in detail (not shown) have equant shapes. C) LNPG-07-15B, 2X. Spodumene hosting secondary fluid inclusions along fractures. D) LNPG-08-23, 40x: Strongly birefringent solid phases in addition to other solid phases in elongate, negative-crystal shape inclusions hosted by spodumene. E) LNPG-07-15A, 20x: Equant-shaped aqueous carbonic fluid inclusions cutting planes of aqueous carbonic inclusions hosted in spodumene. F) As in previous phot 40x: Aqueous carbonic fluid inclusions showing elongation along C axis of the host.

Figure A-4: Top) Sample 08-20: quartz host, Raman peaks: 1284.5 & 1388.7 (CO_2), 2331 (N_2), 2611 (H_2S), 2920 (CH_4). Bottom) Sample 04_1.1: spodumene host Raman peaks: 1281.3 & 1385.7 (CO_2),2333 (N_2).

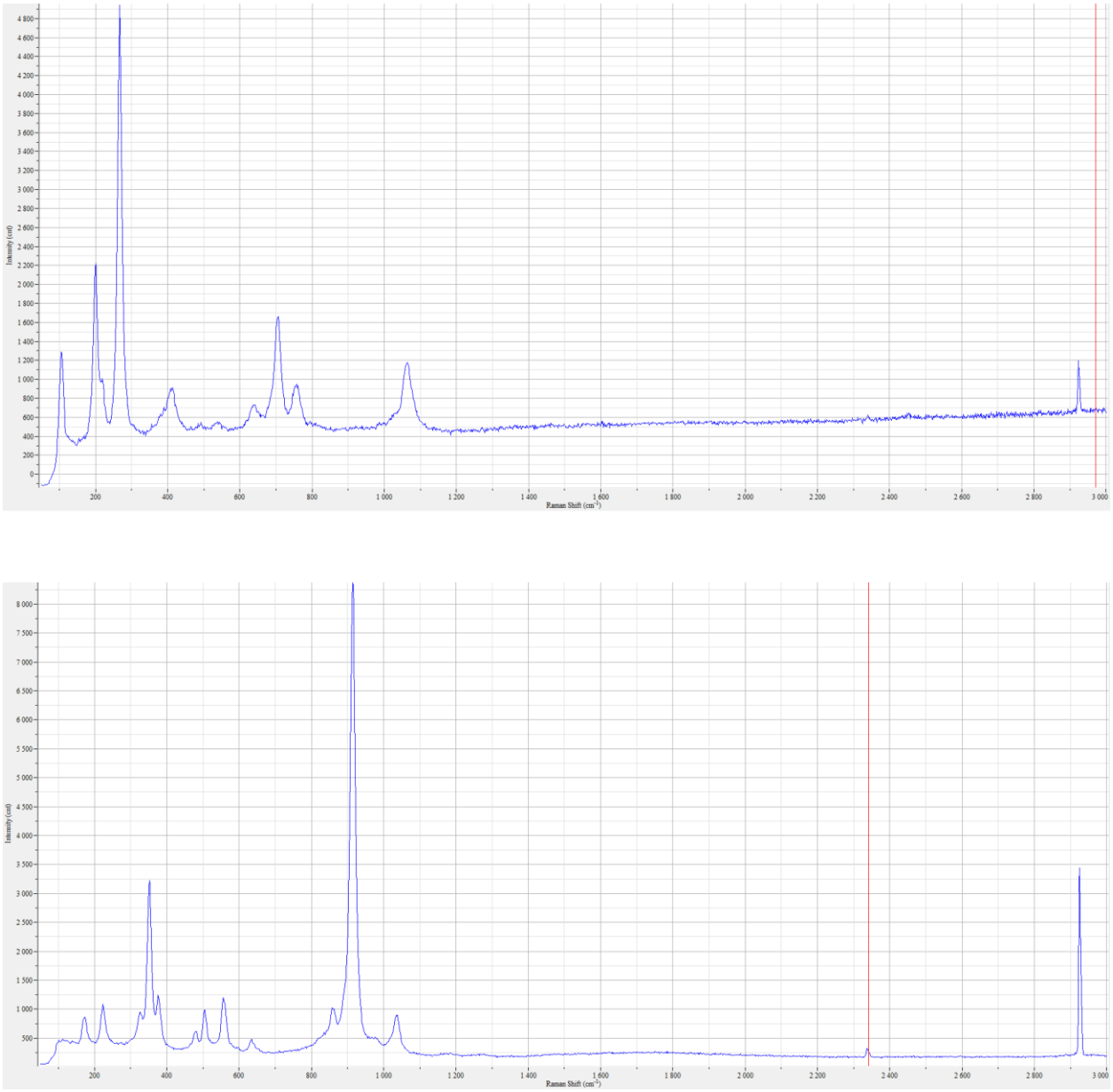

Figure A-5: Top) Sample 08-77: muscovite host, Raman peaks: 2341 (N_2), 2924 (CH_4). Bottom) Sample 07_L9: garnet host, Raman peaks: 2336 (N_2)2924 (CH_4).